UNIVERSIDADE FEDERAL DO RIO GRANDE DO SUL

CENTRO ESTADUAL DE PESQUISAS EM SENSORIAMENTO REMOTO E METEOROLOGIA

PROGRAMA DE PÓS-GRADUAÇÃO EM SENSORIAMENTO REMOTO

DOUGLAS STEFANELLO FACCO

DINÂMICA ESPAÇO-TEMPORAL DA TURBIDEZ NO RESERVATÓRIO DE ITAIPU, NA REGIÃO SUL DO BRASIL, UTILIZANDO DADOS DE SENSORIAMENTO REMOTO

PORTO ALEGRE

2023

DOUGLAS STEFANELLO FACCO

DINÂMICA ESPAÇO-TEMPORAL DA TURBIDEZ NO RESERVATÓRIO DE ITAIPU, NA REGIÃO SUL DO BRASIL, UTILIZANDO DADOS DE SENSORIAMENTO REMOTO

Tese de doutorado apresentada ao Programa de Pós-Graduação em Sensoriamento Remoto como requisito parcial para a obtenção do título de Doutor em Sensoriamento Remoto e Geoprocessamento.

Orientador: Prof. Dr. Laurindo Antonio Guasselli

PORTO ALEGRE

2023

CIP - Catalogação na Publicação

Facco, Douglas Stefanello
DINÂMICA ESPAÇO-TEMPORAL DA TURBIDEZ NO RESERVATÓRIO DE ITAIPU, NA REGIÃO SUL DO BRASIL, UTILIZANDO DADOS DE SENSORIAMENTO REMOTO / Douglas Stefanello Facco. -- 2023.
101 f.
Orientador: Laurindo Antonio Guasselli.

Tese (Doutorado) -- Universidade Federal do Rio Grande do Sul, Centro Estadual de Pesquisas em Sensoriamento Remoto e Meteorologia, Programa de Pós-Graduação em Sensoriamento Remoto, Porto Alegre, BR-RS, 2023.

1. Processamento digital de Imagens. 2. Sensoriamento Remoto . 3. Turbidez da água . 4. Padrões espectrais. 5. Monitoramento . I. Guasselli, Laurindo Antonio, orient. II. Título.

Elaborada pelo Sistema de Geração Automática de Ficha Catalográfica da UFRGS com os dados fornecidos pelo(a) autor(a).

TESE

Submetida como parte dos requisitos
para obtenção do Grau de

DOUTOR EM SENSORIMENTO REMOTO E GEOPROCESSAMENTO

Programa de Pós-Graduação em Sensoriamento Remoto (PPGSR)
Centro Estadual de Pesquisas em Sensoriamento Remoto e Meteorologia (CEPRSM)
Universidade Federal do Rio Grande do Sul (UFRGS)
Porto Alegre, RS, Brasil.

Aprovada em: 31 de março de 2023.
Pela Banca Examinadora:

Homologada em: ___/___/_____.
Por:

Prof. Dr. Laurindo Antonio Guasselli
Orientador

Dr. Daniel Capella Zanotta
(PPGSR/UFRGS)

Dr. Fábio Marcelo Breunig
(UFSM)

Dr. Fernando Luis Hillebrand
(IFRS Rolante)

Observação: Esta Ata não pode ser considerada como instrumento final do processo de concessão de título ao aluno.

AGRADECIMENTOS

Gostaria de agradecer a existência da Universidade pública do Brasil, especialmente a Universidade Federal do Rio Grande do Sul (UFRGS) pela acolhida e ensino de qualidade que me proporcionou.

À Coordenação de Aperfeiçoamento de Pessoal de Nível Superior (CAPES) pela concessão da bolsa de pesquisa.

Ao professor e orientador Laurindo Antonio Guasselli pela disposição e contribuições para minha formação.

O mesmo agradecimento se estende ao meu colaborador Luis Fernando Chimelo Ruiz pela ajuda e contribuição, e não menos importante a banca examinadora, professores Daniel Capella Zanotta, Fabio Marcelo Breunig e Fernando Luis Hillebrand pelas considerações tão importantes para meu trabalho.

Também gostaria de agradecer a todos os professores e funcionários do Programa de Pós-Graduação em Sensoriamento Remoto da Universidade Federal do Rio Grande do Sul (PPGSR-UFRGS).

Aos colegas do Laboratório de Geoprocessamento e Análise Ambiental (LAGAM) e das disciplinas cursadas pelos bons momentos de amizade e descontração.

E a todos os amigos que de alguma forma seja academicamente ou pessoalmente contribuíram para esse momento de conclusão e evolução.

RESUMO

A turbidez da água é um parâmetro crucial na determinação da qualidade da água. A erosão e o assoreamento estão diretamente ligados à turbidez, influenciando a qualidade das águas e o armazenamento de reservatórios. Mapear padrões de turbidez é importante para a gestão e monitoramento de reservatórios. O monitoramento da turbidez em reservatórios, depende de métodos tradicionais com coletas pontuais, analisadas em laboratório que consomem tempo, dinheiro e mão-de-obra exaustiva. Diante disso, o sensoriamento remoto surge como alternativa para complementar programas de monitoramento, preenchendo lacunas temporais e espaciais. Esta Tese aborda métodos para analisar e quantificar padrões de turbidez da água utilizando dados de sensoriamento remoto e técnicas de processamento digital de imagens. Investigou-se a relação entre turbidez, precipitação e reflectância espectral. Os resultados mostraram alta correlação entre o índice de turbidez NDTI e a turbidez (R^2 = 0,91). A precipitação teve influência determinante, sendo o rio Paraná, nos períodos de maior precipitação, o principal agente no transporte de sedimentos. Os compartimentos laterais do reservatório mostraram menor influência no transporte de sedimentos. Também comparou-se o desempenho dos algoritmos Classification and Regression Tree (CART), Naive Bayes (NB) e Random Forest (RF), a partir de classificação supervisionada de imagens, e abordagens em Pixel-Based Image analysis (PBIA) e Geographic Object-Based Image Analysis (GEOBIA), para classificar a turbidez. O classificador RF obteve a maior precisão em ambas as abordagens, seguido por CART e NB. Os índices Kappa e Análise Global das classificações GEOBIA foram superiores às classificações PBIA em ambos os algoritmos. Também avaliou-se o potencial de estimativa da Área de Água Superficial e Nível de Água do Reservatório. Testamos séries temporais de imagens ópticas Landsat 8 e Sentinel-2, radar Sentinel-1, e validação com altimetria Jason-3. A metodologia foi desenvolvida na rotina operacional do Google Earth Engine, que agilizou o mapeamento. Os melhores resultados foram entre Sentinel-2 e NDWI com R^2 = 0,88 e RMSE de 11,59 km². No geral, nossos resultados demonstram o potencial do sensoriamento remoto para identificar e analisar padrões de turbidez no reservatório de Itaipu. O que pode ser extraído deste estudo é que a turbidez da água do reservatório é espectralmente ativa. Em segundo lugar, há uma forte conexão entre materiais suspensos, turbidez e precipitação. Os dados multiespectrais de média

resolução foram ideais na detecção e análise da turbidez. Nosso estudo mostra que mesmo sem dados *in situ*, é possível analisar, e quantificar padrões de turbidez do reservatório de Itaipu a partir de sensores acoplados em satélites espaciais.

Palavras-chave: Sensores orbitais. Padrões espectrais. Monitoramento de reservatório.

ABSTRACT

Water turbidity is a crucial parameter in determining water quality. Erosion and siltation are directly linked to turbidity, influencing water quality and reservoir storage. Mapping turbidity patterns is important for reservoir management and monitoring. The monitoring of turbidity in reservoirs depends on traditional methods with punctual collections, analyzed in the laboratory that consume time, money and exhaustive labor. Given this, remote sensing emerges as an alternative to complement monitoring programs, filling temporal and spatial gaps. This Thesis addresses methods to analyze and quantify water turbidity patterns using remote sensing data and digital image processing techniques. The relationship between turbidity, precipitation and spectral reflectance was investigated. The results showed a high correlation between the NDTI turbidity index and turbidity ($R^2 = 0.91$). Precipitation had a decisive influence, with the Paraná River, in periods of greater precipitation, being the main agent in the transport of sediments. The lateral compartments of the reservoir showed less influence on sediment transport. The performance of the Classification and Regression Tree (CART), Naive Bayes (NB) and Random Forest (RF) algorithms was also compared, based on supervised image classification, and Pixel-Based Image analysis (PBIA) and Geographic Object approaches. Based Image Analysis (GEOBIA), to classify turbidity. The RF classifier achieved the highest accuracy in both approaches, followed by CART and NB. Kappa indices and Global Analysis of GEOBIA rankings were superior to PBIA rankings in both algorithms. The estimation potential of the Surface Water Area and Water Level of the Reservoir was also evaluated. We tested time series of Landsat 8 and Sentinel-2 optical images, Sentinel-1 radar, and validation with Jason-3 altimetry. The methodology was developed in the operational routine of Google Earth Engine, which streamlined the mapping. The best results were between Sentinel-2 and NDWI with $R^2 = 0.88$ and RMSE of 11.59 km². Overall, our results demonstrate the potential of remote sensing to identify and analyze turbidity patterns in the Itaipu reservoir. What can be extracted from this study is that the turbidity of the reservoir water is spectrally active. Second, there is a strong connection between suspended materials, turbidity and precipitation. Medium resolution multispectral data were ideal for detecting and analyzing turbidity. Our study shows that even without in situ data, it is possible to analyze and quantify turbidity patterns in the Itaipu reservoir using sensors attached to space satellites.

Keywords: Orbital sensors. Spectral patterns. Reservoir monitoring

LISTA DE FIGURAS

SUMÁRIO

ORGANIZAÇÃO DA TESE

A tese a seguir foi elaborada de acordo com a política e os procedimentos do PPGSR da Universidade Federal do Rio Grande do Sul com a inclusão de artigos publicados. Este documento é composto por 6 capítulos, 2 capítulos iniciais introdutórios, em seguida apresenta três artigos em forma de capítulo e por fim fechamento do estudo.

O capítulo 1 é uma introdução geral da Tese, contemplando a introdução, os objetivos e a hipótese. Neste capítulo são abordados os principais problemas e limitações da análise de turbidez em reservatórios e prováveis possibilidades.

O capítulo 2 apresenta as principais bases teóricas abarcando principalmente o emprego do sensoriamento remoto e turbidez em estudos aquáticos.

O capítulo 3 apresenta o artigo intitulado: “Spectral Reflectance in the Spatial-temporal Dynamic of Turbidity, Itaipu Reservoir, Brazil”. Publicado na Revista do Anuário do Instituto de Geociências – UFRJ, ISSN: 1982-3908.

O capítulo 4 apresenta o artigo intitulado: “Comparison of PBIA and GEOBIA Classification Methods in Classifying Turbidity in Reservoirs”. Publicado na Revista Geocarto International, ISSN: 1010-6049.

O capítulo 5 apresenta o artigo intitulado: “A timely efficient and robust multi-source and multitemporal routine for determination of surface water area in large water reservoirs”. Publicado na International Journal of Hydrology. ISSN: 2576-4454.

O capítulo 6 apresenta considerações finais.

1 INTRODUÇÃO E JUSTIFICATIVA

A água doce representa apenas 2,5% dos recursos hídricos da Terra, estando presente em diversos processos, sejam físicos, químicos e biológicos, sendo indispensável para a vida no planeta. Além disso, a qualidade de vida da população está diretamente relacionada à disponibilidade de água adequada para consumo, tornando-se uma questão de preocupação global no século 21 (SPERLING, 1996; HELLER *et al*., 2003; ALLAN, 2014; BARBOSA *et al*., 2019).

A construção de reservatórios proporciona o aproveitamento e usos múltiplos dos recursos hídricos e desempenha um papel importante no controle e na gestão, entre eles, destaca-se a geração de energia hidrelétrica, o abastecimento de água, a irrigação agrícola e a recreação (LU *et al*., 2011; YANG; CAI, 2011; WANG; XIE, 2018). Entretanto, gestores dos recursos hídricos têm enfrentado crescentes pressões devido ao aumento da população, exploração de recursos ambientais ou efeitos de mudanças climáticas, e fenômenos como a lixiviação, assoreamento, escoamento superficial, erosão do solo, descarga de resíduos e escoamento urbano, que acarretam na entrada de componentes nocivos para o corpo da água (GOMINHO, 2010; BITTENCOURT, 2014).

A carga de sedimentos suspensos tem grande influência nos parâmetros de qualidade da água, principalmente na elevação da turbidez (LIMA *et al*, 2011; SOMVANSHI *et al*., 2011; CHALOV *et al*., 2015; TRINH *et al*., 2018). Correntes de turbidez são um tipo específico de corrente de densidade de baixa concentração de sedimentos, definidas como fluxos carregados de partículas que se encontram em grande parte ou completamente suspensas, contribuindo na sedimentação de reservatórios (MEIBURG; KNELLER, 2010; TALLING *et al*., 2015; SCHLEISS *et al*., 2016).

Atualmente, a perda anual global da capacidade de armazenamento dos reservatórios é maior do que aquela criada pela construção de novos reservatórios (OEHY; SCHLEISS, 2007). A sedimentação em reservatórios representa um risco de bloqueio e operação insegura de saídas de fundo e entradas de água (SCHLEISS *et al*., 2016).

Segundo a ORGANISATION FOR ECONOMIC CO-OPERATION AND DEVELOPMENT - OECD (2012), a deterioração da qualidade da água resultante da eutrofização reduz a biodiversidade global em rios, lagos e zonas úmidas para cerca

de um terço. Neste contexto desafiador, há uma demanda crescente para melhorar o status de informações sobre a qualidade da água em nível local e global.

Assim, o monitoramento dos reservatórios a fim de subsidiar o planejamento de programas de conservação e o gerenciamento das represas é primordial (BARBOSA, 2019). O monitoramento da qualidade da água em reservatórios serve para verificar seus problemas emergentes, bem como para definir prioridades e programas para o gerenciamento da qualidade da água e avaliar as medidas a serem tomadas (ANGELINI *et al*., 2008; BUZELLI; CUNHA, 2013; MACHADO; BAPTISTA, 2016).

O monitoramento limnológico convencional e pontual de reservatórios de grande extensão torna-se muito árduo, oneroso e inviável quando se considera uma análise espaço temporal com frequência e abrangência necessária para dar conta de entender as dinâmicas atuantes nesses sistemas (BACALHAU, 2022).

Diante disso, novas ferramentas capazes de auxiliar no monitoramento de reservatórios tornam-se necessárias. As alternativas indicadas pela literatura mostram que as tecnologias relacionadas à aquisição de dados remotos, permitem extrair informações sobre a superfície a partir da reflectância ou emitância dos alvos. As características espacial, espectral, radiométrica e temporal dos sensores remotos possibilitam avaliar as diferentes interferências no corpo d'água, permitindo entender o comportamento da água e dos principais usos no seu entorno. Outro ponto a ser destacado é a possibilidade de análise a partir de diversas escalas de mapeamento e faixas espectrais viabilizando o monitoramento de grandes reservatórios (ALMEIDA, 2012; TOLENTINO, 2019).

O uso do sensoriamento remoto para estudo e monitoramento de reservatórios pode ser conduzido de forma qualitativa ou quantitativa. Entretanto, a principal demanda é pela extração de informações quantitativas de parâmetros que permitam uma descrição acurada e detalhada dos processos físicos, químicos e bio-ópticos que ocorrem no meio aquático. Dados derivados de sensoriamento remoto com foco na investigação dos componentes opticamente ativos em ambientes aquáticos são ferramentas capazes de detectar e quantificar os constituintes presentes nas águas dos reservatórios (RITCHIE *et al*., 2003; BUKATA, 2005; BARBOSA, 2019).

Métodos e modelos de análises disponíveis na literatura, podem ser aplicados universalmente, desde que os reservatórios possuem comportamentos semelhantes, sejam eles influenciados pela sua localização geográfica, sazonalidade, clima, uso e

cobertura da terra e fenômenos ao seu entorno, destacando também os constituintes pontuais e difusos resultantes de ação antrópica.

Sendo assim, a síntese de dados derivados de sensoriamento remoto para análise e monitoramento da dinâmica espaço-temporal, oferece uma oportunidade incomparável para entender a estrutura do ecossistema, possibilitando uma visão sinótica dos reservatórios integrada às suas bacias de captação, permitindo acompanhar e compreender sua dinâmica juntamente com os fatores ambientais e antrópicos que a influenciam.

Portanto, esta tese visa utilizar sensores remotos consolidados pela literatura a fim de analisar o comportamento da turbidez em reservatório. Abordar essa lacuna na literatura também oferece uma oportunidade de desenvolver técnicas econômicas, em plataformas livres e de fácil acesso que podem ser combinadas de forma sincronizada com eventos climáticos facilitando insights altamente detalhados sobre o comportamento e as características da turbidez para grandes reservatórios.

1.1 Hipótese

A partir das propriedades ópticas da água, utilizando dados exclusivamente de sensoriamento remoto e processamento digital de imagens orbitais é possível estabelecer relações entre a resposta espectral e a turbidez em reservatórios para extrair padrões e comportamentos espaço-temporais.

1.2 Objetivo Geral

O objetivo da Tese é aplicar métodos para analisar e quantificar a turbidez da água a partir da dinâmica espaço-temporal, utilizando dados ópticos de sensoriamento remoto e técnicas de processamento digital de imagens, no reservatório de Itaipu localizado na região Sul do Brasil.

1.2.1 Objetivos específicos

1) Caracterizar a dinâmica espaço-temporal com base na relação entre a turbidez, precipitação e dados de reflectância espectral para as águas do reservatório Itaipu.

2) Comparar o desempenho de algoritmos de aprendizagem de máquina para classificação de imagem supervisionada, utilizando abordagens de análise de imagem baseada em objetos geográficos (GEOBIA) e análise de imagem baseada em pixels (PBIA), para classificar padrões de turbidez nas águas do reservatório de Itaipu.

3) Empregar um banco de dados multifonte e multitemporal em grande escala para monitoramento do nível e da área de água superficial usando métricas de estimativa consolidadas baseadas em dados de sensoriamento remoto.

4) Analisar a influência de eventos climáticos extremos na dinâmica da turbidez no reservatório bem como na qualidade da água.

1.3 Localização e caracterização da área de estudo

O Reservatório da Usina Hidrelétrica de Itaipu foi adotado como área de estudo para testar as metodologias propostas para análise da turbidez por sensoriamento remoto. Esse reservatório foi formado em 1982, e está inserido na Bacia Hidrográfica do Alto Rio Paraná com área de drenagem de 950.000 km². O reservatório de Itaipu (Fig. 1) está localizado na fronteira Brasil-Paraguai. A barragem separa as cidades de Guaíra no Brasil, Salto de Guayrá no Paraguai, Foz do Iguaçu (Brasil) e Ciudad de Leste (Paraguai) (FONTANA *et al*., 2022).

A sua construção demorou oito anos e teve impactos diretos não só na economia, mas também na ecologia e na geografia da região Sternberg (2010). As florestas foram submersas para dar lugar ao gigantesco projeto, milhares de indígenas foram deslocados e vastas áreas de mata atlântica, juntamente com suas cachoeiras adjacentes, foram inundadas. As Cataratas da Guaíra, as maiores quedas d'água do mundo desapareceram sob o reservatório artificial Santos (2006). Por outro lado, a

barragem produz 90% da energia do Paraguai e 16% da energia do Brasil Rycerz *et al*. (2020), e também é considerada uma das sete maravilhas do mundo moderno pela revista American Society of Civil Engineers Cotrim *et al*. (1984), sendo a maior produtora de energia elétrica do planeta.

Gerenciada pela empresa Itaipu Binacional por se tratar de uma usina construída em conjunto pelo Brasil e Paraguai na fronteira entre os dois países, as características geográficas da região é a maior extensão horizontal do lago - 170 km alinhada na direção norte-sul, na direção leste-oeste, o lago se estende em média por 7 km. A área alagada é de 1.350 km², sendo 770 km² em território brasileiro e 580 km² em território paraguaio é o sétimo maior reservatório de água do Brasil. A profundidade média é de 22 m, chegando a 170 m nas proximidades da barragem. Os níveis de água mínimo e máximo são de 197 e 220m, respectivamente (ITAIPU BINACIONAL, 2023).

O Reservatório de Itaipu, no corpo central, apresenta características de lago monomítico quente, com um padrão de estratificação térmica acentuada nos meses de verão e uma circulação anual no inverno. Este processo é de natureza hidráulica, estando relacionado, principalmente, com a vazão do rio Paraná e com as suas diferentes características de influxo na coluna d'água do reservatório (BRUNKOW *et al*., 1988; IAT, 2017).

A estratificação térmica ocorre, não em função do aquecimento térmico de superfície, mas associada a outros fatores climatológicos, e em função do tipo e do funcionamento do reservatório, sendo denominada de "estratificação hidráulica". Este tipo de estratificação ocorre com maior frequência em reservatórios que apresentam tomadas de água a uma determinada profundidade, mas não próximo ao fundo (TUNDISI, 1983; IAT, 2017).

Com relação ao oxigênio dissolvido na coluna d'água, relatórios históricos mostram que as condições de oxigenação são consideradas boas e satisfatórias em quase todo o período, apresentando uma coluna bem oxigenada, com exceção aos meses mais quentes, onde são observadas depleções acentuadas nas camadas mais profundas. Também destaca-se que as condições hidrológicas e morfométricas deste ecossistema tais como o baixo tempo de residência das águas e a grande profundidade do reservatório, são desfavoráveis ao desenvolvimento do fitoplâncton (IAT, 2017).

Figura 1- Mapa de localização do reservatório de Itaipu.

Fonte: Autor.

A paisagem é dominada pela agricultura anual pelos cultivos de soja e milho, com menor uso e cobertura para urbano, pastagem, pesca, aquicultura e recreação aumentando o risco de erosão do solo e deposição de sedimentos no reservatório Agostinho e Julio, (2018); Fontana *et al*. (2022). Além disso, a mudança do uso da terra de floresta para cultivo aumentou a carga de sedimentos no lago (NORTON *et al*., 2001; FONTANA *et al*., 2022).

Em relação a turbidez no reservatório Pagioro (1999), relata que a maioria dos sedimentos que chegam ao reservatório de Itaipu provém da planície de inundação e de dois afluentes do Paraná, Ivinheima e Ivaí, que drenam através da agricultura e da

pecuária até a planície de inundação de 230 km a montante. Outra característica é a diminuição exponencial bem definida nas taxas de sedimento em suspensão, da porção montante do reservatório até a região jusante próxima da barragem (PAGIORO; THOMAZ, 2002).

Andrade *et al*. (1988), caracterizam o comportamento da turbidez semelhante nas zonas ribeirinha, de transição e lacustre, embora apresentem valores médios decrescentes na direção montante-jusante. Stevaux (1993); Souza Filho e Stevaux (1997); ressaltam que a descarga de sedimentos do rio Paraná é de em torno 30 milhões de toneladas por ano, das quais apenas 10% se referem à carga de material do leito. A carga de material suspenso varia de acordo com os picos de inundação (precipitação).

Na bacia hidrográfica do Paraná, a sedimentação é em grande parte causada por práticas inadequadas de manejo da terra, que causam exposição e erosão do solo. O desmatamento pode aumentar drasticamente os sedimentos que se movem para os rios, e entram no reservatório Rycerz *et al*. (2020). A sedimentação e o fluxo variável do rio, juntamente com os padrões variáveis de precipitação impulsionados pelas mudanças climáticas, reduzem o abastecimento geral de água e a qualidade disponível para a produção de energia hidrelétrica (RYCERZ *et al*., 2020).

2 REFERENCIAL TEÓRICO

2.1 Reservatórios de abastecimento de água

Barragens são construídas desde o início das civilizações humanas, e a pelo menos 5 mil anos são construídos reservatórios represados, que aumentaram de número e de tamanho drasticamente ao longo do último século (WETZEL, 2001; MAYS, 2008; ZARFL *et al*., 2015).

Um reservatório de abastecimento de água é uma estrutura artificial construída para conter água. Estima-se que existam cerca de 16,7 milhões de reservatórios em todo o mundo, armazenando um volume equivalente a 10% em relação aos reservatórios e lagos naturais (LEHNER *et al*., 2011).

Entre as principais finalidades da construção de reservatórios estão a geração de energia elétrica, o abastecimento de água potável, irrigação, navegação, controle das cheias, entre outras. Além de ser uma fonte barata e confiável de energia renovável, a energia hidrelétrica desempenha um papel fundamental na transição para economias de baixo carbono (AGOSTINHO *et al*., 2007; TUNDISI, 2008; EDENHOFER *et al*., 2011).

Os reservatórios forneceram 16,8% da geração global de energia elétrica por meio de hidrelétricas REN21 (2021). A rápida multiplicação de reservatórios em todo o mundo tem oferecido muitas oportunidades socioeconômicas.

Quando comparando diferentes sistemas de geração de energia, estimaram que a liberação de gases de efeito estufa da geração de energia hidrelétrica é uma a duas ordens de magnitude menor que a eletricidade gerada a partir de combustíveis fósseis (TURCONI *et al*., 2013).

A crescente demanda por energia, água e proteção contra inundações exerce pressão crescente sobre governos e organizações para construir novas barragens (ZARFL *et al*., 2015), no entanto, há também um crescente reconhecimento de seus impactos sociais e ambientais (BARBAROSSA *et al*., 2020).

No Brasil, nas décadas de 60 e 70 foram construídos grandes empreendimentos hidráulicos, principalmente para fins de produção de hidroeletricidade e abastecimento humano (TUNDISI, 2008; NOGUEIRA *et al*., 2015). O crescimento populacional e econômico do país, resultou no aumento da demanda energética, doméstica e industrial, nas últimas décadas, levando à exploração do

potencial hidrelétrico no país localizados em regiões com relevo acidentado (AGOSTINHO *et al*., 2007; TUNDISI, 2008).

Existem atualmente 174.526 reservatórios de usinas hidrelétricas (UHEs) artificiais no Brasil. A geração de energia elétrica é um dos principais usos dos recursos hídricos. Destacam-se os dez reservatórios brasileiro de maior área (km²): Sobradinho (BA) 4214 km²; Tucuruí (PA) 2430 km²; Balbina (AM) 2360 km²; Porto Primavera (SP/MS) 2140 km²; Serra da Mesa (GO/TO) 1784 km²; Itaipu (PR) 1350 km²; Furnas (MG) 1340 km²; Ilha Solteira (SP/MG) 1260 km²; Três Marias (MG) 1142 km²; Peixe (GO) 940 km² (SPERLING, 1996; SILVA, 2014).

2.2 Impactos em reservatórios de geração de energia

Na implantação de uma usina hidrelétrica a formação do seu reservatório normalmente modifica as condições naturais do curso d'água. As barragens geram redução na velocidade da corrente provocando a deposição gradual dos sedimentos carregados pelo curso d'água, ocasionando assoreamento. As partículas mais densas depositam-se primeiro, como cascalho e pedregulhos, posteriormente as areias, siltes e argilas (que normalmente mantêm-se em suspensão), podendo inviabilizar a operação de seu aproveitamento, diminuindo gradativamente a capacidade de armazenamento do reservatório (CARVALHO *et al*., 2000; CARVALHO, 2008; DAVRANCHE *et al*, 2010; SOMVANSHI *et al*., 2011; CUNHA *et al*., 2013; CHALOV *et al*., 2015; TRINH *et al*., 2018).

Fenômenos como a lixiviação, escoamento superficial, erosão do solo, descarga de resíduos e escoamento urbano, acarretam na entrada de sedimentos nos reservatórios. Os sedimentos são componentes opticamente ativos que afetam a qualidade das águas dos reservatórios resultando na diminuição da transparência (DAVRANCHE, 2010; SOMVANSHI *et al*., 2011; CUNHA *et al*., 2013; CHALOV *et al*., 2015; TRINH *et al*., 2018).

Os reservatórios apresentam características de ambientes lóticos e lênticos. Próximo do barramento, são parecidos com lagos e sujeitos à mesma ação dos ventos, correntes de densidade e estratificação, e a sua circulação geral é causada pelas entradas e saídas de água advindas dos cursos d'água afluentes (CARDOSO *et al*., 2013; SANTOS *et al*., 2014; BARBOSA, 2019).

Sistemas lênticos são os mais favoráveis a eutrofização que corresponde a elevada proliferação de algas. Essa proliferação é diretamente relacionada com o

aumento populacional e a industrialização em decorrência do aporte de nutrientes trazido pelo esgoto e a poluição difusa, decorrente da fertilização artificial de solos, constituindo as principais causas do aumento da concentração de nutrientes em reservatórios (LIMBERGER, 2011; BATISTA *et al*., 2014).

Devido aos problemas causados pelos sedimentos suspensos e turbidez em sistemas aquáticos, é necessário monitorar sua dinâmica a partir de seu comportamento espaço-temporal. Porém, a maioria dos reservatórios brasileiros e mundiais carece de informações sobre parâmetros limnológicos, devido à falta de medições ou a sua indisponibilidade. Em muitos casos, o monitoramento contínuo dos reservatórios é inviável, visto que estão localizados em regiões remotas ou de difícil acesso (ALSDORF, 2007; ZHANG, 2014; BARBOSA, 2019).

2.3 Turbidez em reservatórios

A turbidez é uma variável limnológica, a partir do qual é possível quantificar a redução da transferência da água e a interferência na passagem da luz na água. Em reservatório, por exemplo, as características da água turva podem ser atribuídas às chuvas de alta intensidade que favorecem a erosão do solo na bacia e o uso excessivo e extensivo de suas terras para atividade agrícola (RUDKE, 2018). Em síntese, quanto maior a quantidade de sedimentos em suspensão, maior é a turbidez (SOMVANSHI *et al*., 2011).

A turbidez além das consequências ambientais e ecológicas nos sistemas fluviais, representa uma ameaça econômica, ao facilitar o assoreamento do reservatório. Isso torna sua medição e monitoramento um exercício valioso. Os métodos tradicionais usados para determinar a turbidez, como medições in situ e análises de laboratório, desempenham um papel significativo no monitoramento da qualidade da água. No entanto, essas técnicas são demoradas, caras e trabalhosas (HE *et al*., 2008; LIU *et al*., 2003; SHAFIQUE *et al*., 2003; SU *et al*., 2008; YANG; JIN, 2010). O uso dessas técnicas é importante e necessário para uma escala temporal e espacial mais ampla, porém continua sendo um desafio (BIERMAN *et al*., 2011).

Comumente, a turbidez é derivada de partículas suspensas de lodo e argila, algas, bolhas de ar, matéria orgânica junto com organismo microscópico em corpos d'água. Esses fatores afetam cor e brilho da água, conferindo-lhe a típica cor turva (RAMOLLO, 2008; OMAR; MATJAFRI, 2009). Geralmente, a turbidez é uma medida

das propriedades ópticas aparentes e inerentes da água responsáveis pela dispersão e absorção da radiação (KOPONEN, 2006; HASMADI; NORSALIZA, 2010). Descreve a redução da transparência de um líquido após a presença de matéria não dissolvida (LAMBROU *et al*., 2010). Alguns autores se referem a ela como a medida de clareza da água (LAMBROU *et al*., 2010; HASMADI; NORSALIZA, 2010).

Partículas suspensas orgânicas absorvem mais luz solar, a temperatura da água é aumentada, levando a uma maior depleção de oxigênio dissolvido como a água morna retém menos oxigênio do que a água fria (RAMOLLO, 2008). A turbidez atua como um indicador da presença de patógenos, fornecendo-lhes alimento e abrigo (LAMBROU *et al*., 2010). Isso pode promover o crescimento do patógeno, consequentemente facilitando surtos de doenças transmitidas pela água (LAMBROU *et al*., 2010). A turbidez também pode levar à perda da capacidade de armazenamento das barragens devido à sedimentação, encurtando sua vida útil (BHATTI, 2007). Consequentemente, a determinação da turbidez da água é crítica para a gestão da qualidade da água.

Duas categorias principais de instrumentos são atualmente reconhecidas em instrumentos de turbidez; os turbidímetros (ou absorciômetros) e os nefelômetros (OMAR & MATJAFRI, 2009; LAMBROU *et al*., 2010). Os turbidímetros medem a absorção da intensidade da luz passando por uma amostra em relação ao feixe inicial (LAMBROU *et al*., 2010; MINELLA *et al*., 2008). São considerados os mais apropriados para amostras com partículas maiores que o comprimento de onda da luz que está sendo usada (LAMBROU *et al*., 2010).

Os nefelômetros, quantificam a porção de luz espalhada pelo feixe incidente dentro de um grande ângulo centrado em 90º, relatado em unidades nefelométricas (NTUs) (LAMBROU *et al*., 2010; OMAR; MATJAFRI, 2009; PENG *et al*., 2009). Nefelômetros são instrumentos mais modernos e internacionalmente reconhecidos, e considerados mais precisos e sensíveis que os turbidímetros, principalmente quando se trata de amostras de baixa turbidez (OMAR; MATJAFRI, 2009).

Embora esses métodos tenham sido críticos no monitoramento da turbidez, eles requerem calibração intensa, amostragem elaborada e análises laboratoriais além de serem lentos, demorados, caros e trabalhosos (KOPONEN, 2006; HE *et al*., 2008). Além disso, essas técnicas não fornecem resultados em tempo real (RAMOLLO, 2008). No entanto, os recentes avanços do sensoriamento remoto

oferecem uma grande oportunidade para (medição ou identificação) de turbidez e uma base para a gestão da qualidade da água.

2.4 Propriedades ópticas da água

O comportamento espectral das águas dos reservatórios está relacionado as substâncias presentes que interagem com radiação solar e, portanto, são responsáveis pelos processos de absorção e de espalhamento da luz, e são denominadas de componentes opticamente ativos (COAs). Esses componentes são substâncias em suspensão que provocam alterações na cor da água pura.

Existem três grandes grupos de componentes opticamente ativos: Matéria inorgânica e orgânica em suspensão, quando não se dissolvem completamente no meio aquático, como a areia, argila, micoorganismos, denominam-se (sedimentos suspensos); Componentes orgânicos dissolvidos no meio aquático, como plantas, animais autóctone e alóctone, classificados como (matéria orgânica dissolvida); E organismos fotossitetizantes como bactérias, algas e plantas fotossintetizantes conhecidas como (clorofila-a) (DE MORAES NOVO, 2010; KIRK, 2010; BARBOSA *et al*., 2019).

Dados de sensoriamento remoto, tanto a nível orbital quanto de campo, para o monitoramento dos aspectos ópticos da água, podem ser utilizados em experimentos para obter medidas da energia refletida, em diferentes faixas de comprimento de onda do espectro eletromagnético, para identificar COAs nos corpos d'água (RUDORFF *et al*, 2006). Diversos pesquisadores buscaram identificar e caracterizar diferentes COAs na água (MANTOVANI e NOVO, 1996; DIAS *et al*., 2007; FERREIRA e PEREIRA FILHO, 2009; TRENTIN, 2009; LOPES *et al*., 2014; BONANSEA *et al*., 2019).

As características de absorção e dispersão da água são determinadas pelas propriedades ópticas inerentes (POIs). A absorção refere-se à transferência de energia luminosa para outra forma de energia (por exemplo, calor) e é quantificada pelo coeficiente de absorção espectral, a (λ) (m-1), que é a fração da luz incidente absorvida dividida pela espessura da camada. A dispersão é definida como a deflexão dos fótons de luz de seu caminho original e pode ser quantificada pelo coeficiente de dispersão espectral b (λ) (m-1), que é a fração da luz incidente que é espalhado, dividido pela espessura da camada (KIRK, 2010).

As propriedades ópticas aparentes (POAs) são determinadas pelos efeitos combinados da estrutura geométrica do campo de luz e constituintes de água (KIRK, 2010). São, portanto, parcialmente determinados pelo ângulo solar e condições atmosféricas locais (BUKATA *et al*., 1995). O coeficiente de atenuação vertical subaquática, a profundidade de Secchi, a reflectância e a irradiância são considerados POA (MOBLEY, 1995).

Em contraste, as propriedades ópticas inerentes (POIs) são afetadas apenas pelo meio aquático e radiativas. A teoria da transferência radiativa descreve a conexão de POIs e POAs (MOBLEY, 1995). Os componentes da água responsáveis por suas propriedades ópticas inerentes são: o material orgânico e inorgânico dissolvido, particulado e em suspensão, material fitoplanctônico e as macrófitas aquáticas. Estes componentes atuam como agentes espalhadores e absorvedores de radiação, influenciando na transmissão da radiação eletromagnética através da coluna d'água e, consequentemente, na produtividade primária.

Água pura se refere à água sem qualquer constituinte, ou seja, livre de matéria orgânica e inorgânica. Os fenômenos de absorção e espalhamento são decorrentes das próprias moléculas d'água (BUKATA *et al*., 1995; DE MORAES NOVO, 2010; BARBOSA, 2019).

A absorção da luz pelas moléculas de água ocorre de forma seletiva (Figura 2) passando a ser muito significativa apenas a partir de 550 nm, com altos valores de absorção no fim do espectro da região do vermelho e do infravermelho-próximo, onde estão as bandas de absorção devido ao estado de vibração fundamental das moléculas de água. Acima de 750 nm, grande parte da radiação incidente é absorvida no primeiro centímetro da coluna de água e convertida em calor (BARBOSA, 2019). O máximo espalhamento da luz pelo corpo d´água limpa se dá na região do azul. De forma geral o espalhamento pela água caracteriza-se por uma redução exponencial do espalhamento em direção a comprimentos de ondas mais longos.

A partir de medidas provenientes de instrumentos de sensoriamento remoto podem ser realizados estudos da inferência de variáveis relacionadas à qualidade da água, de acordo com a análise das feições espectrais da radiação solar refletida pelo volume do corpo da água (LONDE *et al*., 2006; BOWERS *et al*., 2007).

Figura 2 - Curvas de: a) absorção (linha sólida), e b) espalhamento (linha pontilhada) da água pura determinadas em laboratório. Fonte: Smith e Baker (1981).

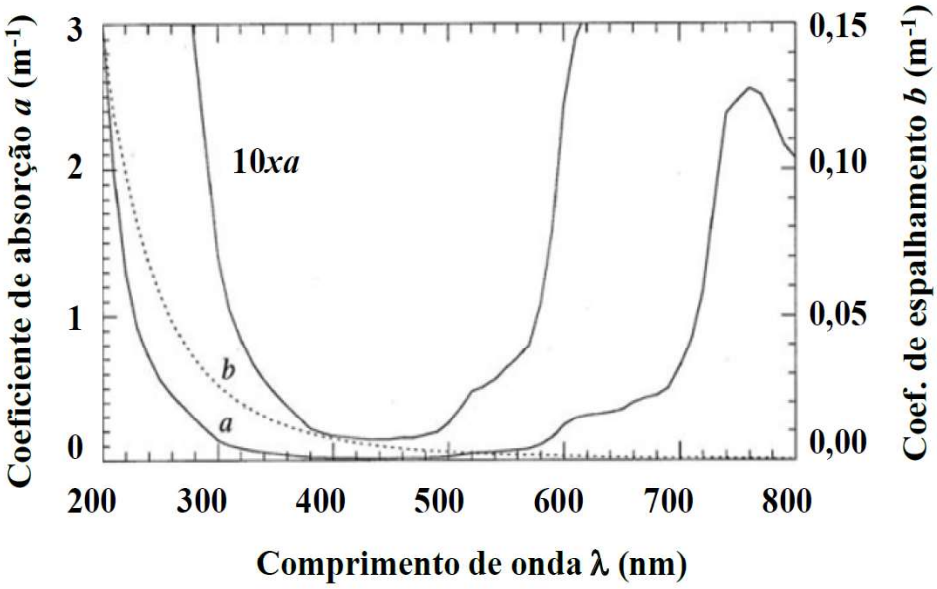

Fonte: Smith e Baker (1981).

Muitos corpos de água naturais contém uma variedade de constituintes orgânicos como a clorofila-a do fitoplâncton e constituintes inorgânicos como minerais em suspensão. Quando esses elementos estão misturados à água pura, é mais difícil em sensoriamento remoto discriminá-los, devido à mútua influência dos mesmos na resposta espectral Jensen e Epiphanio (2009). No entanto, quanto menor a concentração dos COAs na água, mais baixa é sua reflectância, mesmo se tratando da região do visível do espectro eletromagnético, devido ao baixo coeficiente de espalhamento e alta transmitância da água (ROSA, 2009).

O comportamento espectral dos constituintes opticamente ativo (Figura 3) pode estar presentes em uma massa d'água, entre eles sedimentos em suspensão, clorofila (fitoplâncton) e matéria orgânica dissolvida, abordados na sequência deste trabalho.

A concentração de sedimentos em suspensão é o parâmetro de qualidade de água que afeta com maior intensidade o comportamento óptico das águas dos reservatórios. Os sedimentos em suspensão são originários de diversas fontes, incluindo erosão de áreas agrícolas, intemperismo de terrenos montanhosos, erosões costeiras e outros. A erosão do solo na bacia hidrográfica, por exemplo, lança cargas de sedimentos nos corpos d'água, resultando no assoreamento mais rápido dos principais rios e reservatórios, além de afetar a qualidade da água e suas adequações para o consumo humano (JENSEN, 2009).

Figura 3 - Padrão espectral da água e os constituintes opticamente ativos em imagens do sensor hiperespectral Hyperion/EO-1 na região Amazônica.

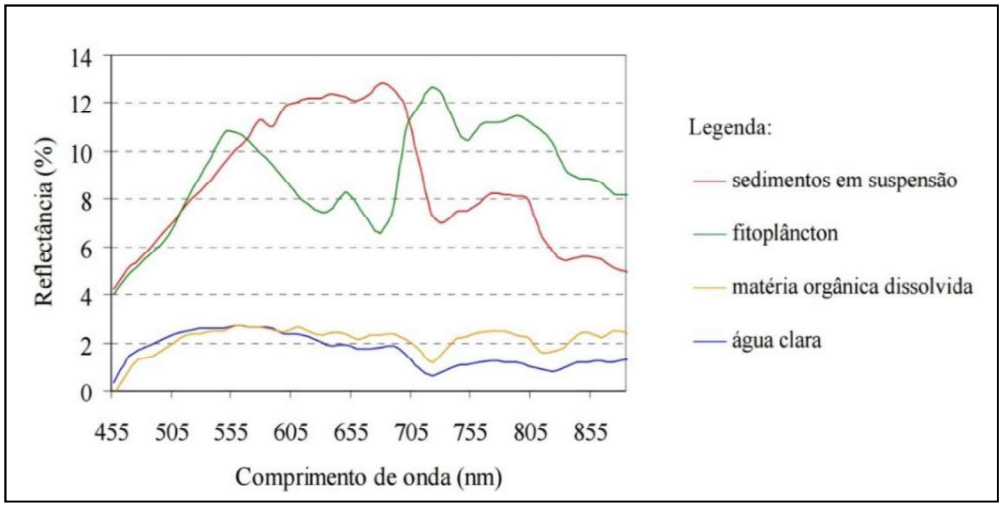

Fonte: Adaptado de Rudorff *et al* (2006).

Os sedimentos em suspensão incluem areia, lodo, argila e outros materiais inorgânicos, bem como matéria orgânica não viva (KOPONEN, 2006). As propriedades ópticas são afetadas pela forma e tamanho da distribuição das partículas, que têm um efeito principal em suas propriedades de absorção e espalhamento (BUKATA *et al*., 1995). Na água limpa, concentrações crescentes de tripton resultam em um aumento linear da reflectância no IR. Nesta área do espectro eletromagnético, o efeito da clorofila-a é desprezível (HAN; RUNDQUIST 1997).

Jensen (2009) descreve a variação espectral da água limpa e da água com diferentes concentrações de sedimentos em suspensão (Figura 4) de solos argilosos e siltosos. Observa-se que a reflectância espectral da água clara sofre um decréscimo após 580 nm, devido à absorção da radiação eletromagnética (REM) pelo corpo d'água. Quando a concentração de sedimentos aumenta, a porcentagem de reflectância também aumenta ao longo de todo o espectro, tanto para argila como para silte, definindo um padrão mais claro nos espectros de reflectância proporcional ao grau de sedimentos suspensos no corpo d'água (DE MORAES RUDORFF *et al.* 2006; JENSEN, 2009).

Com o aumento da concentração de sedimentos em suspensão e consequentemente da turbidez da água, além do aumento geral da reflectância, ocorre a modificação da forma do espectro de reflectância. Porém, a radiação que

sofre espalhamento devido à concentração de sedimentos não tem um comportamento constante e varia em função dos tamanhos das partículas e do material de origem, o que torna difícil a formulação de um algoritmo geral para os sedimentos em suspensão (NOBREGA *et al*. 2002).

Figura 4 - Medida de reflectância espectral da água com vários níveis de concentração de sedimentos em suspensão do tipo argiloso (a), e siltoso (b).

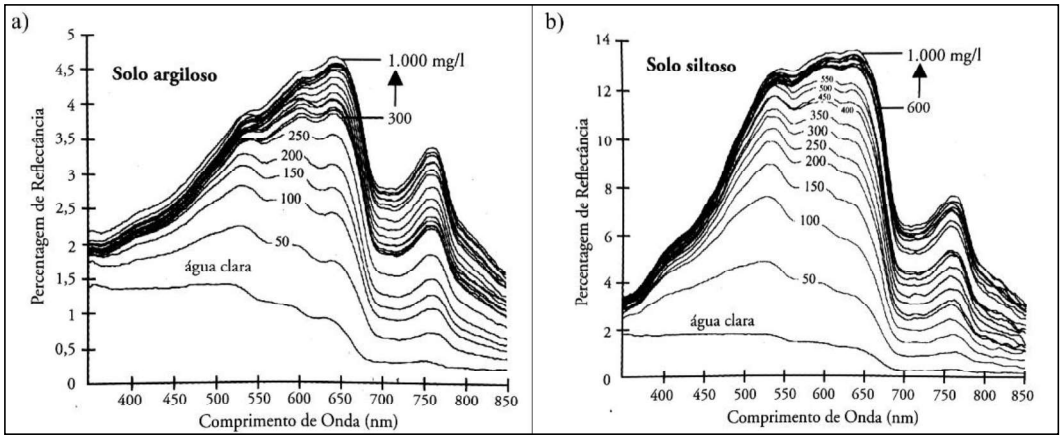

Fonte: Jensen (2009).

A concentração de sedimentos em suspensão e a reflectância da água são aplicadas em dados de sensoriamento remoto para estimar a distribuição espacial de concentração de sedimentos sobre águas costeiras e continentais, como reservatórios, lagos e grandes rios.

Jensen (2009) destaca que nos comprimentos de onda do visível entre 580 e 690 nm, a resposta espectral fornece informações sobre o tipo de sedimentos em suspensão na superfície da água, enquanto o infravermelho próximo (714 a 880 nm) é utilizado para determinar a quantidade de sedimentos na superfície da água. No entanto, essas relações não são sempre aplicadas, pois cada tipo de sedimento deve ser investigado para obter suas características espectrais de absorção e espalhamento, quando em meio aquático.

O fitoplâncton é caracterizado pelas comunidades de vegetais microscópicas que vivem nos ambientes aquáticos, responsável pela produção primária (LAMPERT *et al*., 1986; GHOSAL *et al*., 2000). Esses organismos contêm moléculas que captam e transformam a energia, denominados pigmentos fotossintetizantes, sendo eles as clorofilas (principalmente a), os carotenóides e ficobiliproteínas ou ficobilinas. A água

repleta de algas exibe um pico de reflectância na região do verde, e outro pico de reflectância na região do infravermelho próximo (WETZEL, 2001; JENSEN, 2009).

A matéria orgânica dissolvida na d'água constitui-se de substâncias provenientes da decomposição de organismos terrestres e aquáticos Chen *et al*., (2004). As concentrações dependem da origem, das condições físicas do meio aquático, da bacia de drenagem e dos organismos decompositores (WETZEL, 2001). O espectro de absorção da matéria orgânica dissolvida aumenta exponencialmente em comprimentos de onda mais curtos do espectro visível e há pouca absorção acima de 700 nm (BRICAUD *et al*., 2010).

2.5 Sensoriamento remoto em reservatórios

O sensoriamento remoto nos estudos de reservatórios é uma ferramenta que fornece uma investigação muito mais completa do que métodos tradicionais de amostragem pontual, oferecendo uma visão abrangente e contínua das condições e mudanças em diversas escalas espaciais e temporais desses ambientes, auxiliando na gestão e no monitoramento de informações.

Estudos temporais de grandes reservatórios, entre eles monitoramento da água superficial derivado de imagens ópticas e imagens de elevação topográfica (LI *et al*., 2013); séries temporais de alta resolução temporal e espacial (MISHRA *et al*., 2020), incluindo combinação de limiares em imagens espectrais (LU *et al*., 2011; DU *et al*., 2016), também com índices espectrais como o MNDWI (XU, 2006); NDWI (McFEETERS, 1996); para proliferação de pequenos reservatórios (ARVOR *et al*., 2018); no monitoramento da área superficial (SEATON *et al*., 2020; LING *et al*., 2020a), no mapeamento global de massas da água Landsat (YAMAZAKI *et al*., 2015). No monitoramento da área da superfície, altura da superfície e volume de lagos e reservatórios em escalas regionais e globais (SONG *et al*., 2014; CRÉTAUX *et al*., 2016; YAO *et al*., 2019; CHEN, 2021). Também na dinâmica de lagos e reservatórios em escala de bacia hidrográfica (ZHANG *et al*., 2017; WANG *et al*., 2018; LING *et al*., 2020b; ZHU *et al*., 2020).

Os métodos de sensoriamento remoto passivos envolvem a detecção da luz que é naturalmente emitida ou refletida pelo corpo d'água. Isso inclui sensores óptico e térmicos, que é a detecção da luz ambiente nas porções visíveis e infravermelho do espectro, respectivamente. O sensoriamento remoto óptico passivo pode ser usado

para adquirir parâmetros biogeoquímicos indicativos da qualidade da água, incluindo, turbidez, fitoplâncton, matéria total em suspensão e matéria orgânica dissolvida colorida. Entre os sensores passivos para análise de reservatórios destacam-se MultiSpectral Instrument MSI do Sentinel 2 e Operational Land Imager OLI do Landsat 8.

O sensor MSI do Sentinel 2 de 10 m de resolução espacial, tem sido utilizado em diversas aplicações devido à sua capacidade de capturar imagens de alta qualidade e detalhadas da Terra. Algumas das aplicações comuns do sensor MSI incluem: Monitoramento da eutrofização estimando as concentrações de clorofila-a (LI *et al*., 2023); Monitoramento para análise do volume perdido em reservatório em decorrência da sedimentação, perda de 28% em 92 anos (JAGANNATHAN e KRISHNAVENI, 2021); Algoritmos de aprendizado de máquina para estimativas remotas do conteúdo de Clorofila-a (NGUYEN *et al*., 2021); Estimativa da parte orgânica e inorgânica dos sedimentos suspensos em diferentes águas interiores (ALVADO *et al*., 2021).

O sensor multiespectral OLI do Landsat 8 de 30 m de resolução espacial, muito utilizado em estudos de monitoramento de corpos d'água, foi utilizado para averiguar a distribuição de matéria suspensa total na água de reservatório na China (CAO *et al*., 2021); Detecção e extração da superfície da água na Índia (KULKARNI *et al*., 2022).

Trabalhos combinando os dois sensores para estimativa da transparência da água (CUI *et al*., 2022), analise multi-sensor com o MSI, OLI e veículo aéreo não tripulado (VANT) gerando dados de 30m, 10m e 8cm da qualidade da água em reservatório (CILLERO *et al*., 2020); Investigação de bloons algaes em lagos urbanos (ALCANTRA *et al*., 2021); Geração de modelo de estimativa para sedimentos suspensos as razões de banda espectral resultaram, banda 5/banda 4 do OLI (R^2 = 0,58; RMSE = 7,7) e a banda MSI 8/banda 4 (R^2 = 0,73; RMSE = 6,1) (HA *et al*., 2022).

Os sensores ópticos são facilmente obstruídos por nuvens e de noite não geram imagem da superfície, limitando assim as aplicações de monitoramento. Métodos ativos operam de dia e de noite e permitem obter informações em todas as condições meteorológicas, enviam um sinal conhecido do sensor para a água e o sinal de retorno é detectado e quantificado com base no atraso de tempo e na velocidade conhecida da luz. As imagens Sentinel-1 SAR podem fornecer visualizações desobstruídas e densas do monitoramento da dinâmica da superfície da água devido à sua capacidade de penetração nas nuvens (BIORESITA *et al*., 2018; MARKERT *et*

al., 2020). Com propriedades de detecção de umidade e rugosidade da superfície, possui capacidade de obter imagens tanto diurnas quanto noturnas, com resolução espacial de 5 m. Estudos anteriores têm demonstrado o potencial das imagens Sentinel-1 SAR para delinear a extensão da água e para detectar e mapear os eventos de inundação (BIORESITA *et al*., 2018). Barasa e Wanyama, (2020) usaram dados Sentinel-1 SAR para monitorar a área de inundação de lagos de água doce. Além disso, as imagens Sentinel-1 SAR foram usadas para delinear a água da enchente nos EUA (LIANG e LIU, 2020). Essas pesquisas ilustram o potencial das imagens Sentinel-1 SAR para o monitoramento e a detecção de eventos de inundação em diversas regiões, fornecendo informações valiosas para os tomadores de decisão e ajudando na mitigação dos impactos desses eventos naturais.

A altimetria por satélite tem sido bastante utilizada em estudos de sensoriamento remoto, o sensor radar altimétrico Jason-3, por exemplo, mede a altura instantânea do mar e de grandes reservatórios. A onda de radar emitida pelo satélite reflete na superfície da água do reservatório e é captada pelo satélite que mede e analisa o tempo de ida e volta e a forma que a onda é recebida, permitindo, respectivamente, determinar a distância entre o satélite e a superfície do reservatório. Tortini *et al*. (2020) utilizaram conjunto de dados de vários altímetros incluindo Jason-3 em diversos lagos e reservatórios para geração da série temporal de águas superficiais a nível global; O estudo de Pham-Duc *et al*. (2022) destacou o monitoramento da variação de volume e área superficial de um lago por meio da combinação dos dados dos sensores Sentinel-1 e Sentinel-2. Esses sensores, respectivamente SAR e óptico, fornecem informações complementares sobre as mudanças no lago, permitindo uma análise mais completa das variações de volume e área. Além disso, o estudo de Biswas *et al*. (2019) focou na extração da altura dos rios no sudeste da Ásia. Essa pesquisa utilizou altimetria para medir as alturas dos rios, permitindo o monitoramento da dinâmica fluvial e a avaliação de possíveis riscos associados a inundações e enchentes na região.

O Tropical Rainfall Measuring Mission (TRMM) usa vários sensores ativos e passivos para detectar chuvas, incluindo radar, imagens de micro-ondas que oferecem imagens para acompanhamento, previsão e análise de precipitação. O sensor TMI fornece informações sobre o conteúdo de precipitação da coluna integrada, água líquida da nuvem, gelo da nuvem, intensidade da chuva e tipos de chuva. Martins *et al*. (2019) utilizaram TRMM e dados de turbidez. Dados de

precipitação e imagens sentinel-1 foram utilizados para análise de deslizamentos de terra induzidos na área da borda do Reservatório da Barragem de Bagliha na Índia (MISHRA *et al*., 2022; M OTHMAN *et al*., 2021). Usaram o modelo digital de elevação da Shuttle Radar Topography Mission (SRTM), precipitação do TRMM, e imagens Landsat para estimar a perda anual de solo onde várias barragens estão planejadas e onde faltam estudos básicos sobre erosão do solo na Índia.

Climate Hazards Group InfraRed Precipitation with Station data CHIRPS é outro sensor que estima a precipitação. Yudianto *et al*. (2021) utilizaram o CHIRPS e o TRMM para mapeamento de risco de quebra de barragem em uma região de difícil acesso e com dados limitados na Indonésia.

2.6 Turbidez da água por sensoriamento remoto

O sensoriamento remoto pode auxiliar no entendimento da complexidade dos ecossistemas aquáticos. Em estudos sobre a variação espacial e temporal da qualidade da água é possível a identificação de substâncias específicas em suspensão ou dissolvidas na água (DE MORAES RUDORFF, 2006).

Nas últimas quatro décadas, previsões quantitativas de turbidez e outros parâmetros de transparência da água foram realizadas com sucesso usando satélites espaciais em ambientes lacustres, estuarinos e reservatórios (DÖRNHÖFER e OPPELT, 2016; DÖRNHÖFER *et al*., 2016; CHU *et al*., 2018; RUDORFF *et al*., 2018; LIU *et al*., 2019).

Satélites Landsat 5 e 8 e Sentinel-2 são comumente usados para obter relações de sensoriamento remoto com turbidez (WANG *et al*., 2006; LOBO *et al*., 2015; RUDORFF *et al*., 2018; SURISETTY *et al*., 2018; LIU *et al*., 2019; KUHN *et al*., 2019; GARG *et al*., 2020). Bandas espectrais de comprimentos de onda vermelho e NIR são utilizadas com mais frequência independentemente ou combinadas com outras bandas para desenvolver essas relações (LACAUX *et al*., 2007; LOBO *et al*., 2015; SURISETTY *et al*., 2018; LIU *et al*., 2019; KUHN *et al*., 2019; GARG *et al*., 2020). Os comprimentos de onda da banda verde têm sido utilizados em bandas múltiplas para análise de turbidez (SURISETTY *et al*., 2018; GARG *et al*., 2020).

Análises de regressão com algoritmos de banda única ou multibanda são métodos comuns para avaliar a correlação entre reflectância espectral e medições de turbidez in situ (WANG *et al*., 2006; AL-FAHDAWI *et al*., 2015; LOBO *et al*., 2015).

Esses métodos são simples, eficientes e baratos para prever parâmetros de qualidade da água com cobertura espacial quase contínua.

Estudos qualitativos também são comuns para a previsão de turbidez quando há poucos ou nenhum dado in situ disponível (LACAUX *et al*., 2007; GARG *et al*., 2020). Essas previsões qualitativas podem ser úteis para avaliação geral das condições da qualidade da água quando não são necessárias previsões quantitativas.

Lacaux *et al*. (2007) e Garg *et al*. (2020) utilizaram o Índice de Turbidez por Diferença Normalizada (NDTI) a partir dos valores de reflectância da banda verde e vermelha em substituição a medições in situ com sucesso.

Para Barbosa *et al*. (2019) abordagens por meio das quais dados espectrais de sensoriamento remoto (in situ ou orbital), adquiridos sobre corpos d'água, podem ser utilizados para estimar as concentrações de COAs:

> i) Empírica: que se baseia no desenvolvimento de regressões estatísticas bi ou multivariadas entre medidas concomitantes de Rrs (λ) e de concentrações dos COAs. Quando feições espectrais diagnósticas dos COAs são conhecidas e incluídas nas análises de regressão. Métodos empíricos utilizam técnicas estatísticas para se relacionar diretamente em amostras in situ aos dados de satélite adquiridos simultaneamente. Esses modelos oferecem uma abordagem mais simples, mas têm aplicabilidade espaço-temporal limitada (BARBOSA *et al*., 2019 p.142);
>
> ii) Analítica: fundamenta-se em relações diretas e inversas entre os componentes opticamente ativos as propriedades ópticas inerentes e as propriedades ópticas aparentes por meio de soluções da Equação de Transferência Radiativa. Os métodos analíticos são baseados em modelos bio-ópticos que usam modelagem de transferência radiativa ou simplificações de radiativos modelos de transferência. Modelos bio-ópticos podem ser desenvolvidos independentemente de dados in situ, no entanto, eles requerem conhecimento, ou suposições sobre propriedades ópticas inerentes (BARBOSA *et al*., 2019 p.142).

A aplicabilidade espaço-temporal dos modelos empíricos e analíticos depende da variação das propriedades ópticas inerentes da água, e como estas afetam a água qualidade do parâmetro de interesse.

Diversos artigos utilizaram o índice NDTI, Elhag *et al*. (2019a) Elhag *et al*. (2019b) analisaram diversos parâmetros de qualidade da água em ambientes áridos

na Arábia Saudita, as medições in situ de turbidez da água com alta correlação com os valores de NDTI com R^2 0,94.

Bid *et al*. (2019) analisaram a relação entre o NDTI e concentrações de sedimentos suspensos em reservatório da Índia com R^2 0,90. Mansourmoghaddam *et al*. (2022) utilizaram NDTI e outros índices para avaliar os efeitos da construção da Ilha Palm Jumeirah, nas ilhas do Golfo Pérsico ao redor de Dubai por 19 anos, e constataram um aumento dos valores de NDTI com o passar do tempo, e uma queda de NDTI em 2020 em relação a 2019, atribuindo a diminuição a redução de 63 a 82% no número de turistas em Dubai em 2020 como resultado da pandemia de COVID-19.

Li *et al*. (2023) avaliaram a dinâmica da qualidade da água do lago Chao na China por 30 anos utilizando imagens Landsat 5, 7 e 8, os resultados obtidos indicaram um aumento de sedimentos suspensos, turbidez e na temperatura da superfície da água, com correlações com NDTI próximas a 1.

Ma *et al*. (2020) utilizaram algoritmos de aprendizado de máquina e modelo de regressão para prever turbidez usando sensoriamento remoto. Dentre os diversos algoritmos testados, árvore de decisão de aumento de gradiente (GBDT) e floresta aleatória (RF) produziram valores de R^2 de 0,88 e 0,86, respectivamente.

2.7 Plataforma Google Earth Engine (GEE)

A ferramenta Google Earth Engine - GEE (https://earthengine.google.com/) tem como principal recurso a combinação de um catálogo de múltiplos petabytes de imagens de satélite e conjuntos de dados geoespaciais com recursos de análise em escala planetária (GORELICK *et al*., 2017). O GEE reduz significativamente o tempo necessário para adquirir e processar os dados conforme comparado aos métodos convencionais, fornecendo análise de dados quase em tempo real através de uma interface web simples, sem a necessidade de softwares caros ou outro recurso intensivo soluções (MARKERT *et al*., 2018).

A possibilidade de desenvolvimento de diferentes algoritmos utilizando a ferramenta “code editor” proporciona acesso instantâneo aos dados. Além de um ambiente de desenvolvimento integrado online para prototipagem rápida e visualização de análises espaciais complexas usando a API de JavaScript.

Ao utilizar os recursos do GEE, os usuários podem analisar e visualizar padrões de turbidez em corpos d'água, monitorar mudanças ao longo do tempo e estudar os

impactos do uso da terra, clima ou atividades humanas na qualidade da água. Esta informação é crucial para várias aplicações, incluindo monitoramento ambiental, gestão de recursos hídricos e estudos de ecossistemas aquáticos (Kwong *et al*. 2022).

Google Earth Engine foi utilizado mapeamento de inundação (COLTIN *et al*., 2016) e mudança em superfície alagadas (PEKEL *et al*., 2016). Chang *et al*. (2022) mostraram em variações decadais e sazonais de diferentes zonas de turbidez máxima num período de 38 anos no estuário do rio Amarelo na China com base numa série histórica Landsat no GEE. A morfologia, as correntes e a velocidades do vento combinadas com a estratificação da água do mar têm efeitos diretos nas zonas de turbidez máxima em diferentes escalas de tempo.

Zhang *et al*. (2017) utilizaram recursos de computação em nuvem do Google Earth Engine, para desenvolver um método abrangendo 200 grandes reservatórios no Texas, capturados em 17.811 imagens do Landsat, num período de 32 anos. Com objetivo de estimar a perda evaporativa dos reservatórios, mostraram que esses reservatórios contribuem para uma perda evaporativa anual de 8,0 bilhões/m3, equivalente a 20% de seu armazenamento ativo total ou 53% do uso anual total de água no Texas. Evidenciaram que o modelo pode analisar com eficiência imagens de satélite em grandes escalas espaço-temporais, onde essa análise seria inviável com um único computador.

Jia *et al*. (2019) incorporaram procedimentos de processamento no GEE para desenvolver um fluxo operacional para monitoramento de floração de cianobactérias no lago Taihu, na China, entre 2000 e 2018. Destacam que o GEE fornece uma abordagem rápida e automática para o monitoramento a longo prazo das florações de cianobactérias, o que pode melhorar a automação e a eficiência do gerenciamento ambiental de rotina de lagos podendo ser aplicado a outras águas interiores semelhantes.

Xia *et al*. (2019) utilizaram 16.760 cenas Landsat TM, ETM + e imagens OLI para analisar mudanças na superfície da água na Bacia do Rio Huai, entre 1989 e 2017, utilizando o GEE. Índices espectrais de vegetação e água foram utilizados para quantificar a variabilidade espaço-temporal. As áreas de água de superfície foram positivamente correlacionadas com a precipitação.

Dados de precipitação e imagens Sentinel-1 foram utilizados no GEE para análise de deslizamentos de terra induzidos na área da borda do Reservatório da Barragem de Bagliha na Índia Mishra *et al*. (2022).

Kavzoglu e Goral (2022) utilizaram no GEE imagens do Sentinel-2 e índices espectrais para análise de mucilagem marinha “muco do mar” na extensão do Mar de Mármara. Dentre os índices usados, os da banda do verde foram inferiores para extrair informações de mucilagem das imagens de satélite, o NDTI e o índice de mucilagem (MI).

3 CAPÍTULO 3: SPECTRAL REFLECTANCE IN THE SPATIAL-TEMPORAL DYNAMIC OF TURBIDITY, ITAIPU RESERVOIR, BRAZIL

Anuário do Instituto de Geociências
Universidade Federal do Rio de Janeiro
https://revistas.ufrj.br/index.php/aigeo/

ISSN 0101-9759
e-ISSN 1982-3908

Spectral Reflectance in the Spatial-temporal Dynamic of Turbidity, Itaipu Reservoir, Brazil

Reflectância Espectral na Dinâmica Espaço-temporal da Turbidez, Reservatório de Itaipu, Brasil

Douglas Stefanello Facco[1], Laurindo Antonio Guasselli[1], Luis Fernando Chimelo Ruiz[2], João Paulo Delapasse Simioni[1] & Daiane Gerhardt Dick[3]

[1]Universidade Federal do Rio Grande do Sul, Centro Estadual de Pesquisas em Sensoriamento Remoto e Meteorologia, Porto Alegre, RS, Brasil
[2]Universidade de São Paulo, Escola Superior de Agricultura Luiz de Queiroz, São Paulo, SP, Brasil
[3]Universidade Federal do Rio Grande do Sul, Instituto de Pesquisas Hidráulicas (IPH), Porto Alegre, RS, Brasil
E-mail: douglas.s.facco@gmail.com; laurindo.guasselli@ufrgs.br; ruiz.ch@gmail.com; geojoaopaulo@gmail.com; daiidick@hotmail.com

Abstract

Water quality and the useful life of reservoirs and dams are influenced by the entry of suspended solids, in addition to reducing their transparency and storage capacity. It is primary to monitor and analyses its space-time dynamics. Thus, the objective of this work is to characterize the dynamics of the Itaipu Reservoir waters from turbidity, rainfall and spectral reflectance data. To characterize the dynamics, the reservoir was divided into 18 aquatic compartments between upstream and downstream, using precipitation data from the TRMM sensor and Landsat 8 images in different precipitation situations. NDWI, MNDWI and NDTI water spectral indexes were calculated from Landsat 8 images. The results showed high correlation between the NDTI index and the turbidity ($R^2 = 0.91$). Then the NDTI images were reclassified into low, medium and high turbidity. A strong correlation between turbidity and 4 Band corresponding to the spectral range of red ($R^2 = 0.94$) was also obtained. The precipitation has a determinant influence, being the Paraná River, in the periods of greater precipitation, the main agent in sediment transport. The space-time dynamics showed that the lateral compartments of the reservoir have less influence on sediment transport. In this sense, our analysis brought new elements to understand the turbidity variation in these Itaipu Reservoir compartments, as well as the spectral reflectance dynamics in the space-time characterization related to turbidity.

Keywords: Suspended solids; NDTI; Landsat-8/OLI

Resumo

A qualidade das águas e a vida útil de reservatórios e barragens são influenciados pela entrada de sólidos suspensos, além de diminuir a sua transparência e capacidade de armazenamento. O monitoramento e análise de sua dinâmica espaço-temporal é primordial. Assim, o objetivo desse trabalho é caracterizar a dinâmica a partir de dados de turbidez, da precipitação pluviométrica e da reflectância espectral das águas do reservatório Itaipu. Para caracterizar a dinâmica, o reservatório foi dividido em 18 compartimentos aquáticos entre a montante e jusante, e utilizou-se dados de precipitação do sensor TRMM e imagens Landsat 8 em diferentes situações de precipitação. A partir das imagens Landsat 8 foram calculados índices espectrais de água NDWI, MNDWI e NDTI. Os resultados mostraram alta correlação entre o índice NDTI e a turbidez ($R^2 = 0,91$). Então as imagens de NDTI foram reclassificadas em baixa, média e alta turbidez. Também foi obtido forte correlação entre a turbidez e a Banda 4, correspondente à faixa espectral do vermelho ($R^2 = 0,94$). A precipitação possui influência determinante, sendo o rio Paraná, nos períodos de maior precipitação, o principal agente no transporte de sedimentos. A dinâmica espaço-temporal mostrou que os compartimentos laterais do reservatório possuem menor influência no transporte de sedimento. Nesse sentido, nossa análise trouxe novos elementos para entender a variação da turbidez nesses compartimentos do reservatório de Itaipu, e entender a dinâmica da reflectância espectral na caracterização espaço-temporal relacionada a turbidez.

Palavras-chave: Sólidos suspensos; NDTI; OLI/ Landsat-8

1 Introduction

Large reservoirs and dams are influenced by leaching, silting, surface runoff, soil erosion, waste discharge and runoff phenomena, which lead to the entry of suspended solids. These optically active components affect the quality of reservoir water and its useful life, since they decrease both transparency and storage capacity of water bodies (Chalov et al. 2015; Davranche, Lefebvre & Poulin 2010; Ma et al. 2007; Somvanshi et al. 2011; Trinh et al. 2018). Reservoirs play an important role in the control and management of water resources, hydropower generation, water supply, agricultural irrigation and recreation (Haibo et al. 2011; Lu et al. 2011; Wang et al. 2018).

Turbidity is an important limnological variable that makes it possible to quantify both the reduction of water transparency and the interference in the passage of light in reservoirs. In summary, the higher the total amount of suspended solids, the higher the turbidity, as cited by Somvanshi et al. (2011), for example. In many cases, the continuous monitoring of reservoirs is not feasible, given their location in remote or inaccessible regions (Alsdorf, Rodríguez & Lettenmaier 2007; Barbosa, Novo & Martins 2019; Wang et al. 2004; Zhang & Liu 2014).

Given the difficulties of monitoring large reservoirs and the limitations of conventional methods, remote sensing technology is an alternative with the potential to provide crucial information in space-time monitoring on water bodies in which in-situ networks are not available (Alsdorf, Rodríguez & Lettenmaier 2007; Barbosa, Novo & Martins 2019; Haibo et al. 2011; Zhang & Liu 2014).

The analysis of turbidity in reservoir monitoring from remote sensing tools is very promising. The relationships between turbidity and semianalytical models are highlighted (Abe et al. 2019; Potes, Costa & Salgado 2012; Zhang et al. 2016). By using turbidity estimation models, Garg, Aggarwal & Chauhan (2020) report the sensitivity of both red and near infrared (NIR) bands of the Sentinel-2. Chelotti et al. (2019), by generating an estimation model of suspended solids for a low concentration reservoir, and studying its relations with the rainfall regime, from images Landsat 8, highlighted that the spectral range of red allowed the analysis of the spatial behavior of the water body. Allam, Khan & Meng (2020) developed a regional algorithm to recover surface turbidity with Landsat 8 surface reflectance (L8SR) images, reporting the importance of applying this model in environments of comparable morphological characteristics.

Studies with a space-time approach, such as Pinto et al. (2014), which analyzed 12 years of (Earth and Aqua) MODIS images, pointed out a strong relationship between solids and spectral reflectance, by using turbidity attribute and MODIS NIR/Red sensor bands data, Robert et al. (2016), considering the spectral range of red (Lobo, Costa & Novo 2015; Martins et al. 2019; Quang et al. 2017; Yanti, Susilo & Wicaksono 2016).

Important results have also been obtained with Normalized Difference Turbidity Index (NDTI) (Baughman et al. 2015; Bid & Siddique 2019), Normalized Difference Water Index (NDWI) (Ouni et al. 2019; Saberioon et al. 2020; Wang, Gong & Pu 2018) and Modified Normalized Difference Water Index (MNDWI) (Faye et al. 2020; Maliki et al. 2020; Mi et al. 2019) spectral reflectance indices.

Brazil is the country with the highest availability of fresh water in the world. Most of this water is stored in approximately 19,000 artificial reservoirs whose volume varies in time and space due to both climatic and economic factors, such as energy production and irrigation demands (Barbosa, Novo & Martins 2019). The large extension of Itaipu reservoir, with a flooded area of 1,350 km² Itaipu (2020), deserves attention regarding its monitoring, allowing to explore methodologies with remote sensing techniques. The dynamics of the Itaipu Reservoir have a strong seasonal influence of rainfall (Grimm 1988), which constitutes a significant factor in the fluctuations of the limnological variables of transparency (Toniolo et al. 2019), suspended solids (Silva et al. 2019) and turbidity (Ribeiro Filho 2006; Ribeiro Filho 2008; Ribeiro Filho et al. 2011).

In this context, our goal is to characterize the spatial-temporal dynamic from the relationship between turbidity, rainfall and spectral reflectance data for the Itaipu Reservoir waters.

Our work brings new elements to understand the variation of turbidity in the Itaipu Reservoir and to understand the dynamics of spectral reflectance in spatial-temporal characterization. The products generated are an alternative for monitoring other reservoirs.

2 Area of Study and Methodology

2.1 Area of Study

Itaipu Hydroelectric Power Plant reservoir is located on the Paraná River, on the border between Brazil and Paraguay, and it extends itself from Foz do Iguaçu/Ciudad del Este cities to the city of Guaíra, in the north (Agostinho et al. 1999) (Figure 1). The reservoir is part of the Paraná basin 3. The main tributaries of the Paraná River in Brazilian territory are the São Francisco River, with source in Cascavel, the Guaçu River, which rises in the Toledo city, the São Francisco Falso River, in Céu Azul city, and the Ocoí River, in Matelândia city (Secretaria de Estado do Meio Ambiente e Recursos Hídricos do Paraná 2013).

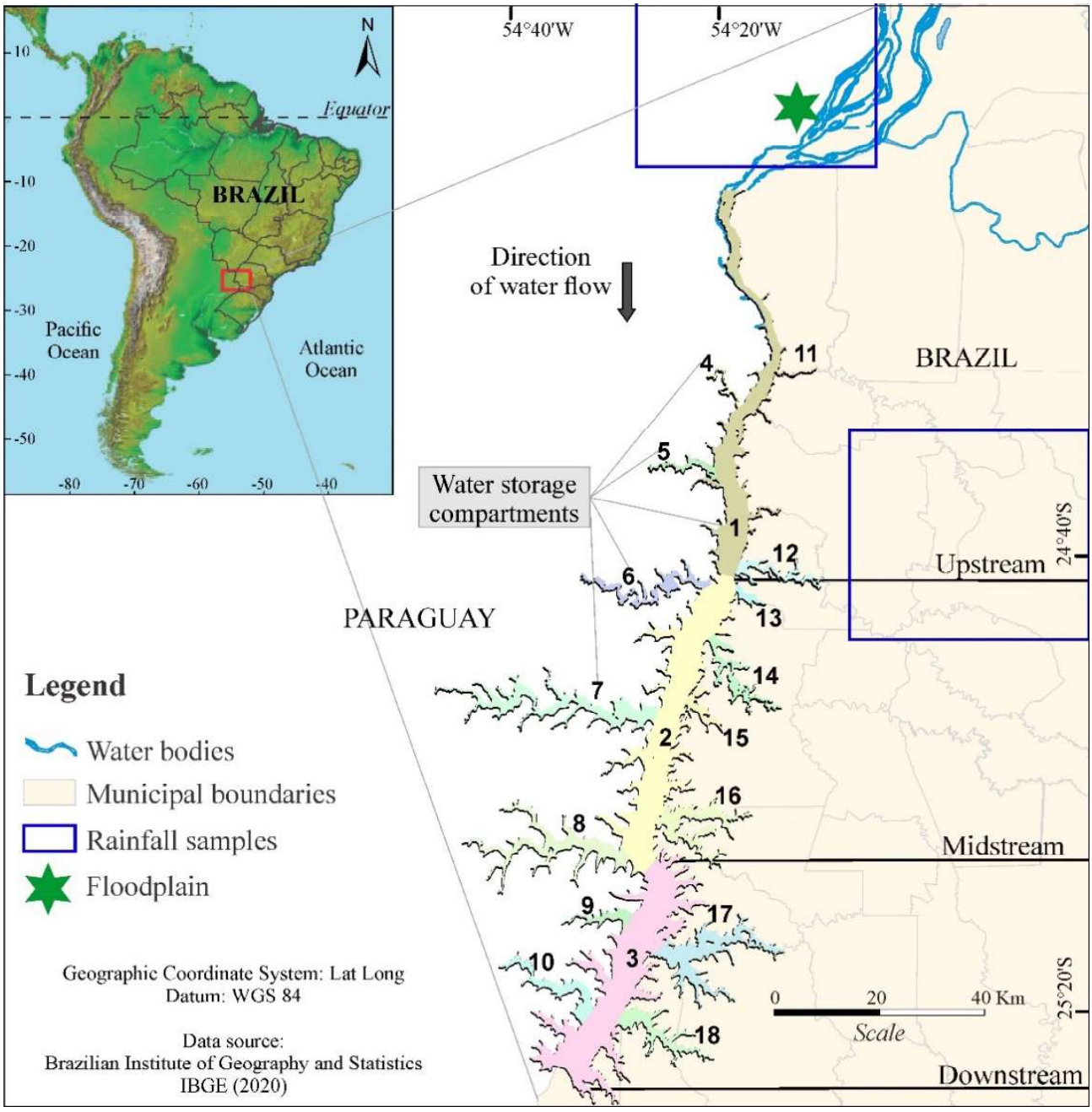

Figure 1 Location map of Itaipu Reservoir Power Plant Reservoir study area: precipitation sampling areas, aquatic compartments and flood plain.

In 2016 Itaipu Binacional was the first hydroelectric plant in the world to exceed the annual generation of 100 million megawatt-hours (MWh), the plant surpassed the 2014 record of 98.8 million MWh set by the Chinese company Três Gargantas and recovered the world's first place in annual production of clean and renewable energy. Itaipu is also the largest hydroelectric plant in the world in accumulated production. Since it started operating in May 1984, more than 2.4 billion MWh have been generated (Itaipu 2020).

In Itaipu Reservoir upstream area there is an extensive flood plain of the Upper Paraná River (Galvão, Stevaux & Saad 2014; Stevaux, Martins & Meurer 2009), with around 230 km long and variable width between 3 km and 8 km. This area is limited between the Engenheiro Sérgio Mota Hydroelectric Power Plant downstream and

the beginning of the backwater of Itaipu Hydroelectric Power Plant reservoir. The flood plain has hygrophilous vegetation with high humidity characteristics as its main modelling agent (Couto, Hayakawa & Souza-Filho 2010).

The predominant climate in the region is classified as Cfa, subtropical humid, which is mesothermal, with annual precipitation average between 1,600 mm and 1,700 mm. There is a higher concentration of rainfall during the summer months, without a defined dry season. The average temperatures of the hottest months are above 22°C and the coldest months are below 18°C (Instituto Agronômico do Paraná 2020; Souza Filho & Fragal 2013).

The main use of the land is agriculture in the basin area. The predominant type of soil is the Latosol that corresponds to soils in advanced stages of weathering, typical of both equatorial and tropical regions, also occurring in subtropical zones. The latosols are mainly distributed by large and old erosion surfaces or river terraces, usually in flat and smooth wavy relief (Rocha & Bade 2018).

2.2 Methodological Flowchart

The methodology used to understand the spatial-temporal variation of turbidity is presented in the methodological flowchart (Figure 2).

2.3 Reservoir Compartmentalization

Due to its large extension, the Itaipu Reservoir presents different dynamics from downstream to upstream, as well as in the compartments of its horizontal arms. Thus, the compartmentation of the reservoir is fundamental to establish areas with similar environmental conditions. A reservoir may have several aquatic compartments with one or more common characteristics, but they communicate with each other in the transportation of energy and matter, directing changes in time and space (Wachholz 2011).

The criteria for the reservoir compartmentalization followed Wachholz, Pereira Filho & Sartor (2011)

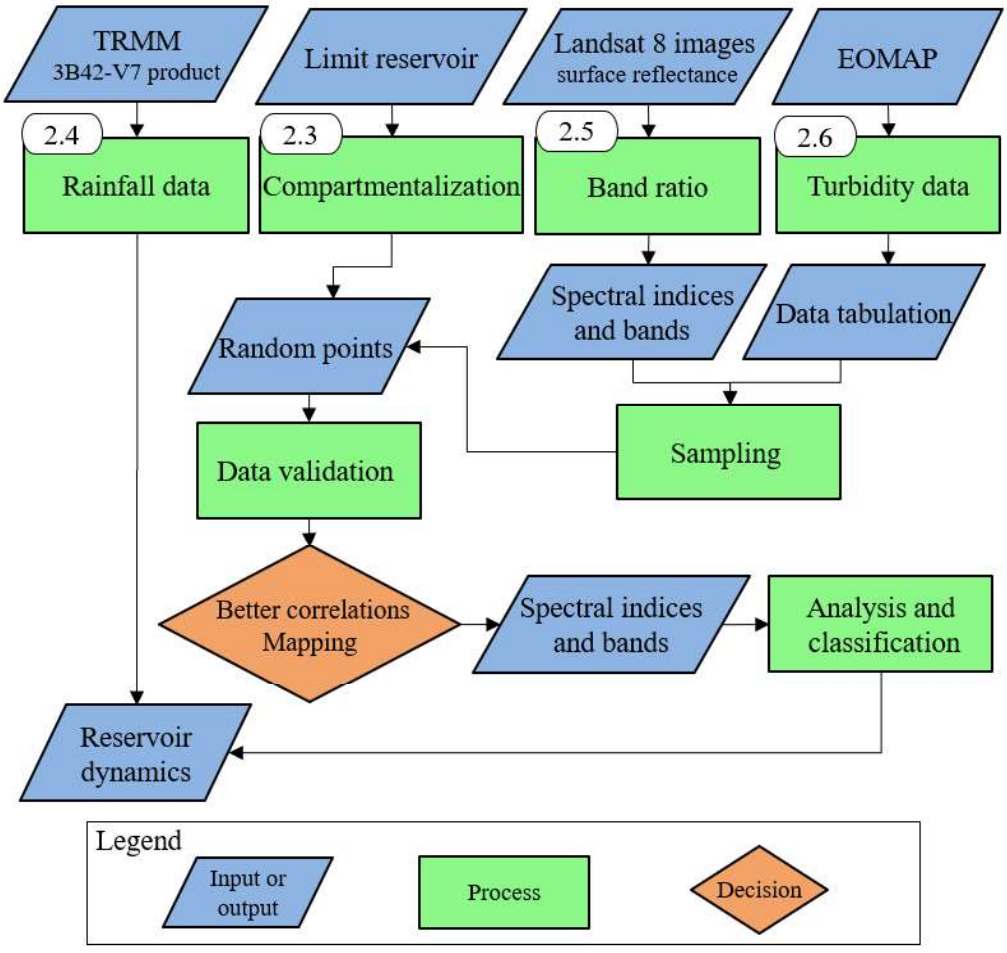

Figure 2 Methodological flowchart

methodology, considering three aspects: (1) the characteristics of the reservoir and its hydrographic basins; (2) the hydrodynamic order of the reservoirs, regarding upstream, intermediate and downstream stations formation; (3) the formation of sequence or non-sequence of reservoirs. It was determined a 100-m zone (measured from the bank) around the reservoir to avoid spectral mixing with other targets than the water.

2.4 TRMM Precipitation Data

One of the main problems in the data collection on rainfall is the lack of pluviometric stations, causing the absence of data, which makes it impossible to use historical series (Moraes et al. 2015; Oliveira Junior et al. 2014). Satellite data have been used in climatological and hydrological studies, being an alternative to overcome the failing of local rainfall stations (Adams, Souza & Costa 2009; Longo, Camargo & Silva Dias 2004; Oliveira Junior et al. 2014).

Almeida et al. (2015); Danelichen et al. (2013); Liu (2015); Pereira et al. (2013); Pessi et al. (2019) and Serrão et al. (2016) highlight that estimates of data sets from the Tropical Rainfall Measuring Mission (TRMM) sensor (3B43 product), made available on NASA's Giovanni platform, are reliable and can be used to estimate precipitation.

The TRMM satellite, launched on November 27, 1997, from a partnership between NASA and the Japanese Aerospace Exploration Agency (JAXA), aims to both monitor precipitation in the tropics and verify its influence on global climate. The satellite's low polar orbit (initially, 350 km, and, since 2001, 403 km), together with its short translation period (91 minutes) allows the collection of high temporal and spatial resolution images (NASA 2018).

TRMM precipitation data (3B42-V7 product), obtained with a 3-hour-time resolution and 0.25° x 0.25° spatial resolution (approximately 27 km x 27 km), have been used to analyze the turbidity variation. Two areas have been defined for precipitation samples (Figure 1): one from the north side of the reservoir, on the coordinates: -54.3459, -23.7262, -53.7087, -23.1879, and another one from the west side of the reservoir, on the coordinates: -54.0512, -24.7856, -53.5019, -24.2912. It was collected, also, the precipitation data for the last 5, 10 and 15 days for the dates: 2016-08-11, 2016-08-27, 2016-09-28 (Table 1), which were compatible with the Landsat 8 images analyzed. These data were used both to analyze the influence of precipitation on the variation of turbidity in the reservoir and to evaluate the water flow in vertical and horizontal directions of the reservoir.

2.5 Landsat 8 Images and Spectral Indices

Landsat 8 satellite's Operational Land Imager (OLI) sensor provides multispectral bands from visible to shortwave infrared (SWIR), with a 185 km bandwidth, a 12-bit radiometry and a 30-m spatial resolution. Three images were purchased on USGS Earth Explorer website (http://earthexplorer.usgs.gov), with dates of August 11, August 27 and September 28, 2016, all with surface reflectance according to Landsat Collection 1 Level 2 product.

The selected dates have different precipitation characteristics: the 08/11 image concentrates the precipitation in the western region of the reservoir and the 08/27 image concentrates the highest precipitation in both north and west regions. In the image of 09/28, there is the lower rainfall in both north and west sides.

For the analysis of the turbidity in Itaipu Reservoir, we used the following water spectral indices: (a) Normalized Difference Water Index (NDWI), in which the water will have positive values while soil and terrestrial vegetation features will tend to have zero or negative values (McFeeters 1996); Modified Normalized Difference Water Index (MNDWI) in which where the NIR band was substituted by the SWIR band to improve distinction of built-up features over water (Xu 2006); and Normalized Difference Turbidity Index (NDTI) in which as turbidity level of water increases due the increase in the suspended particles in the water, the reflectance of the red band is more than that of the green band (Lacaux et al. 2007). Both which were obtained from arithmetic operations of the ENVI 5.3 software (Table 2); and (b) Landsat 8 satellite's B2 (Blue), B3 (Green), B4 (Red), B5 (NIR), B6 (SWIR 1) and B7 (SWIR 2) spectral bands. Both spectral indices and bands were related to the turbidity data, obtained from the correlation coefficient (R), to estimate the association level between two variables and the determination coefficient (R^2). Together, they are indicated to measure the fluctuation of one variable that is explained by another.

Both indices and spectral bands with higher R and R^2 values were used in the characterization of the turbidity in the compartments of the Itaipu Reservoir. Using the maximum and minimum values of the indices, and the spectral data with the highest correlation with turbidity, the reservoir boundary was divided into identical intervals to report and analyze the compartments with the greatest influence of turbidity.

Table 1 Precipitation data from the TRMM sensor, product 3B42-V7 from the last 5, 10 and 15 days for the dates: 2016-08-11, 2016-08-27, 2016-09-28.

	Precipitation North				Precipitation West			
Dates	last 15 days	last 10	last 05	**total mm**	last 15 days	last 10	last 05	**total mm**
08/11	0	0	12	**12 mm**	0	0	64	**64 mm**
08/27	0	150	32	**182 mm**	50	109	0	**159 mm**
09/28	0	21	0	**21 mm**	0	45	0	**45 mm**

Table 2 Water Spectral indices

Index	Equation	Values Range	Source
NDWI	(Green - NIR) / (Green + NIR)	-1 a +1	McFeeters (1996)
MNDWI	(Green - SWIR) / (Green + SWIR)	-1 a +1	Xu (2006)
NDTI	(Red - Green) / (Red + Green)	-1 a +1	Lacaux et al. (2007)

Legend: NDWI - Normalized Difference Water Index; MNDWI - Modified Normalized Difference Water Index; NDTI - Normalized Difference Turbidity Index.

These values were used to classify the reservoir into three turbidity levels: low, medium and high, based on both average and standard deviation statistical parameters, according to (Sharma et al. 2015; Singh, Bhardwaj & Verma 2020; Somvanshi et al. 2011) protocols (Table 3), which were calculated by the R software. Bid & Siddique (2019) followed this methodology of reservoir classification in turbidity analysis.

2.6 Turbidity Validation Samples

Turbidity (TUR) is a key parameter of water quality and it is linearly related to the inverse dispersion of light by both organic and inorganic particles. It is also linearly related to the Total Suspended Solids (TSS) (Sagan et al. 2020).

Earth Observation and Environmental Services (EOMAP) has developed, for the year 2016, algorithms based on modular inversion processing (MIP), a multi-sensors operating processor designed to extract quantitative information about aquatic environments from remote sensing data of Landsat 5/7/8 and Sentinel-2 satellites (Dörnhöfer et al. 2018; EOMAP 2020; Heege et al. 2014). Among the available products, there are historical turbidity series.

These cited algorithms allow recovering atmospheric parameters in the water, including the correction of the terrestrial adjacency effect, essential for the accurate remote detection of any coastal or inland water body. They contain a physical and accurate implementation of the bidirectional effect within the water column, on the surface and in the atmosphere, considering, yet, the full range of reflective, absorbent and dispersion properties of the water body and its limits with the atmosphere (Dörnhöfer et al. 2018; EOMAP 2020; Heege et al. 2014).

To determine the index with the highest level of correlation with turbidity, samples of turbidity were obtained from its historical series for the year 2016, available at EOMAP. Were used 195 random samples in the 18 Formazine Turbidity Unit (FTU) turbidity compartments for each image date, in order to validate both indices and spectral bands from the Landsat 8 images. For the horizontal compartments (4 to 18), were collected 10 samples per compartment and, for the vertical compartments (1 to 3), it were collected 15 samples per compartment.

Table 3 Turbidity classification, according to Somvanshi et al. (2011) and Sharma et al. (2015).

Low Turbidity	Mean − Standard Deviation (> +1σ)
Medium Turbidity	Mean + Standard Deviation
High Turbidity	Value of more than Medium Turbidity

The spectral data most closely related to the validation data underwent statistical evaluation to analyze the degree of similarity of the individual compartments and the reservoir by ANOVA analysis of variance: (1) For the analysis of the dynamics of the individual compartments, the null hypothesis (H0) was that there are no significant differences between the mean values of the compartments; (2) For the analysis of the dynamics of the reservoir, the null hypothesis (H0) was that there are no significant differences between the mean values of all compartments. The null hypotheses were tested by calculating an F value at a significance level of 0.05.

3 Results and Discussion

3.1 Compartmentation

Three compartments in the total were defined in the central body of the reservoir (upstream, intermediate and downstream), as well as 15 compartments were defined in the horizontal arms, corresponding to the tributary river basins (Figure 1). Due to the large extension of the reservoir, compartmentalizing the Itaipu Reservoir into 18 compartments, based on the methodology of Wachholz, Pereira Filho & Sartor (2011), allowed the analysis of turbidity dynamics in more homogeneous areas.

3.2 Bands Ratio

This study showed that the turbidity data obtained from EOMAP showed the higher correlation between band 4 (red region, ~655 nm) of OLI/Landsat 8 and the NDTI index (Table 4). So we chose to discard further analysis with the other bands and indexes that showed low correlation.

In the relationship between turbidity and red band (B4), according to the dispersion graphic on Figure 3A, it can be seen a positive correlation (R) of 0.97 and a determination coefficient of 0.94. Between turbidity and NDTI index, the correlation (R) was 0.95 and the determination coefficient was 0.91 (Figure 3B).

The most of methods to interpret turbidity fluctuation in lakes and reservoirs propose specific empirical relationships by adjusting the in-situ turbidity measurements with the reflectance that is derived from satellite bands (Dogliotti et al. 2015). A single band or the ratio between two bands is routinely used on turbidity analysis, as well as other water component models (Ouillon 2003).

Table 4 Correlation values and determination coefficients for the indices and turbidity versus spectral bands.

Spectral Indices and Bands	Estatísticas	
	R	R²
NDWI	-0.40	0.16
MNDWI	-0.12	0.01
NDTI	**0.95**	**0.91**
B2	0.23	0.05
B3	0.68	0.46
B4	**0.97**	**0.94**
B5	0.42	0.17
B6	0.15	0.02
B7	0.14	0.02

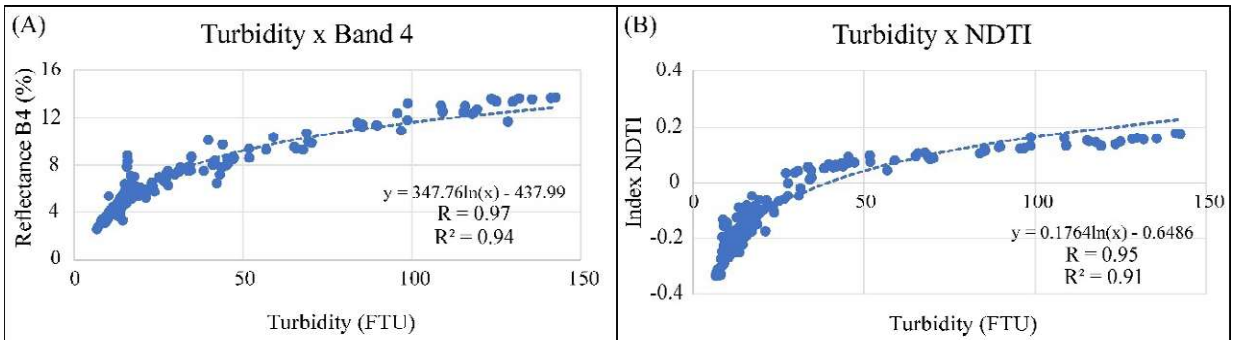

Figure 3 A. relationship between Turbidity and Red band (B4); B. relationship between Turbidity and NDTI in the Itaipu Reservoir.

Several researchers who use remote sensing reflectance for turbidity analysis, as well as for TSS analysis, show high correlation between the red band and its concentrations (Garaba & Zielinski 2015; Güttler, Niculescu & Gohin 2013; Lobo, Costa & Novo 2015; Quang et al. 2017; Vanhellemont & Ruddick 2014). However, few studies in the literature have evaluated the relationship between water turbidity data and the NDTI index. Baughman et al. (2015) used Landsat TM image to analyze the relationships between turbidity and red band and between turbidity and NDTI index, finding 0.55 and 0.53 for R^2, respectively.

Bid & Siddique (2019) analyzed the relations between suspension sediments and NDTI, with R^2 of 0.90, and they found high turbidity from July to September in the Panchet Hill Dam. Among the several factors affecting turbidity, Göransson, Larson & Bendz (2013); Zhang et al. (2016), report that intense rainfall events, from river discharges, are considered one of the main contributors to turbidity increment.

3.3 Turbidity, Spectral Reflectance in the Red Wavelength and NDTI Analysis

The values of turbidity, band 4 and NDTI for the 18 compartments are presented in Figure 4. In the 08/11 image, the compartments located in the western region of the reservoir (11, 12, 13, 14, 15 and 16) have turbidity values between 7 and 68 FTU, the band 4 reflectance varied between 0.02% and 0.09% and the NDTI oscillated between -0.27 and 0.10.

We found similar behavior in the same compartments of 2016-09-28 image (Figure 4), in which the values of turbidity, reflectance in the red wavelength and NDTI varied between 6 and 59 FTU, between 0.03% and 0.08% and between -0.23 and 0.05, respectively. The similarity between the data is directly related to the low precipitation in the northern and western regions in the reservoir.

For the image of 08/11, even with the higher precipitations on the western side of the reservoir (55 mm accumulated in the last 5 days), the lateral compartments did not influence in the increase of sediment transport to the reservoir.

In the image of 08/27, the upstream compartments of the reservoir (1, 4, 11 and 12), in medium course (2), presented the higher values of turbidity, band 4 and NDTI. On this date, according to TRMM data, the highest precipitation occurred in the northern region of the reservoir (192 mm accumulated in the last 15 days), resulting in the contribution of the flood plain in the turbidity transport. According to Quang et al. (2017), the turbidity is strongly influenced by the runoff after high rainfalls, since these brings large amounts of sediment to the water body. Besides, intense water flows cause resuspension after heavy rains. The values of turbidity, band 4 and NDTI for the compartments 11, 12, 13, 14, 15 and 16 varied between 9.1 and 128.41 FTU, between 0.03% and 0.13% and between -0.25 and 0.15, respectively.

ANOVA analysis of variance was used for the 18 individual compartments to verify their dynamics. For the variable Turbidity, an F of 1.32 was obtained with p 0.24, accepting the H0 hypothesis in which the values of the individual compartments are similar to each other and do not present a significant difference. As shown in Figure 4, compartments 1, 11, 12, 4 and 2 have greater variance, the others have very close values. For Band 4 (RED) F 1.31 with p 0.25 also accepting the H0 hypothesis, the compartments with the highest variance were 1, 11, 12, 4 and 2, the others with low variance. For NDTI, F was 3.68 and $p < 0.05$, in which we accept hypothesis H1 in which the compartments do not have similarity, that is, they present a significant difference, with emphasis on compartments 1, 11, 12, 2, 4, 5 and 14.

Our work and the others cited used precipitation to analyze turbidity and all report the importance of this variable in the dynamics of water bodies. Viviano et al. (2017) used precipitation data for turbidity analysis and observed higher concentrations of suspended solids and turbidity some hours after precipitations. Robert et al. (2016) highlight that periods of the year with higher precipitation have higher turbidity in reservoirs. Quang et al. (2017) showed that turbidity is influenced by precipitation in both rainy and dry seasons and that bed sediment resuspension controls turbidity in both shallow and coastal waters, while rainfall is a key factor, affecting turbidity in deep waters. In Martins et al. (2019), the level of turbidity was seasonally dependent, varying from clean water (0-20 NTU), in the dry season, to above 60 NTU, in the rainy season.

Our results are related to Buffon (2016), who analyzed the relationship between the concentration of suspended solids and band 4 of the Landsat 8 satellite in two compartments of the Itaipu Reservoir (12 and 18) (Figure 1). In low precipitation periods, the compartment 18 presented a little higher value in relation to the 12. Robert et al. (2016) observed a significant increase in turbidity values between 2000 and 2015, and highlighted that this increase is related to changes in the land use.

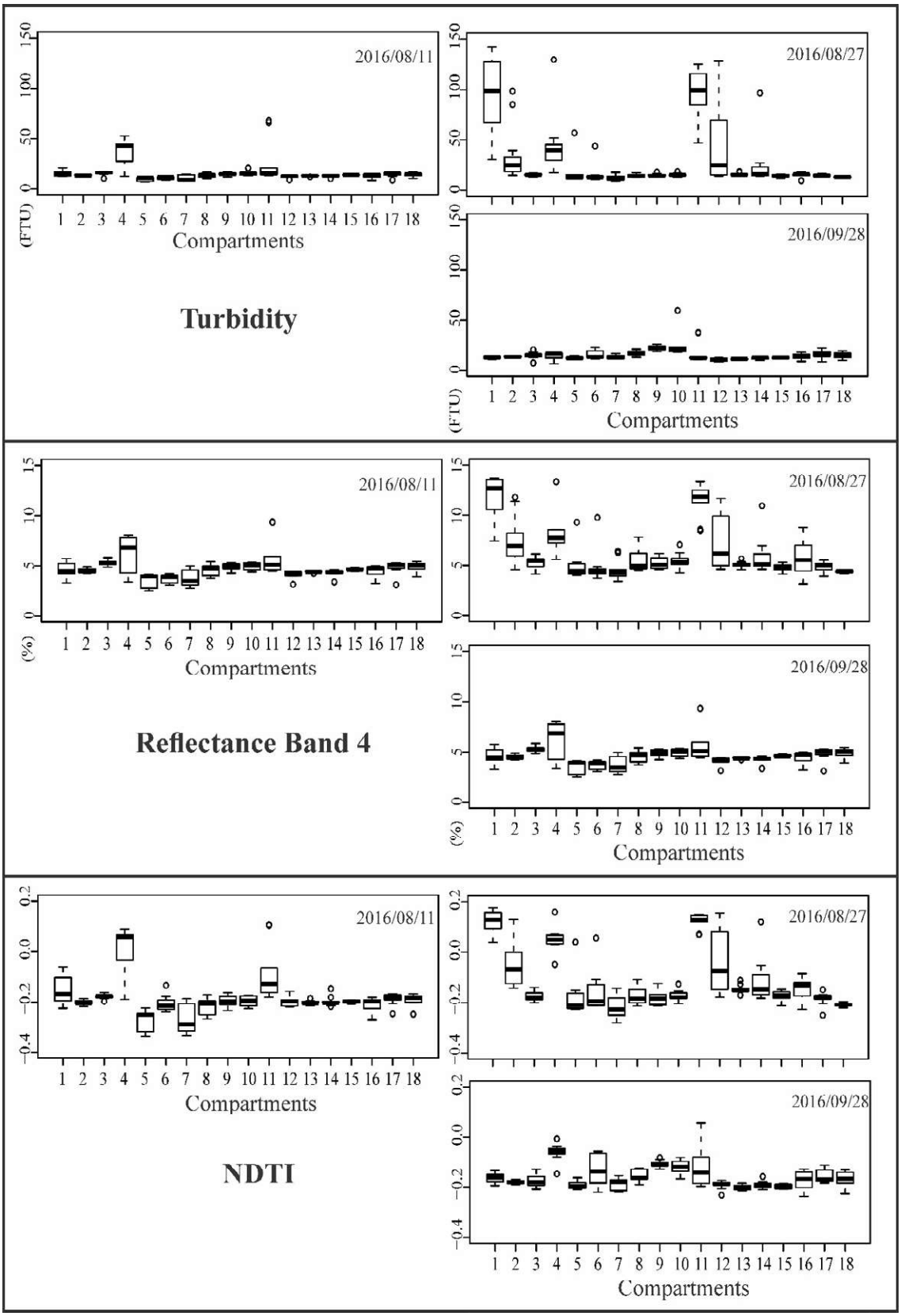

Figure 4 Boxplot of the relationship between turbidity, band 4 (OLI) and NDTI.

3.4 Turbidity Dynamics in the Reservoir

NDTI values were classified into high, medium and low turbidity levels, by using average and standard deviation statistical parameters (Table 5). Both NDTI values map (Figure 5) and turbidity classes map, according to Sharma et al. (2015); Singh, Bhardwaj & Verma (2020); Somvanshi et al. (2011) (Figure 6), show the spatial-temporal variation of these variables.

The 08/27 image shows the highest NDTI values (Figure 5) in the upstream area of the reservoir. Compartments 1 and 2 were classified as high turbidity (Figure 6). Current flow and turbidity variables are positively related, since the flow caused by the rains increases the sediment transportation. In addition, the current flow is strong enough to increase turbidity by causing the resuspension of the sediments deposited at the bottom of the reservoir (Fondriest Environmental Inc 2014; Yu, Zhang & Lemckert 2014).

Table 5 Turbidity Values

NDTI values of Itaipu Reservoir			
Standard deviation	0.093	**Average**	-0.150
Low		-0.243	
Medium		-0.057	
High		> 0.057	

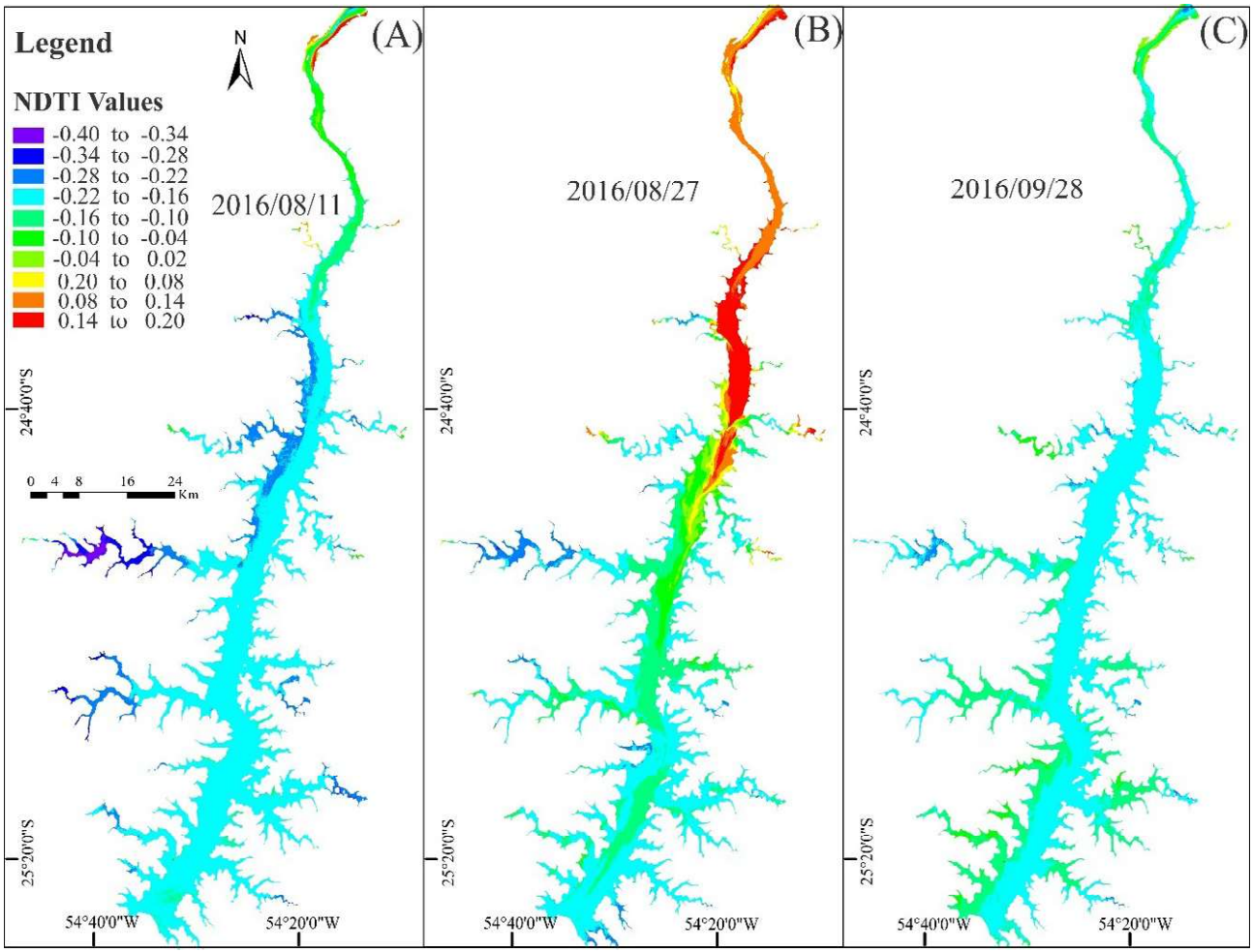

Figure 5 NDTI dynamic for the Itaipu Reservoir.

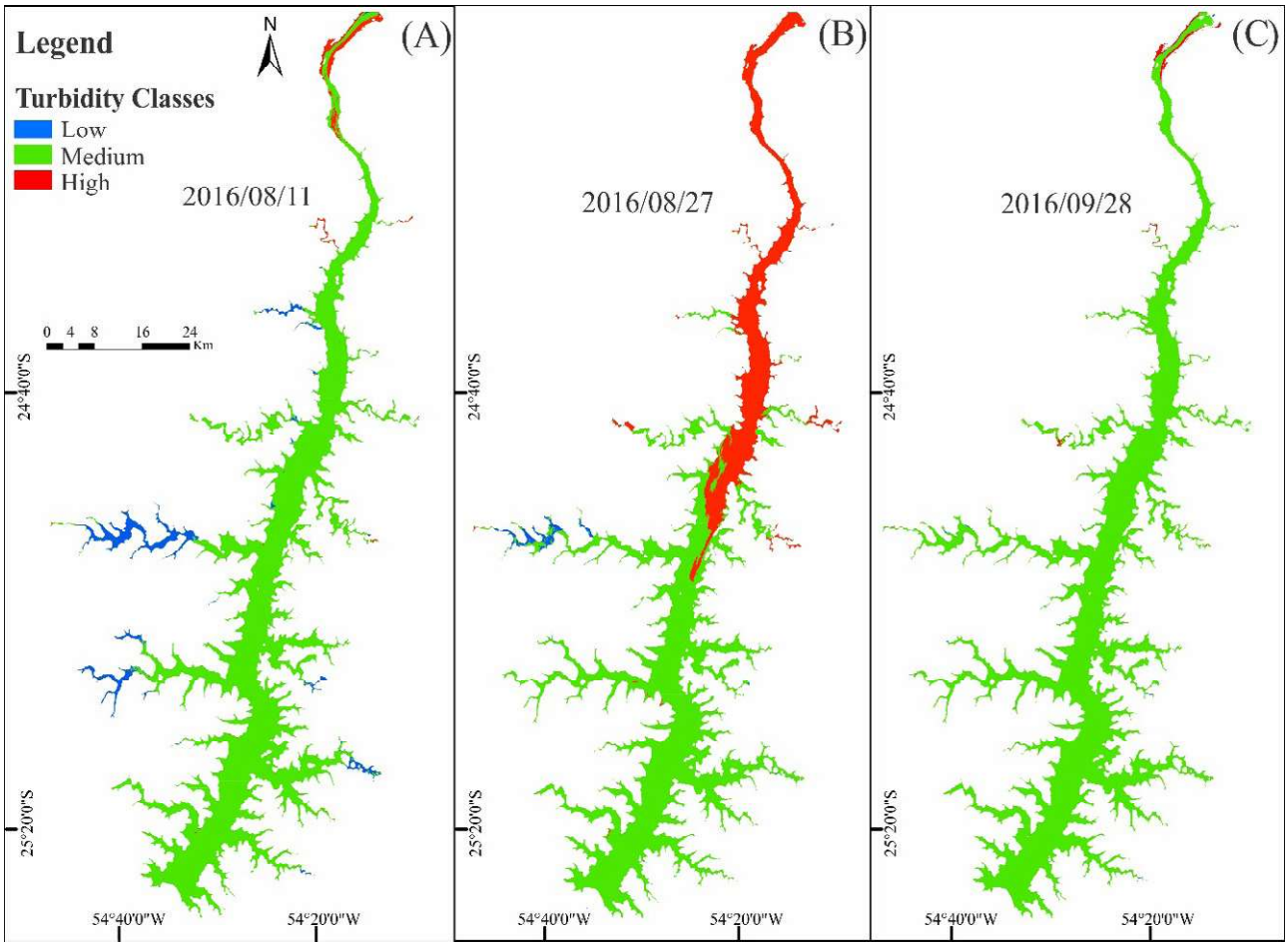

Figure 6 Turbidity classes for the Itaipu Reservoir.

The image of 09/28 showed higher NDTI values than the image of 08/11 in the downstream intermediate compartments (Figure 5). The predominance of the middle turbidity class on 08/11 and 09/28, as well as in the reservoir as a whole (Figure 6), is due to the low rainfall in the north of the reservoir 12 mm and 21 mm respectively (Table 1) and the damming of solids by the flood plain.

Some turbidity patterns were found in the reservoir, even with different periods and precipitation, as is the case of the compartments 3 (medium turbidity), 16 (medium turbidity), 4 (high turbidity and 7, which had low turbidity on the east of the compartment and medium turbidity on the west of the compartment, near the central body.

In the ANOVA analysis to analyze the dynamic space of the reservoir, the variable Turbidity, Band 4 (Red) and NDTI obtained F calculated from 4.93, 6.94 and 8.57 respectively with $P < 0.05$ for all, this means that we accept hypothesis H1 in which for the 3 analyzed dates independently variable the results obtained do not have similarity.

The variability of NDTI values shows that precipitation has a strong influence on the turbidity dynamic in the reservoir, being the Paraná River, in periods of higher precipitation, the main solids transportation agent in the reservoir. In addition, we found that the lateral compartments have little influence on the entrance of solids into the reservoir, as a result of the lower precipitation levels and the few amount of sediment transportation from the western side of the reservoir.

Andrade et al. (1988); Ribeiro Filho (2006) and Ribeiro Filho et al. (2011) point out that both turbidity and suspended solids showed decreasing averages towards downstream in the Itaipu Reservoir, which can be explained by precipitation events. In this sense, the fluvial zone presented the highest concentrations of suspended sediments and turbidity.

Several works report the importance of the flood plain in retaining the solids, as well as highlight the flood periods, in which the water level of the Paraná River is higher. In these periods, characterized by flood pulses, there is the death of vegetation and the entry of solids, as a result of the increment of the water flow (Couto, Hayakawa & Souza-Filho 2010; Hayakawa et al. 2010; Junk, Bayley & Sparks 1989; Souza Filho & Fragal 2013). Similar results were found by Ribeiro, Brandimarte & Kishi (2005), who observed that after the formation of the Salto Caxias reservoir, there were significant increases in water transparency levels, with a tendency to higher values along the central axis.

In our work, values above 50 FTU were found in upstream compartments 1 and 11 on the wettest date of 08/27, and values between 10 and 30 FTU for the least influenced compartments, mainly on 11/08 and 09/28 of less precipitation. Similar values were found by Martins et al. (2019) in which found that the turbidity dynamic in Sobradinho reservoir Northeast Brazil, present strong variability between rainy and dry seasons. Turbidity levels varied from clean water (0-20 NTU) during the dry season, to turbidity (> 50 NTU) during the rainy season.

Silva et al. (2009) found higher turbidity values observed in Peti reservoir, Minas Gerais Brazil, that both variations and high turbidity peaks were higher on the upstream of the reservoir (approximately 200 NTU) in the rainy season, oscillating between 50-80 NTU in the intermediate region. They point out that these values are influenced by anthropic activities, such as livestock, agriculture and urban solids of the cities. The Peti Reservoir and the Itaipu Reservoir are located in the Atlantic Forest Biome, which has been suffering a great deal of deforestation in recent years, according to Santos et al. (2020) the increase in the Brazilian population and the consequent expansion of areas destined for agriculture, livestock, urban centers and forestry were the main reasons for the deforestation of the biome's forests, contributing to the increase in turbidity in the reservoirs.

Agência Nacional das Águas (2021); Silva, Abdon & Rossi (2009); Silva, Neves & Basotti (2017) report that the silting and erosion on the banks of the Paraná River is due to the deforestation of vegetation areas on the coast of the river. The speed of the water flow of the Paraná River, in its main channel, varies between 0.8 and 1.2 m.s-1, and may present slightly higher values during the period of greater precipitation. Places protected by islands or bars, for example, have lower speeds (Galvão, Stevaux & Saad 2014).

Studies in other reservoirs also highlight that land use and land cover is an important factor when talking about the dynamics of turbidity and suspended solids in reservoirs. Wachholz (2011) reports that in Rodolfo Costa e Silva reservoir, Rio Grande do Sul, Brazil, the type of land use is determinant in erosive processes in the watershed, as well as it influences the characteristics of the reservoir. In addition, the author states that positive correlations were found between suspended solids and exposed soil on land prepared for agricultural cultivation. Cabral et al. (2013) point out that the Caçu reservoir, Goiás, Brazil, the highest values of turbidity occurred in the upstream sector, whose main cause are the erosive processes in the margins and unprotected areas of vegetation.

Chelotti et al. (2019) generated models for estimating suspension sediment concentration from MODIS and Landsat 8 data, which allowed investigating their both temporal and spatial behavior, in relation to the rainfall regime and reservoir variation quota. According to Zhang et al. (2016), reservoirs exhibit spatial heterogeneity, significantly greater in arriving rivers than in the main body of the reservoir. According to these authors, and equally to our work the main cause is rainfall. Additionally, they have developed a semiannual model to monitor quantitatively the total of suspended material in slightly turbid inland waters, by using Landsat 8 OLI images.

Bid & Siddique (2019), analyzing seasonal variations on the water turbidity of a dam by the application of NDTI method, showed that the highest levels of turbidity occur in the monsoon, when the indicator jumped from 60 NTU to 700 NTU.

EOMAP's turbidity data were essential to validate both NDTI and band 4 indicators, especially when they are applied to large reservoirs that are located in the remote or difficult to access regions, on which there are lack of information on limnological parameters. The MIP system has been operationally proven in several regional monitoring applications, as well as in global water quality research, such as by UNESCO (Dörnhöfer et al. 2018; EOMAP 2020; Heege et al. 2014; Heege, Schenk & Wilhelm 2019). In Yanti, Susilo & Wicaksono (2016), the band 4 of Landsat 8 OLI sensor had the best precision to detect suspended sediments, presenting a determination coefficient of 0.54.

In this work, we show that the applicability of bands and spectral indices using two bands is a simple method and provided important information about the dynamics of the reservoir. The method proposed by Sharma et al. (2015); Singh, Bhardwaj & Verma (2020); Somvanshi et al. (2011), is efficient for identifying zones with different turbidity levels, helping in the management and monitoring of sediments in a reservoir.

The compartmentation of the Itaipu Reservoir, according to Wachholz (2011) methodology, was essential to

the analysis of the turbidity dynamics of that homogeneous areas, considering the large extension of the reservoir. The upstream compartment 1 is characterized by giving Paraná River's largest contributions at the entrance of suspended solids into the reservoir. In downstream intermediate sector and in reservoir's side arms, the water flow becomes more lentic, because of the low stream.

For Garg, Aggarwal & Chauhan (2020), the remote sensing approach can be used to make qualitative estimates of turbidity, even in the absence of field observations. In this sense, our analysis brought new elements to understand the turbidity fluctuation in the compartments of the Itaipu Reservoir and to comprehend the dynamics of spectral reflectance in the spatial-temporal characterization related to turbidity.

4 Conclusions

This work investigated the relationship between turbidity, precipitation and spectral reflectance in the Itaipu hydroelectric plant reservoir. The results reveal that higher rainfall periods have a strong influence on sediment transportation to the reservoir. The flood plain of the Upper Paraná River, which is upstream from the Itaipu Reservoir, helps in the retention of solids, but in periods of higher precipitation, the Paraná River is the main responsible for transporting sediments to the reservoir, due to its flood and water flow.

The relationship between precipitation, spectral reflectance of Landsat 8 OLI sensor's band 4, NDTI index and EOMAP's turbidity validation data showed itself strong. Both were important to illustrate that the suspended material that affects the spectral reflectance in the spatial-temporal characterization of the reservoir turbidity comes from the upstream, as well as that the horizontal compartments have little influence. The optical properties of the water indicate the red region of the electromagnetic spectrum as the one with the best potential for turbidity analysis, since it is the spectral range with the largest variation, regarding turbidity. The space-time scale approach is essential to determine and correctly interpret the differential effects generated by turbidity control processes. In this sense, this work will continue, aiming at new evaluations with more images to expand the time series. The products and methodology generated by this work are an alternative for monitoring other reservoirs.

5 References

Abe, C.A., Lobo, F.L., Novo, E.M.L.M, Costa, M. & Dibike, Y. 2019, 'Modeling the effects of land cover change on sediment concentrations in a gold-mined Amazonian basin', *Regional Environmental Change*, vol. 19, no. 6, pp. 1801-13. https://doi.org/10.1007/s10113-019-01513-8

Adams, D.K., Souza, E.P.D. & Costa, A.A. 2009, 'Moist convection in Amazonia: implications for numerical modelling', *Revista Brasileira de Meteorologia*, vol. 24, no. 2, pp.168-78. https://doi.org/10.1590/S0102-77862009000200006

Agostinho, A.A., Ambrósio, A.M., Ferreira, V.S., Oliveira, E.F., Okada, E.K & Suzuki, H.I. 1999, '*Reservatório de Itaipu: aspectos biológicos e socioeconômicos da pesca'*. Relatório Anual (1997/98). UEM-Nupélia e Itaipu Binacional, Maringá.

Allam, M., Khan, M.Y. & Meng, Q. 2020, 'Retrieval of Turbidity on a Spatio-Temporal Scale Using Landsat 8 SR: A Case Study of the Ramganga River in the Ganges Basin, India', *Applied Sciences*, vol. 10, no. 11, p. 3702. https://doi.org/10.3390/app10113702

Almeida, C.T.D., Delgado, R.C., Oliveira Junior, J.F.D., Gois, G. & Cavalcanti, A.S. 2015, 'Avaliação das estimativas de precipitação do produto 3B43-TRMM do Estado do Amazonas', *Floresta e Ambiente*, vol. 22, no. 3, pp. 279-86. https://doi.org/10.1590/2179-8087.112114

Alsdorf, D.E., Rodríguez, E. & Lettenmaier, D.P. 2007, 'Measuring surface water from space', *Reviews of Geophysics*, vol. 45, no. 2. https://doi.org/10.1029/2006RG000197

Agência Nacional das Águas 2021, *Região Hidrográfica do Paraná*, viewed 15 May 2021, <http://www2.ana.gov.br/Paginas/portais/bacias/parana.aspx>.

Andrade, L.F., Brunkow, R.F., Xavier, C.F., & Domingues, L.L. 1988, 'Fitoplâncton e características físico-químicas do reservatório de Itaipu (BR)', *Limnologia e manejo de represas. Série Monografias em Limnologia*, vol. 1, pp. 205-68.

Barbosa, C.C.F., Novo, E.M.L.M., & Martins, V.S. 2019, '*Introdução ao Sensoriamento Remoto de Sistemas Aquáticos: princípios e aplicações*', vol. 1. Instituto Nacional de Pesquisas Espaciais.

Baughman, C.A., Jones, B.M., Bartz, K.K., Young, D.B. & Zimmerman, C.E. 2015, 'Reconstructing turbidity in a glacially influenced lake using the Landsat TM and ETM+ surface reflectance climate data record archive, Lake Clark, Alaska', *Remote Sensing*, vol. *7*, no. 10, pp. 13692-710. https://doi.org/10.3390/rs71013692

Bid, S. & Siddique, G. 2019, 'Identification of seasonal variation of water turbidity using NDTI method in Panchet Hill Dam, India', *Modeling Earth Systems and Environment*, vol. *5*, no. 4, pp. 1179-200. https://doi.org/10.1007/s40808-019-00609-8

Buffon, E.C. 2016, 'Caracterização limnológica e espectral de dois compartimentos aquáticos do reservatório Itaipu', Master Dissertation, Universidade Federal de Santa Maria. http://repositorio.ufsm.br/handle/1/9477

Cabral, J.B.P., Wachholz, F., Becegato, V.A. & Nascimento, E.S. 2013, 'Diagnóstico hidrossedimentológico do reservatório da UHE Caçu-Go', *GeoFocus. Revista Internacional de Ciencia y Tecnología de la Información Geográfica*, vol. 13, no. 1, pp. 25-37.

Chalov, S.R., Jarsjö, J., Kasimov, N.S., Romanchenko, A.O., Pietroń, J., Thorslund, J. & Promakhova, E. V. 2015, 'Spatio-temporal variation of sediment transport in the Selenga River Basin, Mongolia and Russia', *Environmental Earth*

Sciences, vol. 73, no. 2, pp. 663-80. https://doi.org/10.1007/s12665-014-3106-z

Chelotti, G.B., Martinez, J.M., Roig, H.L. & Olivietti, D. 2019, 'Space-Temporal analysis of suspended sediment in low concentration reservoir by remote sensing', *Revista Brasileira de Recursos Hídricos*, vol. 24. https://doi.org/10.1590/2318-0331.241920180061

Couto, E.V.D., Hayakawa, E.H. & Souza-Filho, E.E.D. 2010, 'Diagnóstico dos efeitos causados pelas cheias excepcionais de 1982/1983 sobre a planície inundacional do Alto rio Paraná (PR-MS)', *Revista de Geografia, Meio Ambiente e Ensino*, vol. 1, no. 1, pp. 83-99.

Danelichen, V.H., Machado, N.G., Biudes, M.S. & Souza, M.C. 2013, 'TRMM satellite performance in estimated rainfall over the midwest region of Brazil', *Revista Brasileira de Climatologia*, vol. 12, no. 1. http://dx.doi.org/10.5380/abclima.v12i1.31203

Davranche, A., Lefebvre, G. & Poulin, B. 2010, 'Wetland monitoring using classification trees and SPOT-5 seasonal time series', *Remote sensing of environment*, vol. 114, no. 3, pp. 552-62. https://doi.org/10.1016/j.rse.2009.10.009

Dogliotti, A.I., Ruddick, K.G., Nechad, B., Doxaran, D. & Knaeps, E. 2015, 'A single algorithm to retrieve turbidity from remotely-sensed data in all coastal and estuarine waters', *Remote Sensing of Environment*, vol. 156, pp. 157-68. https://doi.org/10.1016/j.rse.2014.09.020

Dörnhöfer, K., Klinger, P., Heege, T. & Oppelt, N. 2018, 'Multi-sensor satellite and in situ monitoring of phytoplankton development in a eutrophic-mesotrophic lake', *Science of The Total Environment*, vol. 612, pp. 1200-14. https://doi.org/10.1016/j.scitotenv.2017.08.219

Earth Observation and Environmental Services 2020, '*Earth Observation and Environmental Services'*, viewed, 1 August 2020, <http://www.eomap.com/services/water-quality/>.

EOMAP - see Earth Observation and Environmental Services.

Faye, C., Grippa, M., Kergoat, L. & Robert, E. 2020, 'Investigating the Drivers of Total Suspended Sediment Regime in the Senegal River Basin Using Landsat 8 Satellite Images', *Journal of Environmental Geography*, vol. 13, no. 1-2, pp. 31-42. https://doi.org/10.2478/jengeo-2020-0004

Fondriest Environmental Inc 2014, *Turbidity, Total Suspended Solids and Water Clarity*, Fundamentals Environmental Measurements. https://www.fondriest.com/environmental-measurements/parameters/water-quality/turbidity-total-suspended-solids-water-clarity/

Galvão, V., Stevaux, J.C. & Saad, A.R. 2014, 'Análise Geoambiental dos Ambientes da Planície Aluvial do Alto Curso do Rio Paraná: Fragilidade e Impactos Ambientais Relativos ao Desenvolvimento do Uso Turístico', *Geociências*, vol. 33, no. 3, pp. 472-91.

Garaba, S.P. & Zielinski, O. 2015, 'An assessment of water quality monitoring tools in an estuarine system', *Remote Sensing Applications: Society and Environment*, vol. 2, pp. 1-10. https://doi.org/10.1016/j.rsase.2015.09.001

Garg, V., Aggarwal, S.P. & Chauhan, P. 2020, 'Changes in turbidity along Ganga River using Sentinel-2 satellite data during lockdown associated with COVID-19', *Geomatics, Natural Hazards and Risk*, vol. 11, no. 1, pp. 1175-95. https://doi.org/10.1080/19475705.2020.1782482

Göransson, G., Larson, M. & Bendz, D. 2013, 'Variation in turbidity with precipitation and flow in a regulated river system–river Göta Älv, SW Sweden', *Hydrology and Earth System Sciences*, vol. 17, no. 7, pp. 2529-42. https://doi.org/10.5194/hess-17-2529-2013

Grimm, A.M. 1988, 'Verificação de variações climáticas na área do lago de Itaipu', *Anais do Congresso Brasileiro de Meteorologia*, Rio de Janeiro.

Güttler, F.N., Niculescu, S. & Gohin, F. 2013, 'Turbidity retrieval and monitoring of Danube Delta waters using multi-sensor optical remote sensing data: An integrated view from the delta plain lakes to the western–northwestern Black Sea coastal zone', *Remote Sensing of Environment*, vol. 132, pp. 86-101. https://doi.org/10.1016/j.rse.2013.01.009

Haibo, Y., Zongmin, W., Hongling, Z., & Yu, G. 2011, 'Water body extraction methods study based on RS and GIS', *Procedia Environmental Sciences*, vol. 10, pp. 2619-24. https://doi.org/10.1016/j.proenv.2011.09.407

Hayakawa, E.H., do Couto, E.V., de Souza Filho, E.E., do Prado, B.R. & Paula, P.F. 2010, 'Análise temporal da planície de inundação do alto rio Paraná (região de Porto Rico–PR) através de dados de sensoriamento remoto', *Boletim de Geografia*, vol. 28, no. 1, pp. 115-26. https://doi.org/10.4025/bolgeogr.v28i1.8086

Heege, T., Kiselev, V., Wettle, M. & Hung, N.N. 2014, 'Operational multi-sensor monitoring of turbidity for the entire Mekong Delta', *International Journal of Remote Sensing*, vol. 35, no. 8, pp. 2910-26. https://doi.org/10.1080/01431161.2014.890300

Heege, T., Schenk, K. & Wilhelm, M.L. 2019, 'Water Quality Information for Africa from Global Satellite Based Measurements: The Concept Behind the UNESCO World Water Quality Portal' in A. Froehlich (ed), *Space in African Society*, Southern Space Studies, Springer, pp. 81-92. https://doi.org/10.1007/978-3-030-06040-4_5

Instituto Agronômico do Paraná 2020, *Cartas climáticas do Paraná*. Londrina, viewed 20 October 2020, <http://www.iapar.br>.

Itaipu 2020, *Itaipu Binacional*, viewed 15 October 2020, <http://www.itaipu.gov.br/>.

Junk, W.J., Bayley, P.B. & Sparks, R.E. 1989, 'The flood pulse concept in river-floodplain systems', *Canadian special publication of fisheries and aquatic sciences*, vol. *106*, no. 1, pp. 110-27.

Lacaux, J.P., Tourre, Y.M., Vignolles, C., Ndione, J.A. & Lafaye, M. 2007, 'Classification of ponds from high-spatial resolution remote sensing: Application to Rift Valley Fever epidemics in Senegal', *Remote Sensing of Environment*, vol. 106, no. 1, pp. 66-74. https://doi.org/10.1016/j.rse.2006.07.012

Liu, Z. 2015, 'Comparison of precipitation estimates between Version 7 3-hourly TRMM Multi-Satellite Precipitation Analysis (TMPA) near-real-time and research products', *Atmospheric Research*, vol. 153, pp. 119-33. https://doi.org/10.1016/j.atmosres.2014.07.032

Lobo, F.L., Costa, M.P. & Novo, E.M.L.M. 2015, 'Time-series analysis of Landsat-MSS/TM/OLI images over Amazonian waters impacted by gold mining activities', *Remote Sensing of*

Environment, vol. 157, pp. 170-84. https://doi.org/10.1016/j.rse.2014.04.030

Longo, M., Camargo, R. & Silva Dias, M.A.F. 2004, 'Análise das características dinâmicas e sinóticas de um evento de friagem durante a estação chuvosa no sudoeste da Amazônia', *Revista Brasileira de Meteorologia*, vol. 19, no. 1, pp. 59-72.

Lu, S., Wu, B., Yan, N. & Wang, H. 2011, 'Water body mapping method with HJ-1A/B satellite imagery', *International Journal of Applied Earth Observation and Geoinformation*, vol. 13, no. 3, pp. 428-434. https://doi.org/10.1016/j.jag.2010.09.006

Ma, M., Wang, X., Veroustraete, F. & Dong, L. 2007, 'Change in area of Ebinur Lake during the 1998–2005 period', *International Journal of Remote Sensing*, vol. 28, no. 24, pp. 5523-5533. https://doi.org/10.1080/01431160601009698

Maliki, A.A., Chabuk, A., Sultan, M.A., Hashim, B.M., Hussain, H.M., & Al-Ansari, N. 2020, 'Estimation of Total Dissolved Solids in Water Bodies by Spectral Indices Case Study: Shatt al-Arab River', *Water, Air, & Soil Pollution*, vol. 231, no. 9, pp. 1-11. https://doi.org/10.1007/s11270-020-04844-z

Martins, V.S., Kaleita, A., Barbosa, C.C., Fassoni-Andrade, A.C., Lobo, F.L. & Novo, E.M.L.M. 2019, 'Remote sensing of large reservoir in the drought years: Implications on surface water change and turbidity variability of Sobradinho reservoir (Northeast Brazil)', *Remote Sensing Applications: Society and Environment*, vol. 13, pp. 275-88. https://doi.org/10.1016/j.rsase.2018.11.006

McFeeters, S.K. 1996, 'The use of the Normalized Difference Water Index (NDWI) in the delineation of open water features', *International Journal of Remote Sensing*, vol. 17, no. 7, pp. 1425-32. https://doi.org/10.1080/01431169608948714

Mi, H., Fagherazzi, S., Qiao, G., Hong, Y. & Fichot, C.G. 2019, 'Climate change leads to a doubling of turbidity in a rapidly expanding Tibetan lake', *Science of The Total Environment*, vol. 688, pp. 952-9. https://doi.org/10.1016/j.scitotenv.2019.06.339

Moraes, B.C., Sodré, G.R.C., Souza, E.B., Ribeiro, J.B.M., Filho, L.G.M., Ferreira, D.B.S. & Oliveira, J.V. 2015, 'Climatology of Seasonal Rainfall in the Eastern Amazon', *Revista Brasileira de Geografia Física*, Recife, vol. 8, no. 5, pp. 1359-73.

NASA - see National Aeronautics and Space Administration.

National Aeronautics and Space Administration 2018, *TRMM Instruments*, viewed 2 October 2020, <http://trmm.gsfc.nasa.gov/overview_dir/ceres.html>.

Oliveira Junior, J.F.D., Delgado, R.C., Gois, G., Lannes, A., Dias, F.O., Souza, J.C. & Souza, M. 2014, 'Análise da precipitação e sua relação com sistemas meteorológicos em Seropédica, Rio de Janeiro', *Floresta e Ambiente*, vol. 21, no. 2, pp. 140-9. http://dx.doi.org/10.4322/floram.2014.030

Ouillon, S. 2003, 'An inversion method for reflectance in stratified turbid waters', *International Journal of Remote Sensing*, vol. 24, no. 3, pp. 535-58. https://doi.org/10.1080/01431160304986

Ouni, H., Kawachi, A., Irie, M., M'Barek, N.B., Hariga-Tlatli, N. & Tarhouni, J. 2019, 'Development of water turbidity index (WTI) and seasonal characteristics of total suspended matter (TSM) spatial distribution in Ichkeul Lake, a shallow brackish wetland, Northern-East Tunisia', *Environmental Earth Sciences*, vol. 78, no. 6, pp. 1-14. https://doi.org/10.1007/s12665-019-8126-2

Pereira, G., Silva, M.E.S., Moraes, E.C. & Cardozo, F.D.S. 2013, 'Avaliação dos dados de precipitação estimados pelo satélite TRMM para o Brasil', *Revista Brasileira de Recursos Hídricos*, vol. 18, no. 3, pp. 139-148.

Pessi, D.D., Santos, C.S.A.D., Nonato, J.J., Dourado, L.G.A., Silva, O.P., Bassini, R.T., & José, J.V. 2019, 'Validação das estimativas de precipitação do satélite TRMM no Estado de Mato Grosso, Brasil', *Revista de Ciências Agrárias*, vol. 42, no. 1, pp. 81-90. https://doi.org/10.19084/RCA18217

Pinto, C.E., Menezes, P.H., Martinez, J.M., Roig, H.L. & Villar, R.A. 2014, 'Uso de imagens MODIS no monitoramento do fluxo de sedimentos no reservatório de Três Marias', *Revista Brasileira de Engenharia Agrícola e Ambiental*, vol. 18, no. 5, pp. 507-516. https://doi.org/10.1590/S1415-43662014000500007

Potes, M., Costa, M.J., & Salgado, R. 2012, 'Satellite remote sensing of water turbidity in Alqueva reservoir and implications on lake modelling', *Hydrology and Earth System Sciences*, vol. 16, no. 6, pp. 1623-33. https://doi.org/10.5194/hess-16-1623-2012

Quang, N.H., Sasaki, J., Higa, H. & Huan, N.H. 2017, 'Spatiotemporal variation of turbidity based on landsat 8 oli in cam ranh bay and thuy trieu lagoon, vietnam', *Water*, vol. 9, no. 8, p. 570. https://doi.org/10.3390/w9080570

Ribeiro Filho, R.A. 2006, 'Relações tróficas e limnológicas no reservatório de Itaipu: uma análise do impacto da biomassa pesqueira nas comunidades planctônicas', PhD Thesis, Universidade de São Paulo.

Ribeiro Filho, R.A. 2008, *Evolução histórica das relações tróficas e limnológicas no reservatório de Itaipu: efeitos top-down e bottom-up na produção pesqueira*, Relatório final de Pós-Doutorado. UNESP, Rio Claro. https://bv.fapesp.br/pt/bolsas/39226/evolucao-historica-das-relacoes-troficas-e-limnologicas-no-reservatorio-de-itaipu-efeitos-top-down/

Ribeiro Filho, R.A., Petrere Junior, M., Benassi, S.F. & Pereira, J.M.A. 2011, 'Itaipu Reservoir limnology: eutrophication degree and the horizontal distribution of its limnological variables', *Brazilian Journal of Biology*, vol. 71, no. 4, pp. 889-902. https://doi.org/10.1590/S1519-69842011000500010

Ribeiro, L.H.L., Brandimarte, A.L. & Kishi, R.T. 2005, Formation of the Salto Caxias Reservoir (PR)- an approach on the eutrophication process. *Acta Limnologica Brasiliensia*, vol. 17, no. 2, pp. 155-65.

Robert, E., Grippa, M., Kergoat, L., Pinet, S., Gal, L., Cochonneau, G. & Martinez, J. M. 2016, 'Monitoring water turbidity and surface suspended sediment concentration of the Bagre Reservoir (Burkina Faso) using MODIS and field reflectance data', *International Journal of Applied Earth Observation and Geoinformation*, vol. 52, pp. 243-51. https://doi.org/10.1016/j.jag.2016.06.016

Rocha, A.S.D. & Bade, M.R. 2018, *Geografia da bacia hidrográfica do Paraná 3: fragilidades e potencialidades socioambientais*, In House, São Paulo.

Saberioon, M., Brom, J., Nedbal, V., Souček, P. & Císař, P. 2020, 'Chlorophyll-a and total suspended solids retrieval and mapping using Sentinel-2A and machine learning for inland waters', *Ecological Indicators*, vol. 113, p. 106236. https://doi.org/10.1016/j.ecolind.2020.106236

Sagan, V., Peterson, K.T., Maimaitijiang, M., Sidike, P., Sloan, J., Greeling, B.A., Maalouf, S. & Adams, C., 2020, 'Monitoring inland water quality using remote sensing: potential and limitations of spectral indices, bio-optical simulations, machine learning, and cloud computing', *Earth-Science Reviews*, p. 103187. https://doi.org/10.1016/j.earscirev.2020.103187

Santos, L.D., Schlindwein, S.L., Fantini, A.C., Henkes, J.A. & Belderrain, M.C.N. 2020, 'Dinâmica do desmatamento da Mata Atlântica: causas e consequências', *Revista Gestão & Sustentabilidade Ambiental*, vol. 9, no. 3, pp. 378-402. http://dx.doi.org/10.19177/rgsa.v9e32020378-402

Secretaria de Estado do Meio Ambiente e Recursos Hídricos Bacias Hidrográficas do Paraná 2013, **Série Histórica**, Secretaria de Estado do Meio Ambiente e Recursos Hídricos Paraná, 2nd edn, Curitiba.

Serrão, E.A.O., Wanzeler, R.T.S., Santos, C.A., Gonçalves, L.J.M. Lima, A.M.M. & Rocha, E.J.P. 2016, 'Statistical evaluation between the constellation of precipitation estimates with GPM satellite TRMM: an analysis of the river basin Solimões', *Revista Brasileira de Climatologia*, vol. 18, pp. 256-75. http://dx.doi.org/10.5380/abclima.v18i0.43059

Sharma, A., Panigrahy, S., Singh, T.S., Patel, J.G. & Tanwar, H. 2015, 'Wetland Information system using remote sensing and GIS in Himach Pradesh, India', *Asian Journal of Geoinformatics*, vol. 14, no. 4.

Silva, A.P.D.S., Dias, H.C.T., Bastos, R.K.X. & Silva, E. 2009, 'Qualidade da água do reservatório da Usina Hidrelétrica (UHE) de Peti, Minas Gerais', *Revista Árvore*, vol. 33, no. 6, pp. 1063-69. https://doi.org/10.1590/S0100-67622009000600009

Silva, B.L., Montanher, O.C., Novo, E.M.L.M., Barbosa, C.C.F., Maciel, D.A. & Carlos, F.M. 2019, 'Relação entre o total de sólidos suspensos em corpos hídricos do alto rio paraná e imagens msi/Sentinel-2: estudo preliminar', *XIX Simpósio Brasileiro de Sensoriamento Remoto*, INPE, Santos.

Silva, J.S.V., Abdon, M.M. & Rossi, M. 2009, 'Identificação de padrões de vegetação ciliar em imagens CBERS e respectivo estado de conservação', *Geografia, Rio Claro*, vol. 34, pp. 629-41. http://www.alice.cnptia.embrapa.br/alice/handle/doc/663285

Silva, J., Neves, S.D.S. & Basotti, I.S., 2017, 'Cobertura vegetal e uso da terra na bacia hidrográfica do rio Paraná no Estado de Mato Grosso do Sul, Brasil', *Encuentro de Geografos de América Latina*, vol. 16. https://www.embrapa.br/busca-de-publicacoes/-/publicacao/1069074/cobertura-vegetal-e-uso-da-terra-na-bacia-hidrografica-do-rio-parana-no-estado-de-mato-grosso-do-sul-brasil

Singh, S., Bhardwaj, A. & Verma, V.K. 2020, 'Remote sensing and GIS based analysis of temporal land use/land cover and water quality changes in Harike wetland ecosystem, Punjab, India', *Journal of environmental management,* vol. 262, p. 110355. https://doi.org/10.1016/j.jenvman.2020.110355

Somvanshi, S., Kunwar, P., Singh, N.B. & Kachhwaha, T.S. 2011, 'Water turbidity assessment in part of Gomti River using high resolution Google Earth's Quickbird satellite data', In Geospatial World Forum, pp. 18-21.

Souza Filho, E.E. & Fragal, E.H. 2013, 'A influência do nível fluviométrico sobre as variações de área de água e da cobertura vegetal na planície do alto rio Paraná', *Revista Brasileira de Geomorfologia*, vol. 14, no. 1. http://dx.doi.org/10.20502/rbg.v14i1.378

Stevaux, J.C., Martins, D.P. & Meurer, M. 2009, 'Changes in a large regulated tropical river: The Paraná River downstream from the Porto Primavera Dam, Brazil', *Geomorphology*, vol. 113, no. 3-4, pp. 230-38. https://doi.org/10.1016/j.geomorph.2009.03.015

Toniolo, G.R., Gross, J.G., Gaida, W., Facco, D.S., Santos, F.C., Pereira Filho, W. 2019, 'Estimativa da transparência da água em uma área piloto do reservatório Itaipu por meio de dados do sensor Oli/Landsat-8', *In*: XIX Simpósio Brasileiro de Sensoriamento Remoto, INPE, Santos -SP.

Trinh, N.X., Quang, T.T., Ha, P.D., Le Xuan, T., Dinh, C.D., Thanh, T.N., Quang, T.T., Duc, T.D. & Thanh, H.N. 2018, 'Delimitating inland aqua-ecological zones under different climate conditions in the Mekong Delta region, Vietnam', *Journal of Water and Climate Change*, vol. 9, no. 3, pp. 463-79. https://doi.org/10.2166/wcc.2018.181

Vanhellemont, Q. & Ruddick, K. 2014, 'Turbid wakes associated with offshore wind turbines observed with Landsat 8', *Remote Sensing of Environment*, vol. 145, pp. 105-15. https://doi.org/10.1016/j.rse.2014.01.009

Viviano, G., Valsecchi, S., Polesello, S., Capodaglio, A., Tartari, G. & Salerno, F. 2017, 'Combined use of caffeine and turbidity to evaluate the impact of CSOs on river water quality', *Water, Air, & Soil Pollution*, vol. 228, no. 9, pp. 1-11. https://doi.org/10.1007/s11270-017-3505-3

Wachholz, F. 2011, '*Influência Da Bacia Hidrográfica E Características Espaço-Temporais de Variáveis Limnológicas Sobre Reservatórios No Rio Jacuí - RS'*, PhD Thesis, Universidade Estadual Paulista. http://hdl.handle.net/11449/104345

Wachholz, F., Pereira Filho, W. & Sartor, S.C.B. 2011, 'Influência do uso da terra e precipitação pluviométrica na formação de compartimentos aquáticos no reservatório Rodolfo Costa e Silva-RS, Brasil', Geografia, vol. 36, no. 3, pp. 551-70.

Wang, G.S., Xia, J., Zhu, Y.Z., Niu, C.W. & Tan, G. 2004, 'Distributed hydrological modeling based on nonlinear system approach', *Advances in Water Science*, vol. 15, no. 4, pp. 521-525.

Wang, H.W., Kondolf, M., Tullos, D. & Kuo, W.C. 2018, 'Sediment management in Taiwan's reservoirs and barriers to implementation', *Water*, vol. 10, no. 8, pp. 1034. https://doi.org/10.3390/w10081034

Wang, X., Gong, Z. & Pu, R. 2018, 'Estimation of chlorophyll a content in inland turbidity waters using WorldView-2 imagery: a case study of the Guanting Reservoir, Beijing, China', *Environmental monitoring and assessment*, vol. 190, no. 10, pp. 1-16. https://doi.org/10.1007/s10661-018-6978-7

Xu, H. 2006, 'Modification of normalised difference water index (NDWI) to enhance open water features in remotely sensed imagery', *International journal of remote sensing*, vol. 27, no 14, pp. 3025-3033. https://doi.org/10.1080/01431160600589179

Yanti, A., Susilo, B. & Wicaksono, P. 2016, 'The aplication of Landsat 8 OLI for total suspended solid (TSS) mapping in Gajahmungkur reservoir Wonogiri regency 2016', *IOP Conference Series: Earth and Environmental Science*, vol. 47, no. 1, p. 012028).

Yu, Y., Zhang, H. & Lemckert, C. 2014, 'Salinity and turbidity distributions in the Brisbane River estuary, Australia', *Journal of hydrology*, vol. 519, pp. 3338-52. https://doi.org/10.1016/j.jhydrol.2014.10.015

Zhang, Q. & Liu, H. 2014, 'Seasonal changes in physical processes controlling evaporation over inland water', *Journal of Geophysical Research: Atmospheres*, vol. 119, no. 16, pp. 9779-92. https://doi.org/10.1002/2014JD021797

Zhang, Y., Zhang, Y., Shi, K., Zha, Y., Zhou, Y. & Liu, M. 2016, 'A Landsat 8 OLI-based, semianalytical model for estimating the total suspended matter concentration in the slightly turbid Xin'anjiang Reservoir (China)', *IEEE journal of selected topics in applied earth observations and remote sensing*, vol. 9, no. 1, pp. 398-413. https://doi.org/10.1109/JSTARS.2015.2509469

Received: 30 January 2021

Accepted: 25 August 2021

How to cite:

Facco, D.S., Guasselli, L.A., Ruiz, L.F., Simioni, J.P.D. & Dick, D.G. 2021, 'Spectral Reflectance in the Spatial-temporal Dynamic of Turbidity, Itaipu Reservoir, Brazil', *Anuário do Instituto de Geociências,* vol. *44*: 41228. https://doi.org/10.11137/1982-3908_2021_44_41228

4 CAPÍTULO 4: COMPARISON OF PBIA AND GEOBIA CLASSIFICATION METHODS IN CLASSIFYING TURBIDITY IN RESERVOIRS

Geocarto International

ISSN: (Print) (Online) Journal homepage: https://www.tandfonline.com/loi/tgei20

Comparison of PBIA and GEOBIA classification methods in classifying turbidity in reservoirs

Douglas Stefanello Facco, Laurindo Antonio Guasselli, Luis Fernando Chimelo Ruiz, João Paulo Delapasse Simioni & Daiane Gerhardt Dick

To cite this article: Douglas Stefanello Facco, Laurindo Antonio Guasselli, Luis Fernando Chimelo Ruiz, João Paulo Delapasse Simioni & Daiane Gerhardt Dick (2021): Comparison of PBIA and GEOBIA classification methods in classifying turbidity in reservoirs, Geocarto International, DOI: 10.1080/10106049.2021.1899302

To link to this article: https://doi.org/10.1080/10106049.2021.1899302

Published online: 22 Jun 2021.

GEOCARTO INTERNATIONAL
https://doi.org/10.1080/10106049.2021.1899302

Comparison of PBIA and GEOBIA classification methods in classifying turbidity in reservoirs

Douglas Stefanello Facco[a], Laurindo Antonio Guasselli[a], Luis Fernando Chimelo Ruiz[b], João Paulo Delapasse Simioni[a] and Daiane Gerhardt Dick[c]

[a]Research Center on Remote Sensing and Meteorology (CEPSRM), Federal University of Rio Grande do Sul (UFRGS), Porto Alegre, Brazil; [b]Superior School of Agriculture "Luiz de Queiroz" (ESALQ), University of Sao Paulo (USP), Piracicaba, Brazil; [c]Hydraulic Research Institute (IPH), Federal University of Rio Grande do Sul (UFRGS), Porto Alegre, Brazil

ABSTRACT

Our goal is to compare the performance of Classification and Regression Tree, Naive Bayes and Random Forest algorithms, from supervised image classification, and approaches on Pixel-Based Image analysis (PBIA) and Geographic Object-Based Image Analysis (GEOBIA), to classify turbidity in reservoirs. Tod do so, we use Landsat 8 image and bands and spectral indices, as predictive parameters, as well as the classification algorithms based on PBIA and GEOBIA. The Brazilian Itaipu reservoir was adopted, as a case study. Our results show that the RF classifier obtained the highest accuracy in both classification approaches, followed by CART and NB. The KA and OA indices of the GEOBIA classifications were superior to the PBIA classifications in both algorithms. This study contributes with an approach to quickly and accurately delineating turbidity spectral limits in reservoirs.

ARTICLE HISTORY
Received 15 September 2020
Accepted 3 February 2021

KEYWORDS
Image segmentation; turbidity; reservoir

1. Introduction

Insufficient monitoring, low frequency of in situ collections and sample density, associated with financial, political or legal problems, have been the main obstacles (Beskow et al. 2016) for analysis of both spatial and limnological parameters of reservoirs worldwide (Alsdorf et al. 2007; Zhang and Liu 2014).

Turbidity is an eutrophication indicator that is related to Total Suspended Solids (Petus et al. 2010; Guttler et al. 2013; Cazassa et al. 2018; Pereiraand Fernandes 2018; Zhou et al. 2020). Thus, mapping and knowing turbidity patterns are tasks that can contribute to the management and monitoring of reservoirs, since they influence water quality and its useful life (WMO 2013; Potes et al. 2018; Chelotti et al. 2019; Arias-Rodriguez et al. 2020).

Turbidity gradients allow the identification of hydrologic processes of sediment transport, deposition and resuspension (Wilkes et al. 2019). In addition, identifying the sources and distribution of suspended materials allows deducing spatial information on nutrient

CONTACT Douglas Stefanello Facco douglas.s.facco@gmail.com

availability (Guttler et al. 2013) and diagnosing their behavior from remote analysis and observations.

However, a limited number of point samples show that conventional methods do not reveal the turbidity dynamics in large water bodies due to their significant heterogeneity (Zhou et al. 2020). The limitations of conventional methods, monitoring at different scales and the large extent of reservoirs require other monitoring sources (Zhang and Liu 2014; Bonansea et al. 2019; Zhou et al. 2020).

Remote sensing of water bodies demonstrates that orbital data can be complementary to traditional methods of collection (Chelotti et al. 2019; Arias-Rodriguez et al. 2020), but they are essential in situations in which there are lack of information, such as in remote areas and spaces with no in situ monitoring networks, since they reveal the interaction between solar radiation and water constituents (Alsdorf et al. 2007; Haibo et al. 2011; Zhang 2014).

Image classification methods can be efficient tools for mapping and knowing turbidity patterns. The supervised methods are based on class samples, from user-defined spectral signatures in Pixel and Geographic Object approaches (Huang et al. 2009; Blaschke 2010; Pillay et al. 2014; Wulder et al. 2018).

The Pixel-Based Image Analysis (PBIA) approach uses individual pixel spectral information and presents "salt and pepper" effect problems (Zhang et al. 2015; Yang and Chen 2017). The Geographic Object-Based Image Analysis (GEOBIA) forms homogeneous regions by segmentation and considers context and geometry of geographic objects (Mitkari et al. 2017). Non-parametric techniques are used to recognize patterns that neglect data distribution (Laliberte et al. 2011; Pande-Chhetri et al. 2017).

In reservoir waters, GEOBIA can be a valuable method, because it allows both the creation of sets of objects by different spectral heterogeneity thresholds and the adaptation of form criteria, since geometry is often not distinct (Blaschke et al. 2014), as well as it supports the use of various bands for segmentation and many classification solutions. (Zhang et al. 2010; Sun et al. 2012; Zhou et al. 2014; Shirke et al. 2016; Wu et al. 2016; Kaplan and Avdan 2017; Du et al. 2020; Mao et al. 2020; Yang et al. 2020) used GEOBIA to classify water bodies.

The spatial resolution of images is an important factor in the selection of classification techniques (Blaschke 2010). GEOBIA is superior to (PBIA) classification for high spatial resolution images (Blaschke 2010; Hossain and Chen 2019). For medium and low-resolution images, both PBIA and GEOBIA classifications are recommended (GIS Gisgeography 2020).

Data mining algorithms decrease the dimensionality of data sets and select more informative attributes for classification (Laliberte et al. 2011; Hamedianfar and Shafri 2014). It is possible to manipulate big data volumes by inserting pattern recognition methods. Machine learning automates the construction of analytical models, based on which systems can learn from data, identifying patterns and making decisions with minimal human intervention (Alpaydin 2014).

Water has high spectral similarity and the lack of in situ turbidity data generates uncertainties in its partitioning. It is a challenge to evaluate the accuracy and performance of the classification methods in the classification of turbidity from training samples and validation of algorithms. Spatial image resolution, segmentation thresholds and the most relevant attributes should be considered, as well as the PBIA and GEOBIA approaches.

This work proposes to contribute with a classification approach to quickly delineate spectral limits of turbidity in reservoirs, considering different scales of segmentation,

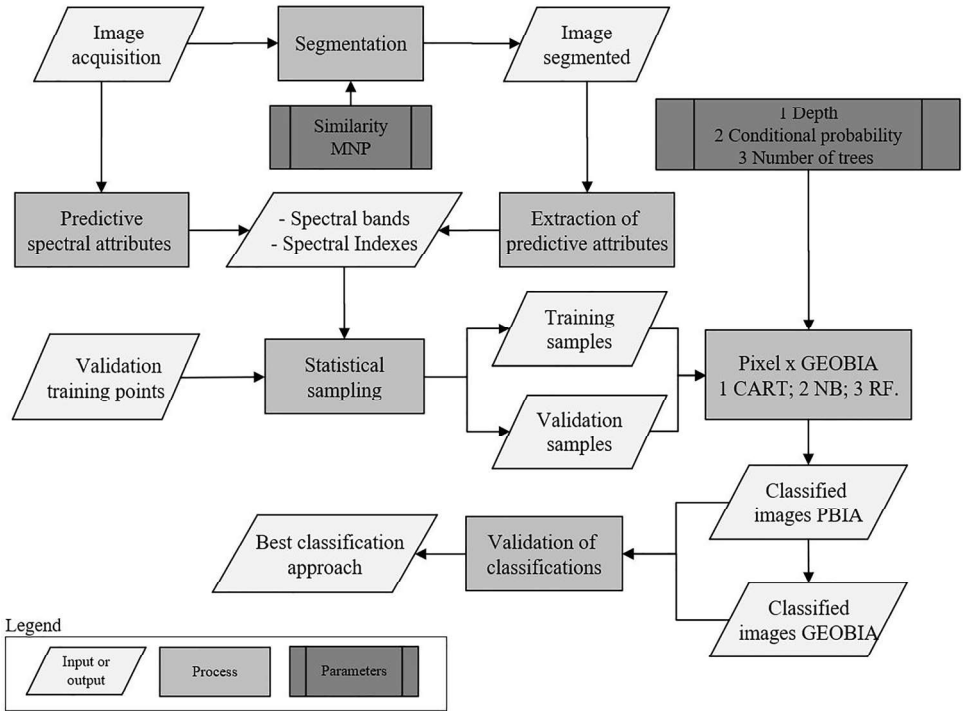

Figure 1. Methodological flowchart.

evaluating its accuracy. Our proposal points out a semi-automated and multiscale strategy, seeking greater precision to identify turbidity classes.

In this sense, our objective is to compare the performance of Classification and Regression Tree (CART), Naive Bayes (NB) and Random Forest (RF) machine learning algorithms from supervised image classification, as well as the approaches based on PBIA and GEOBIA, to classify turbidity patterns in reservoir waters.

2. Methodology

The flowchart (Figure 1) shows the methodological procedures to compare the performance of algorithms in the classification of turbidity patterns in reservoirs.

2.1. Study area

As a study area, it was adopted the Itaipu Hydroelectric Power Plant reservoir, located on the Paraná River, on the border between Brazil and Paraguay, which is part of the Paraná hydrographic basin 3. The Brazilian side has a total area of 8.707 km^2, which is around 4% of the area of the Paraná state (Bade et al. 2016).

In the South, the reservoir extends from Foz do Iguaçu (Brazil) and Ciudad del Leste (Paraguay) to the cities of Guaíra (Brazil) and Salto del Guairá (Paraguay), in the North (Figure 2). The downstream limit is given by the Itaipu dam. The reservoir is 150 km long and 7 km width (average), while its average depth is 22 m and 170 m near the dam.

Figure 2. Location map of Itaipu UHE Reservoir, on the Brazil-Paraguay border.

The minimum and maximum water levels are 197 m and 220 m, respectively. It is the seventh largest reservoir in Brazil. The flooded area is 1.350 km^2, being 770 km^2 in Brazilian territory and 580 km^2 in Paraguayan territory. The drainage area is 820.000 km^2 (Itaipu 2020).

2.2. Landsat images

It was acquired an image from Landsat 8 satellite Operational Land Imager (OLI) sensor to the date of August 27, 2016, from the USGS Earth Explorer (http://earthexplorer.usgs.gov), which was geometrically processed, considering its surface reflectance, from both Landsat Ecosystem Disturbance Adaptive Processing System (LEDAPS) and Landsat Surface Reflectance Code (LaSRC) algorithms, according to Landsat Collection 1 Level 2. OLI sensor data have been widely used in surface water detection (Du et al. 2014; Yang et al. 2015; Gao et al. 2016; Li et al. 2016; Liu et al. 2016). The choice of the image date depends on the availability of turbidity data from EOMAP company on the same date, for validation, covered in secession 2.5.

2.3. Segmentation

Segmentation at various scales is important in GEOBIA. A single scale or similarity threshold does not correctly represent different objects in the image (Hossain and Chen 2019). It is necessary to identify the specific scales for the dominant image objects in a

Table 1. Spectral attributes used for sampling.

Bands Spectral - OLI	Spectral Indexes		
Banda 2 (Blue)	Index	Equation	Sources
Banda 3 (Green)	MNDWI	(Green - SWIR)/(Green + SWIR)	(Xu 2006)
Banda 4 (Red)	NDPI	(SWIR - Green)/(SWIR + Green)	(Lacaux et al. 2007)
Banda 5 (NIR)	NDTI	(Red - Green)/(Red + Green)	(Lacaux et al. 2007)
Banda 6 (SWIR 1)	NDWI	(NIR - SWIR)/(NIR + SWIR)	(Gao 1996)
Banda 7 (SWIR 2)	NDWI2	(Green - NIR)/(Green + NIR)	(McFeeters 1996)

Legend: MNDWI - Modified Normalized Difference Water Index; NDPI - Normalized Difference Pond Index; NDTI - Normalized Difference Turbidity Index NDWI - Normalized Difference Water Index.

scene. Segmenting on various scales generates homogeneous landscape objects. In GEOBIA, the classification depends on the quality of segmentation (Su and Zhang 2017; Hossain and Chen 2019).

OLI spectral bands 1 to 7 were used on GEOBIA segmentation. Region growth was used in the QGIS 3.8 software, with GeoPatterns plugin (Ruiz 2019) and the Segmentation tool, interface to configure segmentation using the tool i.segment from the Geographic Resources Analysis Support System (GRASS-GIS) software, integrated with QGIS3. (Alves et al. 2014; Duarte et al. 2018; Ruiz 2019; Lennert et al. 2019) used GRASS-GIS segmentation to classify images, and highlighted its potential and accuracy.

To generate the geographic objects, we used a random seeds' set of pixels, analyzing the similarities with their neighbors. Pixels with similar values were grouped, forming objects (Espindola et al. 2006; Ruiz 2019).

The region growth segmentation groups a set of spatially neighboring pixels (regions). Based on spectral similarity, it is verified whether the average between two contiguous regions is consistent with a predetermined threshold. It is controlled by the similarity threshold, which varies between 0 and 1 (the higher the value, the greater the freedom of growth for the regions) (Espindola et al. 2006; Ruiz 2019). Another parameter is the minimum size of objects (the smaller the value, the smaller the generated geographical objects). Thresholds were tested from 0 to 0,2, ranging from 0,01. For scale, the minimum size of the objects was evaluated from 0 to 200, ranging from 10.

2.4. Extraction of predictive attributes

Predictive attributes represent the information of the images and facilitate the classification of these objects (Blaschke et al. 2014). The object-based approach usually adopts spectral, textural and geometric attributes.

However, this study analyzes only the water category. Water has great spectral similarity, generating uncertainties on its partitioning. Due to the large extent of the Itaipu reservoir, the complexity of analyzing only the water category requires an heterogeneous sets of rules. Also, it was used spectral attributes, relative to spectral bands and indices, derived from the ratio between bands (Table 1), in the classification. In water, textural attributes do not contribute with information, since this target do not show roughness or smoothness in remote sensing images. Water has a continuous and homogeneous feature that is distinguishable and amenable to repetition (Moreira 2005).

We obtained the individual average of the spectral attribute for each segment, in the segmentation process, by using both the GeoPatterns plugin and the Sampling tool, creating a field in the attribute table of each segment (Ruiz 2019).

2.5. Sampling for training and validation

Training and validation samples were obtained from turbidity images available by the EOMAP company on the eoApp portal. EOMAP developed algorithms to extract quantitative information in aquatic environments, using the Modular Inversion Processing (MIP) feature from Landsat 7/8, Sentinel-2 and MODIS satellites. The algorithms retrieve physical parameters from water, including correction of the Earth adjacency effect. The model contains physical and accurate implementation of the water column bidirectional effect, surface and atmosphere, and considers reflective, absorbent and dispersion properties of the water body and its limits to the atmosphere (Heege et al. 2014; Broszeit 2015; Dörnhöfer et al. 2018; EOMAP. 2020).

Some considerations are required to use EOMAP product information. MIP system data were validated with in situ data from several water bodies in the world. The turbidity model presented $R^2 = 0.73$. In situ data, which were used as "truth" to calculate correlations and relative errors, have a probability of 95% and relative error between $\sim$ 7% and $\sim$ 25% (Broszeit 2015; EOMAP. 2020).

The samples were generated in two forms, in regular and irregular grids, both well distributed and representative, in relation to the turbidity classes: (a) training, which was based on a grid of regular points with equidistance of 1 km, covering the area of the reservoir (totaling 1051 points); (b) validation, with 1000 samples of irregular turbidity distributed in the reservoir.

Both training and validation samples were divided into five classes: very low turbidity (VLT); low turbidity (LT); medium turbidity (MT); high turbidity (HT); and very high turbidity (VHT). The maximum and minimum turbidity values of the validation points were used to separate the classes from the GI geometric interval method (Wu and Rao 2006) in the Arcgis software.

2.6. Machine learning classifiers

Classification and Regression Tree (CART), Naive Bayes (NB) and Random Forest (RF) were used to evaluate machine learning algorithms performance, by means of both PBIA and GEOBIA classifications. In Google Earth Engine (GEE), the classifications with PBIA analysis unit were performed, while the classifications with the GEOBIA analysis unit in the QGis plugin GeoPatterns platform.

CART uses statistics without probabilistic premises, selecting the variables automatically (Friedl and Brodley 1997). The goal of a decision tree is to reduce the impurities of the nodes using combinations of the most informative variables that best explain the variation of the dependent variable and obtain the relevance of the input variables (Hellesen and Matikainen 2013). Both complexity and size of the tree can be controlled by the depth and number of samples, at its internal nodes (Ruiz et al. 2014). In the PBIA approach, depths from 5 to 30 were tested, ranging from 5. In GEOBIA, six depth values from 5 to 30 were tested, ranging from 5, and numbers of six child nodes 5 to 30, ranging from 5, seeking the best fit. Gini index was used to measure the impurity of the branches of the tree.

NB is a machine learning method for classification, which considers input variables as independent. For this reason, it is considered naive, since in most cases the assumption of independence of the characteristics of an instance is false (Raschka 2014). It is based on Bayes' theorem, which deals with conditional probability. That is, the probability of the occurrence of an event A, given the event B (Montgomery et al. 2004). The NB parameter for both PBIA and GEOBIA approaches was an a priori probability of the true classes.

RF or random forests, introduced by (Breiman 2001), is based on the generation of several trees that are aggregated to evaluate a classification (Breiman et al. 1984; Breiman

Table 2. Classification categories for the Kappa index.

Kappa	Quality
0.0 – 0.2	Bad
0.2 – 0.4	Reasonable
0.4 – 0.6	Good
0.6 – 0.8	Very Good
0.8 – 1.0	Excellent

Fonte: (Landis and Koch 1977).

Table 3. Turbidity classes values, number of training and validation points that were used for training and validation.

Class	Value (FTU)	No. of training points	No. of validation points
Very low turbidity (VLT)	00.00 – 16.50	628	588
Low turbidity (LT)	16.50 – 20.50	109	105
Medium turbidity (MT)	20.50 – 38.00	103	115
High turbidity (HT)	38.00 – 90.00	106	80
Very high turbidity (VHT)	> 90.00	105	112
Total of points		**1051**	**1000**

2001). It explores trained trees with the same number of samples, but with different samples entered by the user. On RF trees, it is assigned a vector of the data, according to the majority of votes from the result of the classification of each tree. Thus, the size of resources and the number of trees are important adjustment parameters that should be considered, when using the RF classifier (Wieland and Pittore 2014; Ma et al. 2015). For both PBIA and GEOBIA approaches, it were tested trees from 5 to 50, ranging from 5.

2.7. Accuracy assessment of classifications

To validate the classifications, it was applied Kappa Index (KA) and Overall Accuracy (OA) measurements (for total accuracy) and User Accuracy (UA) and Producer Accuracy (PA) (for individual accuracies) (Acharya et al. 2018).

According to (Cohen 1960; Landis and Koch 1977; Rosenfield and Fitzpatrick-Lins 1986), KA considers the actual concordance, given by overall accuracy and the concordance by chance, expressed by the product of rows and columns. It considers all the error matrix elements, rather than only those that lie on the main diagonal, that is, estimates the sum of the marginal columns and rows.

The OA is calculated by the sum of the total of correctly classified pixels, divided by the total number of pixels of the confusion matrix. The UA calculates the probability of a classified pixel, representing the category (Story and Congalton 1986; Congalton 1991). The PA indicates the probability of a reference pixel being correctly classified (Story and Congalton 1986; Congalton 1991; Gu et al. 2015).

The Table 2 presents the quality categories of the Kappa index.

3. Results

3.1. Turbidity classes

Based on the turbidity samples obtained from EOMAP data, five turbidity classes were defined for the Itaipu reservoir. These classes were used as parameters for machine learning classifiers training. Table 3 shows the values of the classes and the total of both training and validation points used in the classification.

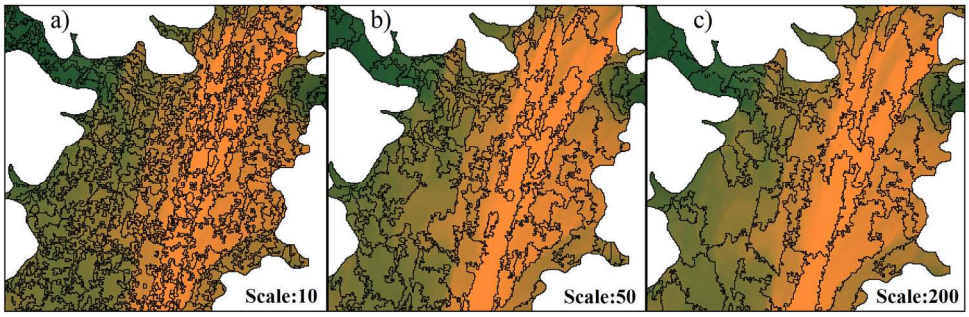

Figure 3. Example of different segmentation scales: a) Scale 10; b) Scale 50; c) Scale 200, superposed on R4G3B2 true composition, from the August 27 of 2016 Landsat OLI image, in the intermediate region of the reservoir. The blank areas on the images are not part of the flooded region of the reservoir, being other types of coverage.

Table 4. Results of the best segmentation for each classifier in the GEOBIA approach and its Similarity Threshold, Minimum Number of Pixels (MNP) and Total Number of Objects (TNO) parameters.

Best Classification	Threshold	MNP	TNO
CART	0.04	20	7885
NB	0.13	50	4319
RF	0.07	10	13609

3.2. Segmentation accuracies

It were generated 380 segmentations with different thresholds and minimum number of pixels for the reservoir area. Figure 3 presents an example of segmentation in scales 10, 50 and 200, in a section of the Itaipu reservoir.

To evaluate the influence of the segmentation parameters, we categorize the image using CART, NB and RF classifiers and determine the best accuracy. The results of the best segmentation and threshold similarity, minimum number of pixels and total number of objects parameters for each classifier, considering the GEOBIA approach, are presented in Table 4.

The RF classifier obtained the most accurate similarity threshold data set (0.07), minimum number of pixels (MNP) per segment (10), and total number of objects (TNO) (13609). CART classifier obtained the most accurate similarity threshold data set (0.04), the highest among the classifiers. However, the MNP per segment was 20 and the TNO was 7885 for CART, which is approximately half in relation to the RF. The NB achieved 0.13 as the best accuracy for similarity threshold, 50 for MNP and 4319 for TNO.

Among the similarity thresholds, the NB obtained the highest value, allowing a larger freedom of growth that represents the main factor of the highest MPN per segment (50). Thus, according to Figure 3b, of scale 50, the generated objects did not discriminate the turbidity classes, producing objects with two or even three classes for the same segment.

Both CART and NB classifiers achieved the largest MNP, 20 and 50 (Figure 4), and the smallest accuracies for KA (0.83 and 0.79 respectively) (Figure 5).

3.3. PBIA and GEOBIA classification accuracies

To analyze the potential of both PBIA and GEOBIA machine learning algorithms, it were evaluated the Kappa Index (KA), Overall Accuracy (OA), User Accuracy (UA) and Producer Accuracy (PA) variables. For PBIA ratings, KA and OA values for a 20-knot CART tree were 0.75% and 0.85% respectively; for NB, using prior probability, the values were 0.53% and

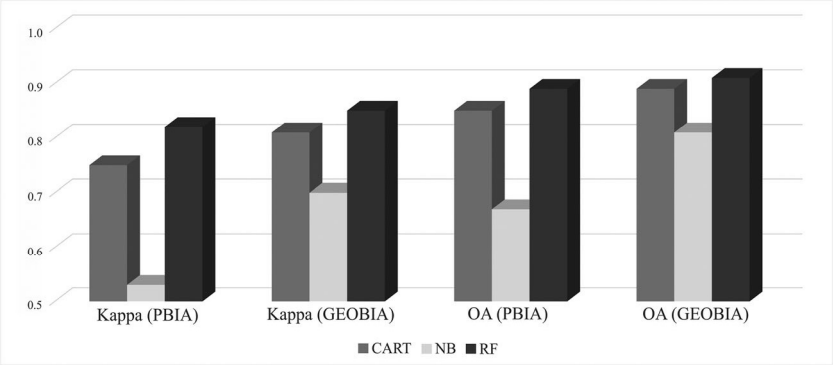

Figure 4. Graphics comparing KA and OA accuracies for both PBIA and GEOBIA classifications of CART, NB and RF sorters.

PBIA						
CART						
OA= 0.85	VLT	LT	MT	HT	VHT	UA(%)
VLT	587	46	8	5	0	0.91
LT	40	53	12	0	0	0.50
MT	0	10	74	13	0	0.76
HT	0	0	8	78	5	0.86
VHT	1	0	1	10	100	0.89
PA(%)	0.93	0.49	0.72	0.74	0.95	KA= 0.75
NAVE BAYES						
OA= 0.68	VLT	LT	MT	HT	VHT	UA(%)
VLT	429	28	5	0	0	0.93
LT	84	27	5	3	0	0.23
MT	115	54	87	14	0	0.32
HT	0	0	5	71	5	0.88
VHT	0	0	1	18	100	0.84
PA(%)	0.68	0.25	0.84	0.67	0.95	KA= 0.53
RANDOM FOREST						
OA= 0.89	VLT	LT	MT	HT	VHT	UA(%)
VLT	615	41	2	0	0	0.93
LT	13	59	11	0	0	0.71
MT	0	9	86	20	0	0.75
HT	0	0	3	82	7	0.89
VHT	0	0	1	4	98	0.95
PA(%)	0.98	0.54	0.83	0.77	0.93	KA= 0.82

GEOBIA						
CART						
OA= 0.89	VLT	LT	MT	HT	VHT	UA(%)
VLT	608	41	7	2	0	0.92
LT	15	71	10	0	0	0.74
MT	0	3	84	20	1	0.78
HT	0	0	1	77	10	0.88
VHT	0	0	0	7	94	0.93
PA(%)	0.98	0.62	0.82	0.73	0.90	KA= 0.81
NAVE BAYES						
OA= 0.81	VLT	LT	MT	HT	VHT	UA(%)
VLT	554	22	0	0	0	0.96
LT	62	39	10	3	0	0.34
MT	7	54	86	12	0	0.54
HT	0	0	6	81	11	0.83
VHT	0	0	0	10	94	0.90
PA(%)	0.89	0.34	0.84	0.76	0.90	KA= 0.70
RANDOM FOREST						
OA= 0.92	VLT	LT	MT	HT	VHT	UA(%)
VLT	640	12	0	0	0	0.98
LT	22	54	10	0	0	0.63
MT	3	6	89	3	1	0.87
HT	0	0	20	82	4	0.77
VHT	0	0	0	8	97	0.92
PA(%)	0.96	0.75	0.75	0.88	0.95	KA= 0.85

Figure 5. KA, OA, UA and PA indices' matrix of confusion for both PBIA and GEOBIA approaches, considering CART, NB and RF classifiers.

0.68%; and for RF, using 15 trees, 0.82% and 0.89%. The highest accuracy of PBIA classification was estimated by the RF classifier and the lowest, by the NB classifier.

For GEOBIA ratings, the KA and EG values for CART were 0.81 and 0.89 respectively, using a 20-node tree; for NB, using prior probability, the numbers were 0.70 and 0.81; and for RF, using 15 trees, 0.85 and 0.92. Both RF and CART also exceeded the NB algorithm, but with less discrepant results.

KA and OA values for both PBIA and GEOBIA classifications are presented in Figure 4 and the classification errors' matrix and the KA, OA, UA and PA indices for the classification methods, in Figure 5. According to Figures 4 and 5, the RF classifier obtained the highest KA and OA accuracy in the two classification approaches, followed by CART and NB, respectively.

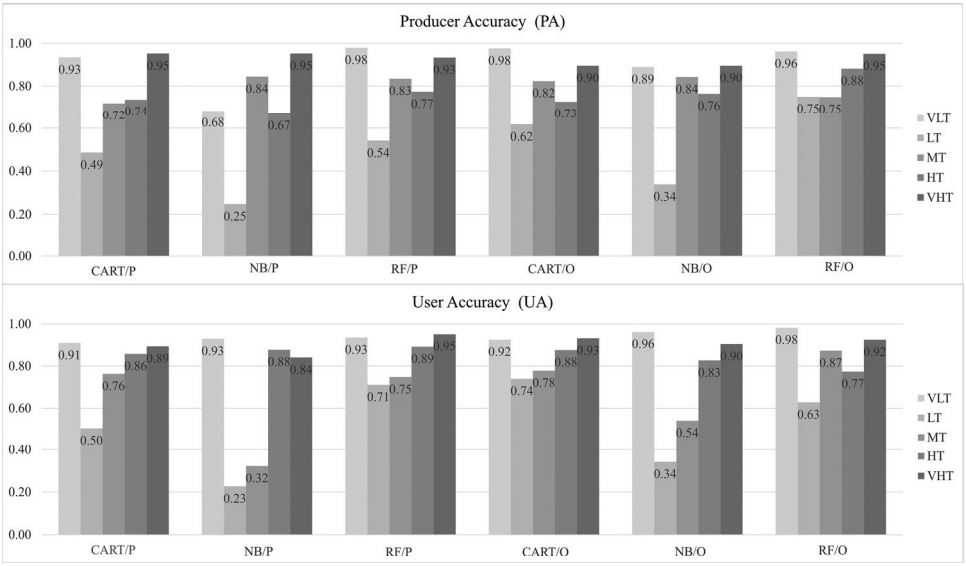

Figure 6. Graphics comparing UA and PA for VLT, LT, MT, HT and VHT classes in both PBIA (P) and GEOBIA (G) approaches.

In PA and UA estimations (Figure 6), the values for PA were over 67%, except for the LT class. In general, VLT and VHT classes presented higher precision, except for the NB/P classifier, in which MT and VHT were more precise. The LT class presented the least precision for the six methods. This is the least accuracy class, in relation to the reference values. The NB classifier had the lowest accuracy.

The best accuracy for both VLT and VHT classes were obtained by UA, indicating a higher percentage of correctness of the reference samples. In all methods, the lowest accuracy occurred for the LT class, followed by MT, except in the RF/O LT and HT classifiers. The PBIA approach classifiers had the lowest UA. We point out that the smallest PA and UA occurred in the transition values between classes, mainly between LT classes.

3.4. Turbidity classification maps

The CART, NB and RF classification models, based on both PBIA and GEOBIA, were applied to the data set with the best configuration parameters, generating thematic maps of the Itaipu reservoir for each method.

Figure 7 shows the Landsat 8 satellite OLI image (RGB 432, true color composition) and the classifications: a) CART/P; b) NB/P; c) RF/P; d) CART/O; e) NB/O; and f) RF/O. We highlight Figures 7b and 7e, NB classifier, in which NB/P classified a large area as MT, reaching down to the reservoir downstream. The most abrupt confusions of the sorter occurred in the PBIA classification.

The classifications were similar in the upstream and intermediate region of the reservoir for both CART/O and RF/O classifiers. The analysis on Figure 8 shows that the classifiers in the PBIA approach (Figures 8a–8c) produced "salt and pepper" effect noises. The GEOBIA approach showed better results.

In all classifiers, the biggest confusions occurred in both LT and MT classes, according to UA and PA (Figure 6). The intermediate region of the reservoir shows that NB misclassified the areas from LT to MT (Figure 9). We point out that the spectral response of

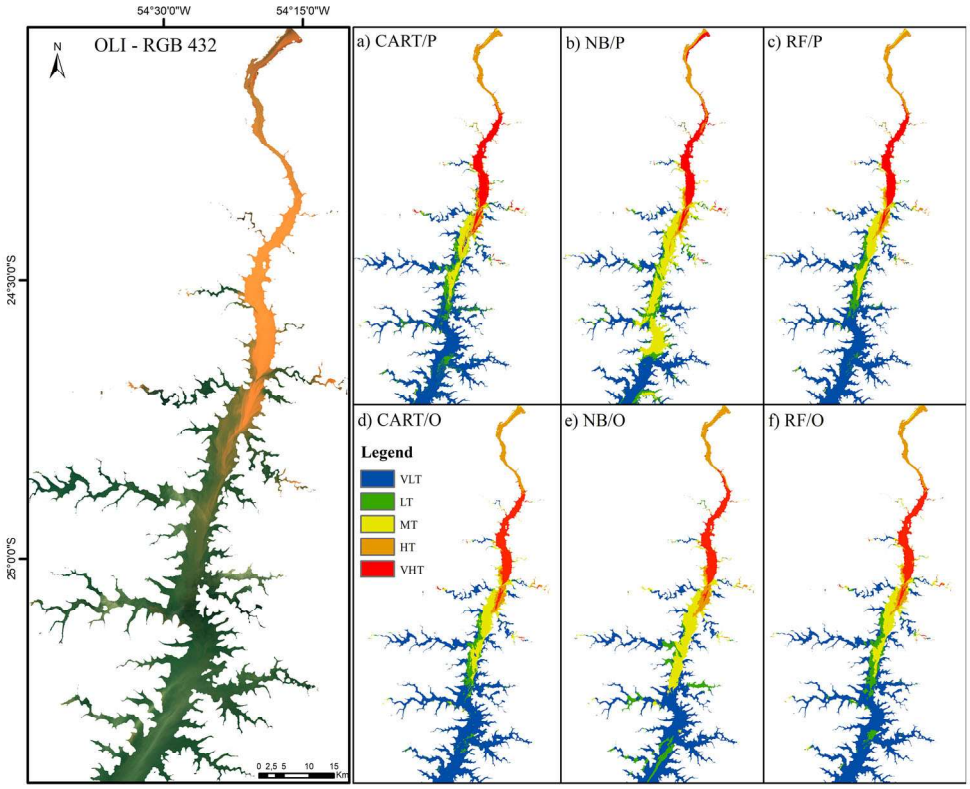

Figure 7. On the right side, the result of the classifications by methods: a) CART/P; b) NB/P; c) RF/P; d) CART/O; e) NB/O; and f) RF/O. On the left, the satellite image, with a 30-m spatial resolution, od Itaipu reservoir, on August 27, 2016. The blank areas in the images represent other types of coverage.

both LT and MT classes is very close and RF/O classifier successfully presented values closer to the validation data (Figure 9f). Both CART and NB classifiers ranked LT areas as MT in both classification approaches, accenting that NB rated a large region as MT.

In the upstream area of the reservoir, the NB classifier is the least close to the validation data in both approaches (Figure 10). Both CART/P (Figure 10a) and NB/P (Figure 10b) classified HT regions as VHT.

3.5. Most relevant spectral attributes

GEOBIA RF was the most accurate classifier. In the analysis of the most relevant attributes in the classification, at Figure 11, the five most relevant variables were Band 4 (27.9%); NDTI (17.8%); Band 3 (12.1%); NDWI (10.1%); and Band 5 (7.1%).

4. Discussion

This study evaluated the performance of classification methods using PBIA and GEOBIA spatial analysis units to identify turbidity classes in the Itaipu reservoir. One of our greatest challenges in classifying turbidity in this reservoir was the acquisition of both training and validation samples of algorithms, since the use of machine learning algorithms

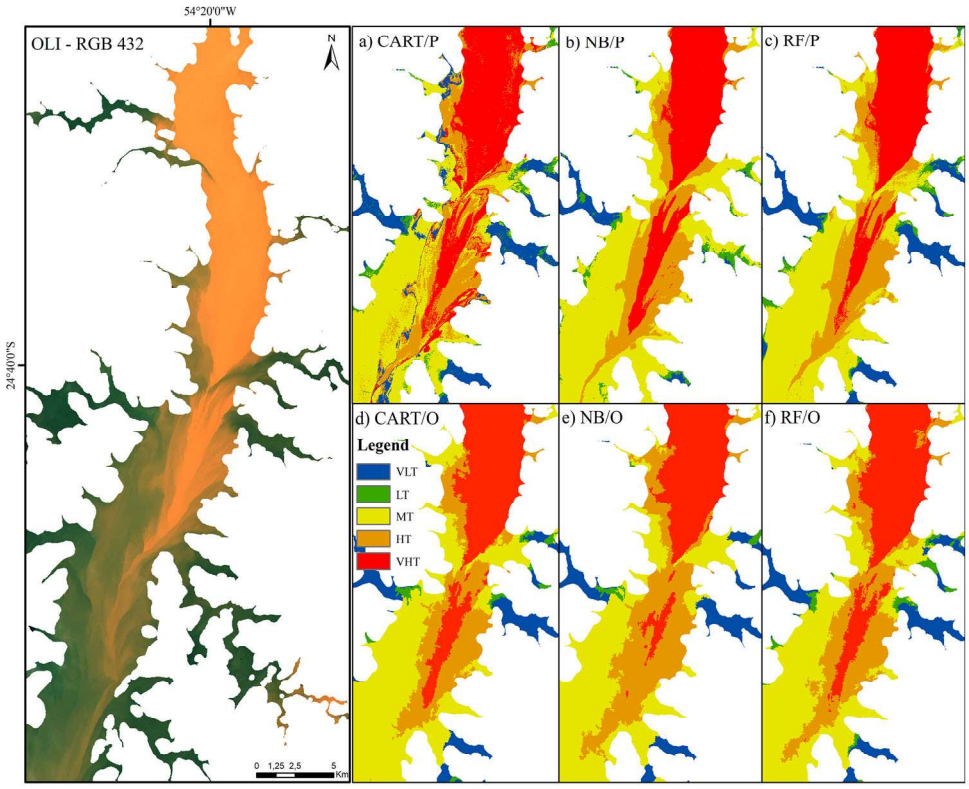

Figure 8. Result of the classifications in the transition upstream and intermediate regions, highlighting the "salt and pepper" effect from PBIA classifications: a) CART/P; b) NB/P; and c) RF/P.

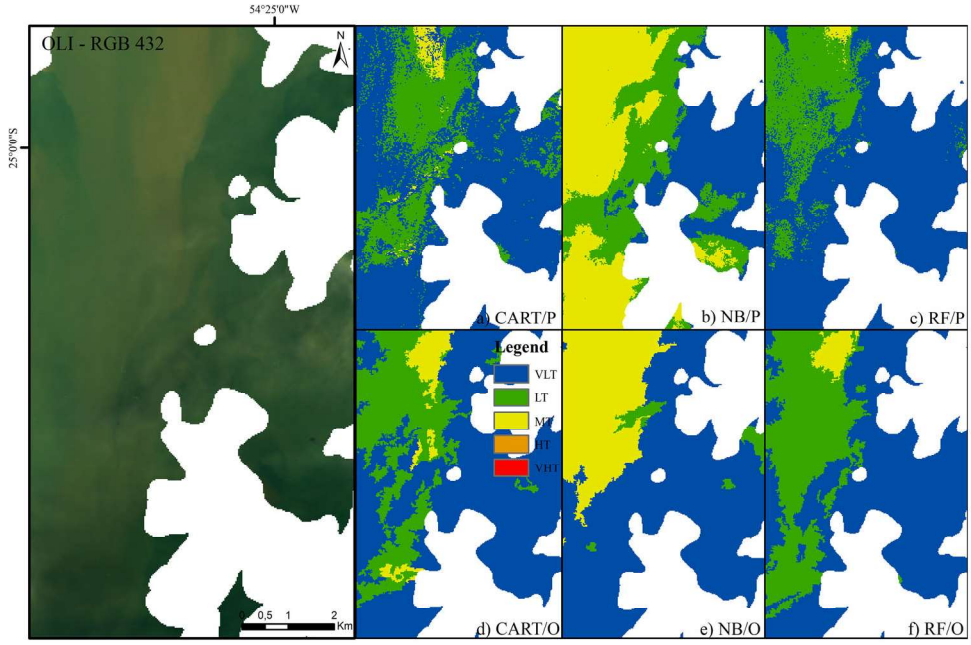

Figure 9. Result of the classifications in the intermediate region of the reservoir, highlighting that both LT and MT classes had the lower accuracy: a) CART/P; b) NB/P; c) RF/P; d) CART/O; e) NB/O; and f) RF/O.

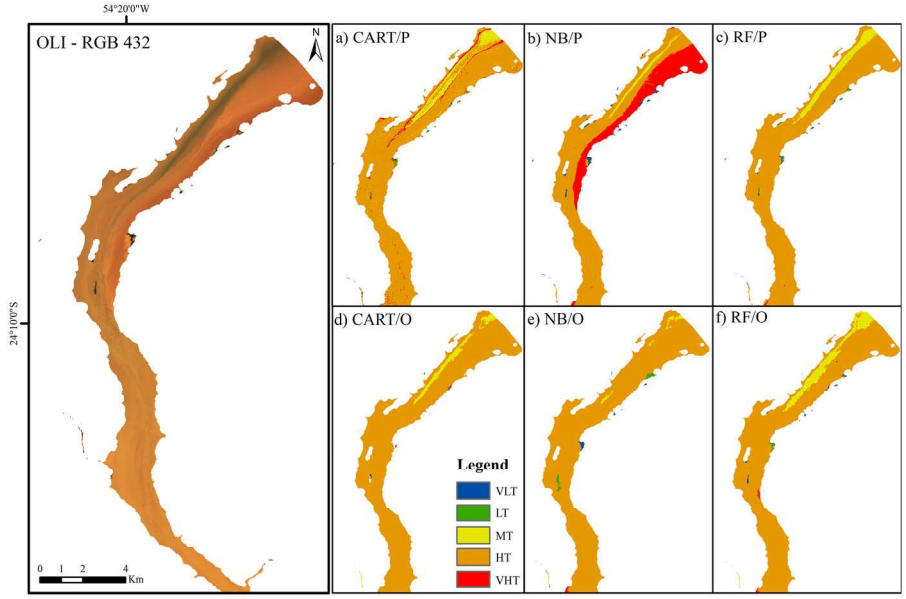

Figure 10. Result of the classifications in the region upstream of the reservoir, highlighting the NB classifier in both PBIA and GEOBIA approaches, in which it obtained the largest class confusion: b) NB/P; and e) NB/O.

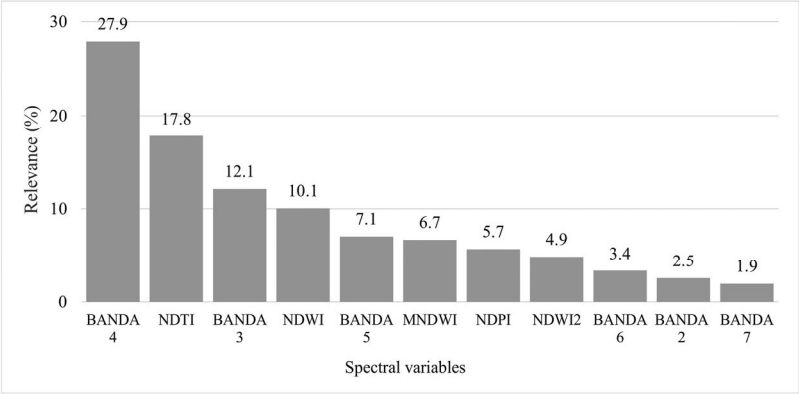

Figure 11. Graphic highlighting the most relevant spectral variables derived from the RF/O classification on Landsat 8 image.

requires a large number of samples for training and validation of classifiers (Li et al. 2014; Gong et al. 2016; Wulder et al. 2018).

Roy et al. (2014), Acharya et al. (2016), Page et al. (2019) and Wang et al. (2019) showed that the better quality of Landsat 8 OLI images, in relation to previous Landsat sensors, has allowed more accurate reservoir monitoring.

4.1. Classification methods

Separating the water class from other classes of use and coverage is generally easy. But, in this study we seek to separate turbidity classes in the water in a large reservoir. Seeking greater efficiency in this mapping, we used PBIA and GEOBIA sorters, as well as spatially

varied classification rules, to delineate the turbidity classes. For this purpose, we use a semi-automated controllable approach in different parameters, in the classification process.

In countries like Brazil, with great availability of fresh water stored in approximately 19,000 artificial reservoirs (Barbosa et al. 2019), classification methods with good accuracy can better monitor the quality of the waters.

The definition of five classes for turbidity classification was efficient and allowed the spatial representation of the Itaipu reservoir waters. However, different approaches have also been efficient to generate water classes from concentrations of optically active constituents (Reinart et al. 2003), the inherent optical properties (Mckee et al. 2007), the water color (Wernand et al. 2013), as well as classifications based only on satellite data, such as reflectance spectra (Shi et al. 2013; Shen et al. 2015; Eleveld et al. 2017; Garg et al. 2017; Jackson et al. 2017; Spyrakos et al. 2018; Uudeberg et al. 2019).

Spectral reflectance data have also been used in different approaches. Some researchers have used data in scale, while others, widely used statistical methods, as clustering and k-means (Vantrepotte et al. 2012; Shi et al. 2013; Eleveld et al. 2017; Spyrakos et al. 2018).

Our results indicate that both KA and OA indices of GEOBIA classifications were superior to PBIA classifications in the identification of turbidity classes. They softened local noise at the object level and reduced the "salt and pepper" effect of the PBIA classification. The noise reduction in the GEOBIA classification was also described in (Brauchler and Stoffels 2020; Imane et al. 2020; Liu et al. 2020; Vlachopoulos et al. 2020).

The analysis of the best performances of PBIA classification concerning the KA index analysis shows that RF was 29% more accurate than NB and 7% more accurate than CART algorithm. For the GEOBIA classifications, in the analysis of the KA index, the RF was 15% more accurate than NB and 4% more accurate than CART algorithm. The RF classifier algorithm had the best performance in both approaches. (Shaik and Srinivasan 2019; Stevenson and Bravo 2019; Wang et al. 2019) also highlighted the efficiency and higher accuracy of this sorter.

It is worth mentioning that both KA and OA indices of GEOBIA classifications were superior to the PBIA classifications for both algorithms. (Kaplan and Avdan 2017; Du et al. 2020; Mao et al. 2020; Yang et al. 2020), also highlight the GEOBIA method in classifying water bodies.

Besides the good quantity of data for model validation and training, the joint use of spectral bands and indices had a great contribution, in which the RF classifier, using the GEOBIA approach, was the most accurate.

But, we emphasize that GEOBIA classifications' accuracy was totally dependent on the various segmentation scales generated until it reached the best accuracy (Hossain and Chen 2019), providing a realistic local optical scale and a better understanding of land cover and its objects (Gonzalo-Martín et al. 2016).

Although several studies seek to identify the ideal scale for segmentation, there is still no consensus, even more considering different image objects in a scene, in the remote sensing area. The scale has a complex hierarchy, considering its multidimensional nature and variability (Malenovský et al. 2007; Wu and Li 2009; Hossain and Chen 2019).

Some studies have applied GEOBIA with spatially varied classification and machine learning techniques to very high spatial resolution images (Teodoro and Araújo 2014; Ruiz et al. 2017). These works, however, resulted in much larger MNP per segment in relation to medium-resolution multispectral images, such as Landsat 8, due to pixel size.

In our work, with medium spatial resolution images, the lower values of both similarity and MNP showed higher accuracy. However, (Teodoro and Araújo 2014; Ruiz et al. 2017)

when evaluating the segmentation of regions by growth, point out that, for very high-resolution images, there are low similarity values and MNP per segment (9), result in worst Kappa index values. They also point out that low values generate many similar objects, causing over-segmentation, which makes discrimination almost impossible. (Ruiz et al. 2017) used high resolution images and obtained better accuracy for similarity equal to 10 and MNP equal to 100.

In segmentation, the selection of a scale-based object is the key to GEOBIA. The wrong scale will lead to a super or sub-segmentation (Ming et al. 2012). Besides the problems of supersegmentation, (Teodoro and Araújo 2014; Ruiz et al. 2017) report that high MNP values per segment resulted in bad Kappa values, decreasing the classification accuracy. The behavior of high and medium resolution images are similar for high MNP values per segment.

Colkesen and Kavzoglu (2017) and Hossain and Chen (2019) report the importance of evaluating different segmentation scales in the accuracy of the classification. The heterogeneity of the segments is analyzed by the evaluation of the relation of the corresponding scale, indicating the scale levels, in which the image can be segmented in the most appropriate way, in relation to the properties, resulting in the highest accuracy.

GEOBIA classification applications have been used to extract water bodies (Zhou et al. 2014; Kaplan and Avdan 2017), improve methods to identify water bodies (Sun et al. 2012; Mao et al. 2020), generate space-time analysis (Wu et al. 2016; Du et al. 2020) and estimate the extent of water bodies (Yang et al. 2020), among others.

In the absence of turbidity data, (Mustafa and Bayat 2020) used hybrid K-SVM classification, combining unsupervised K-means clusters for training and supervising SVM classification. (Wu et al. 2014; Kar et al. 2016; Garg et al. 2017) used hyperspectral imaging classification based on spectral similarity between continuous imaging spectra and field radio spectrometer.

4.2. Turbidity mapping in reservoirs

The spatial patterns of turbidity for the image of August, 27, 2016, were satisfactorily explained by the interaction of hydrological factors, mainly river sediment discharges caused by the rains (Ribeiro Filho 2006; Ribeiro Filho et al. 2011).

Studies on turbidity in the Itaipu reservoir, between 1986 and 2008, showed higher historical averages in the reservoir upstream, or fluvial zone, with 22.6 NTU and a peak of 142 NTU, in 1990. In the intermediate region, or transition zone, the numbers were 15.9 NTU and peak of 187 NTU, in 2004. In the downstream, or lake zone, it had occurred smaller and homogeneous values of 10.9 NTU and lower value of 2 NTU.

In reservoirs, the turbidity presents very similar values between the riparian, transitional and lacustrine zones, although it presents decreasing average values in the upstream direction (Pagioro et al. 2005; Ribeiro Filho et al. 2013).

The EOMAP turbidity data proved feasible to derive harmonized and consistent water quality parameters, such as turbidity, for various types of lakes and ecological states. Studies have demonstrated the potential of MIP for long-term monitoring of lakes and reservoirs (Broszeit 2015; Dörnhöfer et al. 2016; Dörnhöfer et al. 2018; Roelfsema et al. 2018; Karle et al. 2019; León-Pérez et al. 2019; Garaba and Zielinski 2015; Lobo et al. 2015; Yanti et al. 2016; Quang et al. 2017; Shahzad et al. 2019) by mapping TSS-related turbidity in lakes and reservoirs, indicated that the red band allows the best results in turbidity prediction. So, it was no surprise that Band 4 and the NDTI spectral index were the most relevant predictive attributes in our mapping.

Other approaches have also been used, such as: NDTI spectral index (Lacaux et al. 2007; Gardelle et al. 2009; Baughman et al. 2015; Bid and Siddique 2019); empirical models in the relationship between surface feedback and concentration of optically active water components (Zhang et al. 2016; Huang et al. 2019; Liu and Wang 2019); semi-analytic models, using Inherent Optical Properties (IOP) of water (Wang 2007; Zhang et al. 2010; Zhang et al. 2018). However, establishing turbidity patterns in water bodies still remains a major challenge.

5. Conclusions

The methodological approach, which is based on machine learning classifiers, for turbidity detection that is built on Landsat 8 satellite bands and spectral indices, in the Itaipu reservoir, showed that, when comparing the performance of techniques to classify turbidity patterns in reservoir waters, the RF classifier obtained higher KA and OA values in both PBIA and GEOBIA classification approaches. But both KA and OA number for the GEOBIA classifications were better than the PBIA classifications in both algorithms. Our results showed that GEOBIA and machine learning classifiers, together with Landsat 8 and MIP validation data, were satisfactory for classifying and identifying turbidity classes. The thresholds and parameters resulting from this work can serve as guidance for other work on the same topic. In this sense, this study contributes with an approach to quickly and accurately delineate spectral turbidity limits in reservoirs, considering different segmentation scales and evaluating their accuracy. Our results suggest a semi-automated and multiscale strategy to define similarity thresholds and MNP, emphasizing that this classification strategy can support to a higher accuracy in the identification of turbidity classes in reservoirs.

Disclosure statement

No potential conflict of interest was reported by the authors.

Funding

The present work was carried out with the support of Brazilian Coordination for the Improvement of Higher-Level Personnel (CAPES) and the National Council for Scientific and Technological Development (CNPq), represented by the Research Productivity scholarship. Research Productivity Fellowship.

ORCID

Douglas Stefanello Facco http://orcid.org/0000-0002-6731-9724
Laurindo Antonio Guasselli http://orcid.org/0000-0001-8300-846X
Luis Fernando Chimelo Ruiz http://orcid.org/0000-0003-3800-6902
João Paulo Delapasse Simioni http://orcid.org/0000-0001-7426-4584
Daiane Gerhardt Dick http://orcid.org/0000-0001-5037-4404

References

Acharya TD, Lee DH, Yang IT, Lee JK. 2016. Identification of water bodies in a Landsat 8 OLI image using a J48 decision tree. Sensors. 16(7):1075.
Acharya UR, Oh SL, Hagiwara Y, Tan JH, Adeli H. 2018. Deep convolutional neural network for the automated detection and diagnosis of seizure using EEG signals. Comput Biol Med. 100(100):270–278.

Alpaydin E. 2014. Introduction to Machine Learning. 3rd ed. Cambridge, MA: The MIT Press.
Alsdorf DE, Rodríguez E, Lettenmaier DP. 2007. Measuring surface water from space. Rev Geophys. 45(2):1–24.
Alves ED, Accioly ID, Cavalcanti JE, Menezes R, da Silva EA, da Silva AB. 2014. Mudanças no uso e na cobertura do solo em uma área piloto da mesorregião agreste de Pernambuco. Geotecnologias: inovações e desenvolvimento: anais. Simpósio regional de geoprocessamento e sensoriamento remoto. Brasil (SE) Aracaju: UFS; p. 487–493.
Arias-Rodriguez LF, Duan Z, Sepúlveda R, Martinez-Martinez SI, Disse M. 2020. Monitoring water quality of Valle de Bravo reservoir, Mexico, using entire lifespan of MERIS data and machine learning approaches. Remote Sens. 12(10):1586.
Bade MR, Da RA, Da CJ, de Nóbrega MT. 2016. Compartimentação geomorfológica das bacias hidrográficas do Paraná III (Brasil/Paraguai). Rev Bras Geografia Física. 9(05):1370–1383. 2016
Barbosa CC, de Moraes Novo EM, Martins VS, editors. 2019 Apr 14. Introdução ao Sensoriamento Remoto de Sistemas Aquáticos: princípios e aplicações. São José dos Campos (São Paulo/ Brazil): Instituto Nacional de Pesquisas Espaciais.
Baughman CA, Jones BM, Bartz KK, Young DB, Zimmerman CE. 2015. Reconstructing turbidity in a glacially influenced lake using the Landsat TM and ETM + surface reflectance climate data record archive, Lake Clark, Alaska. Remote Sens. 7(10):13692–13710.
Beskow S, Timm LC, Tavares VE, Caldeira TL, Aquino LS. 2016. Potential of the LASH model for water resources management in data-scarce basins: a case study of the Fragata River basin, southern Brazil. Hydrol Sci J. 61(14):2567–2578.
Bid S, Siddique G. 2019. Identification of seasonal variation of water turbidity using NDTI method in Panchet Hill Dam, India. Model Earth Syst Environ. 5(4):1179–1122.
Blaschke T. 2010. Object based image analysis for remote sensing. ISPRS J Photogramm Remote Sens. 65(1):2–16.
Blaschke T, Hay GJ, Kelly M, Lang S, Hofmann P, Addink E, Feitosa RQ, Van der Meer F, Van der Werff H, Van Coillie F, et al. 2014. Geographic object-based image analysis - towards a new paradigm. ISPRS J Photogramm Remote Sens. 87(100):180–191.
Bonansea M, Ledesma M, Rodriguez C, Pinotti L. 2019. Using new remote sensing satellites for assessing water quality in a reservoir. Hydrol Sci J. 64(1):34–44.
Brauchler M, Stoffels J. 2020. Leveraging OSM and GEOBIA to create and update forest type maps. Int J Geo-Inform. 9(9):499.
Breiman L. 2001. Random forests. Mach Learn. 1(1):5–32.
Breiman L, Friedman JH, Olshen RA, Stone CJ. 1984. Classification and regression trees. Monterey, CA: Wadsworth.
Broszeit BS. 2015. Assessing long-term inland water quality using satellite imagery: a feasibility and validation study of different lake types [master's thesis]. Würzburg: Julius Maximilian University.
Cazassa GC, dos Santos MC, de Oliveira TG, Pereira PH, Gonçalves JA, Vieira EM. 2018. Monitoramento de desastres em rios empregando sensoriamento remoto: análise comparativa da turbidez e da reflectância no Rio Doce. Rev Ibero-Am Ciênc Ambientais. 24(9(5):308–318.
Chelotti GB, Martinez JM, Roig HL, Olivietti D. 2019. Space-temporal analysis of suspended sediment in low concentration reservoir by remote sensing. RBRH. 24:1–15.
Cohen J. 1960. A coefficient of agreement for nominal scales. Educ Psychol Meas. 20(1):37–46.
Colkesen I, Kavzoglu T. 2017. The use of logistic model tree (LMT) for pixel-and object-based classifications using high-resolution WorldView-2 imagery. Geocarto Int. 2(1):71–86.
Congalton RG. 1991. A review of assessing the accuracy of classifications of remotely sensed data. Remote Sens Environ. 37(1):35–46.
Dörnhöfer K, Göritz A, Gege P, Pflug B, Oppelt N. 2016. Water constituents and water depth retrieval from Sentinel-2A—A first evaluation in an oligotrophic lake. Remote Sens. 8(11):941.
Dörnhöfer K, Klinger P, Heege T, Oppelt N. 2018. Multi-sensor satellite and in situ monitoring of phytoplankton development in a eutrophic-mesotrophic lake. Sci Total Environ. 612(612):1200–1214.
Du Z, Li W, Zhou D, Tian L, Ling F, Wang H, Gui Y, Sun B. 2014. Analysis of Landsat-8 OLI imagery for land surface water mapping. Remote Sens Lett. 5(7):672–681.
Du B, Wang Z, Mao D, Li H, Xiang H. 2020. Tracking lake and reservoir changes in the nenjiang watershed, northeast China: patterns, trends, and drivers. Water. 12(4):1108.
Duarte L, Silva P, Teodoro AC. 2018. Development of a QGIS plugin to obtain parameters and elements of plantation trees and vineyards with aerial photographs. ISPRS Int J Geo-Inf. 7(3):109.
Eleveld MA, Ruescas AB, Hommersom A, Moore TS, Peters SW, Brockmann C. 2017. An optical classification tool for global lake waters. Remote Sens. 9(5):420.

EOMAP. 2020. Viewed 1 August 2020, http://www.eomap.com/services/water-quality/.
Espindola GM, Câmara G, Reis IA, Bins LS, Monteiro AM. 2006. Parameter selection for region-growing image segmentation algorithms using spatial autocorrelation. Int J Remote Sens. 27(14):3035–3040.
Friedl MA, Brodley CE. 1997. Decision tree classification of land cover from remotely sensed data. Remote Sens Environ. 61(3):399–409.
Gao BC. 1996 Dec 1. NDWI-A normalized difference water index for remote sensing of vegetation liquid water from space. Remote Sens Environ. 58(3):257–266.
Gao H, Wang L, Jing L, Xu J. 2016. An effective modified water extraction method for Landsat-8 OLI imagery of mountainous plateau regions. IOP Conf Ser: Earth Environ Sci. 34(1):012010. 2016.
Garaba SP, Zielinski O. 2015. An assessment of water quality monitoring tools in an estuarine system. Remote Sens Appl: Soc Environ. 2(2):1–0.
Gardelle J, Hiernaux P, Kergoat L, Grippa M. 2009. Less rain, more water in ponds: a remote sensing study of the dynamics of surface waters from 1950 to present in pastoral Sahel (Gourma region, Mali). Hydrol Earth Syst Sci Discuss. 6(4):309–324.
Garg V, Kumar AS, Aggarwal SP, Kumar V, Dhote PR, Thakur PK, Nikam BR, Sambare RS, Siddiqui A, Muduli PR, Rastogi G. 2017. Spectral similarity approach for mapping turbidity of an inland waterbody. J Hydrol. 550(550):527–537.
GIS Geography. 2020. Image classification techniques in remote sensing. Available from: https://gisgeography.com/image-classification-techniques-remote-sensing/.
Gong P, Yu L, Li C, Wang J, Liang L, Li X, Ji L, Bai Y, Cheng Y, Zhu Z. 2016. A new research paradigm for global land cover mapping. Ann GIS 22(2):87–102.
Gonzalo-Martín C, Lillo-Saavedra M, Menasalvas E, Fonseca-Luengo D, García-Pedrero A, Costumero R. 2016. Local optimal scale in a hierarchical segmentation method for satellite images. J Intell Inf Syst. 146(3):517–529.
Gu J, Congalton RG, Pan Y. 2015 Jan. The impact of positional errors on soft classification accuracy assessment: a simulation analysis. Remote Sens. 7(1):579–599.
Guttler FN, Niculescu S, Gohin F. 2013. Turbidity retrieval and monitoring of Danube Delta waters using multi-sensor optical remote sensing data: an integrated view from the delta plain lakes to the western–-northwestern Black Sea coastal zone. Remote Sens Environ. 132(132):86–101.
Haibo Y, Zongmin W, Hongling Z, Yu G. 2011. Water body extraction methods study based on RS and GIS. Procedia Environ Sci. 10(10):2619–2624.
Hamedianfar A, Shafri HZ. 2014. Development of fuzzy rule-based parameters for urban object-oriented classification using very high resolution imagery. Geocarto Int. 3(3):268–292.
Heege T, Kiselev V, Wettle M, Hung NN. 2014. Operational multi-sensor monitoring of turbidity for the entire Mekong Delta. Int J Remote Sens. 18(8):2910–2926.
Hellesen T, Matikainen L. 2013. An object-based approach for mapping shrub and tree cover on grassland habitats by use of LiDAR and CIR orthoimages. Remote Sens. 5(2):558–583.
Hossain MD, Chen D. 2019. Segmentation for Object-Based Image Analysis (OBIA): a review of algorithms and challenges from remote sensing perspective. ISPRS J Photogramm Remote Sens. 150(150): 115–134.
Huang CC, Lai YG, Lai JS, Tan YC. 2019. Field and numerical modeling study of turbidity current in Shimen Reservoir during typhoon events. J Hydraul Eng. 1(5):05019003.
Huang SL, Wang SH, Budd WW. 2009. Sprawl in Taipei's peri-urban zone: responses to spatial planning and implications for adapting global environmental change. Landscape Urban Plann. 90(1–2):20–32. 15
Imane S, Mohamed R, Mustapha H. 2020. A comparison of GEOBIA Vs PBIA machine learning methods for lithological mapping using Sentinel 2 imagery: case study of Skhour Rehamna, Morocco. In: IEEE International Conference of Moroccan Geomatics (Morgeo). Vol. 11; p. 1–6.
Itaipu. 2020. Bacia do Rio Paraná. [Accessed 2020 Dec 09] https://www.itaipu.gov.br/energia/bacia-do-rio-parana
Jackson T, Sathyendranath S, Mélin F. 2017. An improved optical classification scheme for the ocean colour essential climate variable and its applications. Remote Sens Environ. 203(203):152–161.
Kaplan G, Avdan U. 2017. Object-based water body extraction model using Sentinel-2 satellite imagery. Eur J Remote Sens. 1(1):137–143.
Kar S, Rathore VS, Champati Ray PK, Sharma R, Swain SK. 2016 Jun 1. Classification of river water pollution using Hyperion data. J Hydrol. 537:221–233.
Karle N, Wolf T, Heege T, Schenk K, Klinger P, Schulz K. 2019. Satellite remote sensing of chlorophyll and Secchi depth for monitoring lake water quality: a validation study. In: Earth Resources and Environmental Remote Sensing/GIS Applications X 3. Vol. 11156; p. 111561Q.

Lacaux JP, Tourre YM, Vignolles C, Ndione JA, Lafaye M. 2007. Classification of ponds from high-spatial resolution remote sensing: application to Rift Valley Fever epidemics in Senegal. Remote Sens Environ. 15(1):66–74.
Laliberte AS, Goforth MA, Steele CM, Rango A. 2011. Multispectral remote sensing from unmanned aircraft: image processing workflows and applications for rangeland environments. Remote Sens. 3(11): 2529–2551.
Landis JR, Koch GG. 1977. An application of hierarchical kappa-type statistics in the assessment of majority agreement among multiple observers. Biometrics. 33(2):363–374.
Lennert M, Grippa T, Radoux J, Bassine C, Beaumont B, Defourny P, Wolff E. 2019. Creating Wallonia's new very high resolution land cover maps: combining grass GIS Obia and OTB pixel-based results. Int Arch Photogramm Remote Sens Spatial Inf Sci. XLII-4/W14:151–157.
León-Pérez MC, Hernández WJ, Armstrong RA. 2019. Characterization and distribution of seagrass habitats in a Caribbean nature reserve using high-resolution satellite imagery and field sampling. J Coastal Res. 35(5):937–947.
Li Y, Gong X, Guo Z, Xu K, Hu D, Zhou H. 2016. An index and approach for water extraction using Landsat–OLI data. Int J Remote Sens. 17(16):3611–3635.
Li C, Wang J, Wang L, Hu L, Gong P. 2014. Comparison of classification algorithms and training sample sizes in urban land classification with Landsat thematic mapper imagery. Remote Sens. 6(2):964–983.
Liu B, Du S, Du S, Zhang X. 2020. Incorporating deep features into GEOBIA paradigm for remote sensing imagery classification: a patch-based approach. Remote Sens. 12(18):3007.
Liu LW, Wang YM. 2019. Modelling reservoir turbidity using landsat 8 satellite imagery by gene expression programming. Water. 11(7):1479.
Liu Z, Yao Z, Wang R. 2016. Assessing methods of identifying open water bodies using Landsat 8 OLI imagery. Environ Earth Sci. 1(75(10):873.
Lobo FL, Costa MP, Novo EM. 2015. Time-series analysis of Landsat-MSS/TM/OLI images over Amazonian waters impacted by gold mining activities. Remote Sens Environ. 157:170–184. 1
Ma X, Guo J, Sun X. 2015. Sequence-based prediction of RNA-binding proteins using random forest with minimum redundancy maximum relevance feature selection. Biomed Res Int. 2015:425810.
Malenovský Z, Bartholomeus HM, Acerbi-Junior FW, Schopfer JT, Painter TH, Epema GF, Bregt AK. 2007. Scaling dimensions in spectroscopy of soil and vegetation. Int J Appl Earth Obs Geoinf. 1(2): 137–164. 9
Mao D, Wang Z, Du B, Li L, Tian Y, Jia M, Zeng Y, Song K, Jiang M, Wang Y. 2020. National wetland mapping in China: a new product resulting from object-based and hierarchical classification of Landsat 8 OLI images. ISPRS J Photogramm Remote Sens. 164:11–25. 1
McKee D, Cunningham A, Dudek A. 2007. Optical water type discrimination and tuning remote sensing band-ratio algorithms: application to retrieval of chlorophyll and Kd (490) in the Irish and Celtic Seas. Estuarine Coastal Shelf Sci. 73(3–4):827–834. 1
McFeeters SK. 1996. The use of the Normalized Difference Water Index (NDWI) in the delineation of open water features. Internat J Remote Sens. 17(7):1425–1432.
Ming D, Ci T, Cai H, Li L, Qiao C, Du J. 2012. Semivariogram-based spatial bandwidth selection for remote sensing image segmentation with mean-shift algorithm. IEEE Geosci Remote Sens Lett. 13(9(5): 813–817.
Mitkari KV, Arora MK, Tiwari RK. 2017. Extraction of glacial lakes in gangotri glacier using object-based image analysis. IEEE J Sel Top Appl Earth Obs Remote Sens. 1(12):5275–5283.
Montgomery DC, Runger GC, Hubele NF. 2004. Data summary and presentation. Eng Stat. 3:18–22.
Moreira MA. 2005. Fundamentos do Sensoriamento Remoto e Metodologias de Aplicação. 3a edição. Viçosa: Editora UFV.
Mustafa FA, Bayat O. 2020. Knowledge technologies based on fabrication process composite materials and remote sensing applications. Adv Compos Lett. 29:2633366X19895989.
Page BP, Olmanson LG, Mishra DR. 2019. A harmonized image processing workflow using Sentinel-2/MSI and Landsat-8/OLI for mapping water clarity in optically variable lake systems. Remote Sens Environ. 231:111284. 15
Pagioro TA, Roberto MD, Thomaz SM, Pierini SA, Taka M, 2005. Zonação longitudinal das variáveis limnológicas abióticas em reservatórios. In: Rodrigues L, Thomaz SM, Agostinho AA, Gomes, LC, editors. Biocenoses em reservatórios: padrões espaciais e temporais. São Carlos: RiMa; p. 39–46.
Pande-Chhetri R, Abd-Elrahman A, Liu T, Morton J, Wilhelm VL. 2017. Object-based classification of wetland vegetation using very high-resolution unmanned air system imagery. Eur J Remote Sens. 1(1): 564–576.

Petus C, Chust G, Gohin F, Doxaran D, Froidefond JM, Sagarminaga Y. 2010. Estimating turbidity and total suspended matter in the Adour River plume (South Bay of Biscay) using MODIS 250-m imagery. Cont Shelf Res. 30(5):379–392. 30

Pillay K, Agjee NH, Pillay S. 2014. Modelling changes in land cover patterns in Mtunzini, South Africa using satellite imagery. J Indian Soc Remote Sens. 1(1):51–60.

Potes M, Rodrigues G, Penha AM, Novais MH, Costa MJ, Salgado R, Morais MM. 2018. Use of Sentinel 2–MSI for water quality monitoring at Alqueva reservoir, Portugal. Proc Int Assoc Hydrol Sci. 380: 73–79.

Quang N, Sasaki J, Higa H, Huan N. 2017. Spatiotemporal variation of turbidity based on landsat 8 oli in Cam Ranh Bay and Thuy Trieu lagoon, Vietnam. Water. 9(8):570.

Raschka S. 2014. Naive bayes and text classification i-introduction and theory. arXiv preprint arXiv: 1410.5329. https://scholar.google.com/scholar_lookup?hl=en&publication_year=2014&author=S.+Raschka&title=Naive+Bayes+and+text+classification+I+-+Introduction+and+theory

Reinart A, Herlevi A, Arst H, Sipelgas L. 2003. Preliminary optical classification of lakes and coastal waters in Estonia and south Finland. J Sea Res. 49(4):357–366.

Ribeiro Filho RA, Petrere Junior M, Benassi SF, Pereira JM. 2011. Itaipu Reservoir limnology: eutrophication degree and the horizontal distribution of its limnological variables. Braz J Biol. 71(4):889–902.

Ribeiro Filho R, Julia Myriam de Almeida P, Miguel Petrere J, Simone Frederigi B. 2013. Eutrophication indexes used as fish production parameters in the Itaipu Reservoir (Brazil). J Environ Prot. 9:2013.

Ribeiro Filho R. 2006. Relações tróficas e limnológicas no reservatório de Itaipu: uma análise do impacto da biomassa pesqueira nas comunidades planctônicas [master's thesis]. São Paulo: Universidade de São Paulo.

Roelfsema C, Kovacs E, Ortiz JC, Wolff NH, Callaghan D, Wettle M, Ronan M, Hamylton SM, Mumby PJ, Phinn S. 2018. Coral reef habitat mapping: a combination of object-based image analysis and ecological modelling. Remote Sens Environ. 208(208):27–41.

Rosenfield GH, Fitzpatrick-Lins K. 1986. A coefficient of agreement as a measure of thematic classification accuracy. Photogramm Eng Remote Sens. 52(2):223–227.

Roy DP, Wulder MA, Loveland TR, C.E W, Allen RG, Anderson MC, Helder D, Irons JR, Johnson DM, Kennedy R, et al. 2014 Apr 5. Landsat-8: science and product vision for terrestrial global change research. Remote Sens Environ. 145:154–172.

Ruiz LF, Caten AT, Dalmolin RS. 2014. Árvore de decisão e a densidade mínima de amostras no mapeamento da cobertura da terra. Cienc Rural. 44(6):1001–1007.

Ruiz LF, Guasselli LA, Caten AT. 2017. Object based analysis and decision tree for the classification of submetrical spatial resolution images captured by UAV. Bol Ciênc Geod. 23(2):252–267.

Ruiz LF. 2019. Proposed object-based classification and postclassification of land cover and use by unmanned aerial vehicle images [master's thesis]. Porto Alegre: Federal University of Rio Grande do Sul.

Shahzad A, Kazmi SJ, bin Farhan S, Shaikh S, Aziz A, Khan HU, Ahmed AF, Ahmed F. 2019. Mapping turbidity levels in the lake's water using satellite remote sensing technique. Int J Econ Environ Geol. 15:40–43.

Shaik AB, Srinivasan S. 2019. A brief survey on random forest ensembles in classification model. In: International Conference on Innovative Computing and Communications. Singapore: Springer; p. 253–260.

Shen Q, Li J, Zhang F, Sun X, Li J, Li W, Zhang B. 2015. Classification of several optically complex waters in China using in situ remote sensing reflectance. Remote Sens. 7(11):14731–14756.

Shi K, Li Y, Li L, Lu H, Song K, Liu Z, Xu Y, Li Z. 2013. Remote chlorophyll-a estimates for inland waters based on a cluster-based classification. Sci Total Environ. 444:1–5.

Shirke S, Pinto SM, Kushwaha VK, Mardikar T, Vijay R. 2016. Object-based image analysis for the impact of sewage pollution in Malad Creek, Mumbai, India. Environ Monit Assess. 1(2):95. 188

Spyrakos E, O'Donnell R, Hunter PD, Miller C, Scott M, Simis SGH, Neil C, Barbosa CCF, Binding CE, Bradt S, et al. 2018. Optical types of inland and coastal waters. Limnol Oceanogr. 63(2):846–870.

Stevenson M, Bravo C. 2019. Advanced turbidity prediction for operational water supply planning. Decis Support Syst. 119(119):72–84.

Story M, Congalton RG. 1986. Accuracy assessment: a user's perspective. Photogramm Eng Remote Sens. 1(3):397–399.

Su T, Zhang S. 2017. Winter wheat mapping using landsat 8 images and geographic object-based image analysis. Transactions of the ASABE. 60(3):625–633. 2017

Sun F, Sun W, Chen J, Gong P. 2012. Comparison and improvement of methods for identifying waterbodies in remotely sensed imagery. Int J Remote Sens. 10(21):6854–6875.

Teodoro AC, Araújo R. 2014. Exploration of the OBIA methods available in SPRING non-commercial software to UAV data processing. In: Earth resources and environmental remote sensing/GIS applications. Vol. 9245. Amsterdam (Netherlands): International Society for Optics and Photonics; p. 92451F.
Uudeberg K, Ansko I, Põru G, Ansper A, Reinart A. 2019. Using optical water types to monitor changes in optically complex inland and coastal waters. Remote Sens. 11(19):2297.
Vantrepotte V, Loisel H, Dessailly D, Mériaux X. 2012. Optical classification of contrasted coastal waters. Remote Sens Environ. 123:306–323. 1
Vlachopoulos O, Leblon B, Wang J, Haddadi A, LaRocque A, Patterson G. 2020. Delineation of crop field areas and boundaries from UAS imagery using PBIA and GEOBIA with random forest classification. Remote Sens. 12(16):2640.
Wang M. 2007 Mar. Remote sensing of the ocean contributions from ultraviolet to near-infrared using the shortwave infrared bands: simulations. Appl Opt. 46(9):1535–1547. 20
Wang D, Ronghua M, Xue K, Li J. 2019. Improved atmospheric correction algorithm for Landsat 8–OLI data in turbid waters: a case study for the Lake Taihu. Opt Express. 27(20):A1400–18. 30
Wang C, Shu Q, Wang X, Guo B, Liu P, Li Q. 2019. A random forest classifier based on pixel comparison features for urban LiDAR data. ISPRS J Photogramm Remote Sens. 148:75–86. 1
Wernand MR, Hommersom A, van der Woerd HJ. 2013. MERIS-based ocean colour classification with the discrete Forel-Ule scale. Ocean Sci. 1(3):477.
Wieland M, Pittore M. 2014 Apr. Performance evaluation of machine learning algorithms for urban pattern recognition from multi-spectral satellite images. Remote Sens. 6(4):2912–2939.
Wilkes MA, Gittins JR, Mathers KL, Mason R, Casas–Mulet R, Vanzo D, Mckenzie M, Murray–Bligh J, England J, Gurnell A, et al. 2019. Physical and biological controls on fine sediment transport and storage in rivers. Wiley Interdiscip Rev Water. 6(2):e1331.
WMO (World Meteorological Organization). 2013. Planning of water quality monitoring systems. Geneva (Switzerland): Chair, Publications Board World Meteorological Organization (WMO).
Wu P, Cai N, Chen Q, Jiang C, Wu Y, Li J. 2016. Water area annual variations of nine plateau lakes in Yunnan province, China: a brief spatiotemporal analysis with landsat time series. In: International Geoscience and Remote Sensing Symposium (IGARSS). Vol. 10; p. 6233–6236.
Wu H, Li ZL. 2009. Scale issues in remote sensing: a review on analysis, processing and modeling. Sensors (Basel)). 9(3):1768–1793.
Wu W, Rao SS. 2006. Fuzzy analysis of geometric tolerances using interval method. Proc Inst Mech Eng, Part C: J Mech Eng Sci. 1(4):489–497.
Wu LC, Zarnescu L, Nangia V, Cam B, Camarillo DB. 2014 Apr 25. A head impact detection system using SVM classification and proximity sensing in an instrumented mouthguard. IEEE Trans Biomed Eng. 61(11):2659–2668.
Wulder MA, Coops NC, Roy DP, White JC, Hermosilla T. 2018. Land cover 2.0. Int J Remote Sens. 18(12):4254–4284.
Xu H. 2006. Modification of normalised difference water index (NDWI) to enhance open water features in remotely sensed imagery. Internat J Remote Sens. 20;27(14):3025–3033.
Yang X, Chen L. 2017. Evaluation of automated urban surface water extraction from Sentinel-2A imagery using different water indices. J Appl Remote Sens. 11(2):026016.
Yang Y, Liu Y, Zhou M, Zhang S, Zhan W, Sun C, Duan Y. 2015. Landsat 8 OLI image based terrestrial water extraction from heterogeneous backgrounds using a reflectance homogenization approach. Remote Sens Environ. 171(171):14–32.
Yang X, Qin Q, Yésou H, Ledauphin T, Koehl M, Grussenmeyer P, Zhu Z. 2020. Monthly estimation of the surface water extent in France at a 10-m resolution using Sentinel-2 data. Remote Sens Environ. 244(244):111803.
Yanti A, Susilo B, Wicaksono P. 2016. The aplication of Landsat 8 OLI for total suspended solid (TSS) mapping in Gajahmungkur reservoir Wonogiri regency. IOP Conf Ser: Earth Environ Sci. 47(1): 012028.
Zhang Y, Cao G, Li X, Wang B. 2018. Cascaded random forest for hyperspectral image classification. IEEE J Sel Top Appl Earth Obs Remote Sens. 16(4):1082–1094.
Zhang G, Jia X, Hu J. 2015. Superpixel-based graphical model for remote sensing image mapping. IEEE Trans Geosci Remote Sens. 853(11):5861–5871.
Zhang Q, Liu H. 2014. Seasonal changes in physical processes controlling evaporation over inland water. J Geophys Res: Atmos. 27(16):9779–9792.
Zhang Y, Shi K, Zhang Y, Moreno-Madrinan MJ, Li Y, Li N. 2018. A semi-analytical model for estimating total suspended matter in highly turbid waters. Opt Express. 24(26):34094–34112.

Zhang M, Tang J, Dong Q, Song Q, Ding J. 2010 Feb 15. Retrieval of total suspended matter concentration in the Yellow and East China Seas from MODIS imagery. Remote Sens Environ. 114(2):392–403.
Zhang Y, Zhang Y, Shi K, Zha Y, Zhou Y, Liu M. 2016. A Landsat 8 OLI-based, semianalytical model for estimating the total suspended matter concentration in the slightly turbid Xin'anjiang Reservoir (China). IEEE J Sel Top Appl Earth Obs Remote Sens. 9(1):398–413.
Zhang T, Li Q, Yang X, Zhou C, Su F. 2010 Jun 18–20. Automatic mapping aquaculture in coastal zone from TM imagery with OBIA approach. 18th International Conference on Geoinformatics, Beijing, China; p. 1–4.
Zhou YN, Luo J, Shen Z, Hu X, Yang H. 2014. Multiscale water body extraction in urban environments from satellite images. IEEE J Sel Top Appl Earth Obs Remote Sens. 7(10):4301–4312. 2
Zhou B, Shang M, Feng L, Shan K, Feng L, Ma J, Liu X, Wu L. 2020. Long-term remote tracking the dynamics of surface water turbidity using a density peaks-based classification: a case study in the Three Gorges Reservoir, China. Ecol Indic. 116(116):106539.

5 CAPÍTULO 5: A TIMELY EFFICIENT AND ROBUST MULTI-SOURCE AND MULTI-TEMPORAL ROUTINE FOR DETERMINATION OF SURFACE WATER AREA IN LARGE WATER RESERVOIRS

MedCrave
Step into the World of Research

International Journal of Hydrology

Research Article

Open Access

CrossMark

A timely efficient and robust multi-source and multi-temporal routine for determination of surface water area in large water reservoirs

Abstract

The Brazilian electrical system has gone through conflicts resulting from recent water crisis. Timely indicators are crucial for properly acting in order to mitigate upcoming problems. In this work we evaluate the potential of Reservoir Water Level (RWL) and Surface Water Area (SWA) indices for estimating physical parameters in the management of water resources. We tested Landsat 8 (L8) and Sentinel-2 (S2) optical image time series, Sentinel-1 (S1) radar, spectral indices and validation with Jason-3 (J3) altimetry. The methodology was developed in the Google Earth Engine (GEE) operational routine, which streamlined the SWA mapping. The best results were between S2 and NDWI and threshold 0, with $R^2 = 0.88$ and RMSE of 11.59 km². As main limitations, we highlight the cloud cover for the optical images, which can decrease the temporal sampling, as well as the SAR backscatter response in the presence of bare soil and aquatic vegetation. We could attest that periodic remote sensing data are particularly useful for timely updating spatial variations of RWL and SWA in reservoirs.

Keywords: water resources, spectral indexes, google earth engine, sentinel-1, sentinel-2, landsat 8, Jason-3

Volume 6 Issue 5 - 2022

Douglas Stefanello Facco,[1] Laurindo Antonio Guasselli,[1] Daniel Capella Zanotta,[1] Luis Fernando Chimelo Ruiz[2]

[1]Research Center on Remote Sensing and Meteorology, Federal University of Rio Grande do Sul, Brazil

[2]Research and development (R&D) at Santos Lab Digital, Brazil

Correspondence: Douglas Stefanello Facco, Research Center on Remote Sensing and Meteorology, Federal University of Rio Grande do Sul, Porto Alegre, Brazil, Tel 55 55 9 96236952, Email douglas.s.facco@gmail.com

Received: September 30, 2022 | **Published:** October 12, 2022

Introduction

The Brazil has experienced water crises that have affected human supply, agriculture, navigability and energy generation.[1] According to[2] conflicts involving the Brazilian Electric System are caused by recent water crisis involving their companies and their management sector. As popularly known, most of it is caused by critical low dam reservoirs levels. Sedimentation is another important reason that affects the level of dam reservoirs, being the most important factor in reducing the volume and their useful life.[3] Reservoir Water Level (RWL) and Surface Water Area (SWA) are crucial physical parameters in water resource management, and stand for good indicators of climate change impacts.[4–6] Accurate and up-to-date databases on RWL and SWA and their spatial distribution are needed in surface water mapping, periodic estimates for consumption and irrigation, wetland conservation, and ecological environmental assessment.[7] Traditional approaches to monitoring RWL in reservoirs use in situ measurement. However, in large reservoirs, it is impractical to install and maintain the sufficient number of measurement stations.[8,9] It is necessary a huge amount of measuring devices to monitor every subbasin and finally compute the entire reservoir volume. Althought, water level is found to be intimately associated with superficial area for a particular reservoir and can be adequately used to estimate RWL.[10–12]

Remote sensing (RS) data is ideal for estimating SWA. Relationship between RWL and SWA in reservoirs, derived from orbital sensors, allows the estimation of these parameters based on the dynamic behavior of the covering area. Many studies have demonstrated that Optical L8 and S2 images are very useful to separate the water sheet from other covers.[13] Although, there are several methods for water volume and level estimation, they lack generalization. One reason is that there are widespread differences in the parameters of many remote sensing sensors, and classification rules are often defined for remote sensing images from several sensors.[14]

Literature has demonstrated that differences in reflectivity for water and non-water bodies can be adequately extracted from spectral indices.[15] Spectral water indices are more accurate compared to other methods such as classification techniques, or linear unmixing.[7,16,17] Among the spectral indices of water most used in the literature, in[18] the authors developed the Normalized Difference Water Index (NDWI) using green and near-infrared (NIR) spectral ranges to maximize water characteristics.[18] replaced NIR with shortwave infrared (SWIR) and derived the modified NDWI (MNDWI).

Radar images are used to separate water sheets from other covers, with the advantage that clouds and fog are not a concern.[20] Radar backscatter is sensitive to the moisture content and harshness of the landscape. The Sentinel-1 sensor's C-band penetrates clouds and thick canopies.[21] Satellite altimetry (RA), originally used for ocean surface topography, has been tested for rivers, lakes, and reservoirs with great results.[22] In the case of small reservoirs, the precision of water level time series derived from satellite altimetry is mainly ruled by the seasonal variability of the water storage.[23]

The cloud-based platform Google Earth Engine (GEE) is very convenient in large-scale analysis to understand long-term[24] changes in reservoirs.[25] There are many advantages for using radar data over optical satellite data. The wavelength of the radar signal together with the active satellite sensor allows data acquisition at any time of the day and regardless of weather conditions.[26] Bodies of water are seen as dark regions in the image, due to the reduced back scattering of the radio signal transmitted from a smooth surface. The roughness of the water is what defines its value and not its color properties as we are used to with optical images.[26]

In this work, we aim to employ a large-scale multi-source and multi-temporal database to estimate RWL and SWA in reservoirs using consolidated estimation metrics based on invariant indices and remote sensing data. For optical imaging, the water spectral index method is a multiband extraction method commonly used in remote sensing to select significance thresholds between a body of water and non-water. For radar images, backscatter data is used, appropriate thresholds in decibels (dB) are selected to measure wave scattering.

Based on L8 and S2 optical images of 30 meters and 10 meters of spatial resolution respectively, S1 radar images of 10 meters and J3 altimetry data with 3.3 cm accuracy used for validation, satellite measurements (or orbital data) are used to update the spatial and temporal variations of SWA in reservoirs. Studies have already tested the accuracy of the estimates of these sensors separately, but none has verified the accuracy of both for a reservoir, indicating the best parameters and thresholds, operating within a dynamic, accessible, fast and free cloud platform.

Materials and methods

We selected as a study area the reservoir of the Itaipu hydroelectric plant, located in South America on the Brazil-Paraguay border (Figure 1). The Itaipu Reservoir, one of the largest producers of hydroelectric power in the world, is located in the western region of the State of Paraná, in southern Brazil. The reservoir is 170 km² long, has an average width of 7 km, an average depth of 22 m, 170 m close to the dam, a minimum water level of 197 m and a maximum of 220 m. The Itaipu dam is the most down-stream in the Paraná Basin, and receives a positive contribution from all Paraná Basin reservoirs. Regardless of change in the country's energy storage, the flooded area of the reservoirs around Itaipu, does not vary substantially.[26]

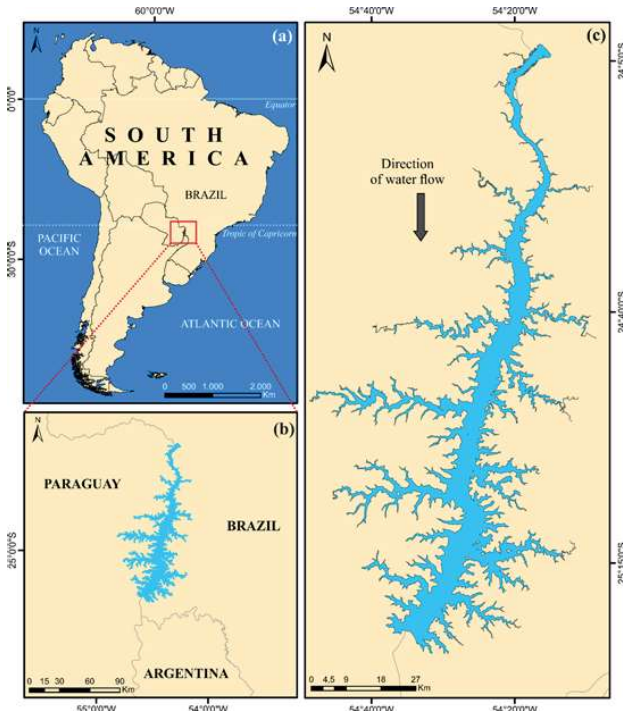

Figure 1 (a) Location of the Itaipu reservoir (red square) in relation to South America; (b) Regional location of the Itaipu reservoir on the Brazil-Paraguay border; (c) Expanded map of the extension of the Itaipu reservoir.

The climate of the western region of Paraná State is classified as humid subtropical (Cfa, according to the Köppen classification). The average monthly temperature is above 22°C in the summer period. The average annual precipitation varies from 1600 to 1700 mm in the studied region. Agriculture is the main land use in the basin area. The predominant soil type is the Latosol, which corresponds to soils in advanced stages of weathering, typical of both equatorial and tropical regions, also occurring in sub-tropical zones. Latosols are mainly distributed over large and old erosion surfaces or river terraces, usually in flat and undulating relief.[28]

Methodological flowchart

The flowchart shown in Figure 2 provides the general structure of the pipeline methodology for determining the surface water area in large reservoirs. Methodology steps will be detailed in what follows.

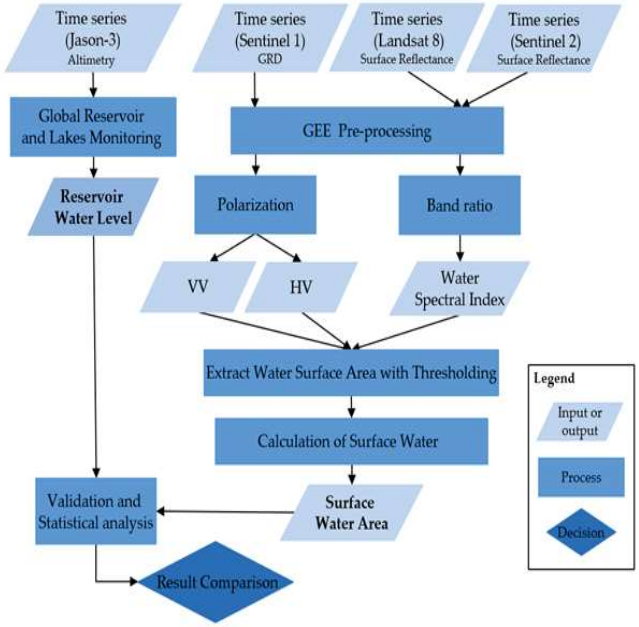

Figure 2 Summary flowchart of the methodology.

Data set: time series of satellite imagery and altimetry

We used data from synthetic aperture radar S1 and multispectral L8 and S2 images, processed in the GEE platform. All the data was validated using J3 altimeter. The analysis period was between 2019 and 2021, due to the availability of S2. Images have a maximum delay of 5 days with J3. The products used are described below.

a) S1: C-band data from Sentinel-1 in Interferometric Wide Swath (IW) mode was designed to acquire images of Earth surfaces. In IW mode it has dual polarization with vertical transmission and vertical reception (VV) and vertical transmission and horizontal reception (VH) and spatial resolution of 10-meter. We used the Level 1 Ground Range Detected (GRD) product pre-processed in the GEE to derive the backscatter co-efficient at each pixel. The VV and VH polarized data were selected to map the water surface. To cover the reservoir, it was necessary to mosaic two SAR images for each date, totaling 66 dates;

b) L8: The Landsat 8 Surface Reflectance Tier 1 multispectral images available on the GEE are derived from the Landsat 8 OLI / TIRS sensors. The images were orthorectified and atmospherically corrected to obtain surface reflectance. The bands used were 3 (green), 4 (red), 5 (near infrared) and 6 (medium infrared) with a spatial resolution of 30 meters. Two Lansdat-8 images were merged to cover the reservoir on each date, totaling 16 dates;

c) S2: S2 multispectral images with level 2A processing are available in the GEE, orthorectified and atmospherically corrected for surface reflectance values. Bands 3 (green), 4 (red) and 8 (near infrared) with a spatial resolution of 10-meter and band 11 (short wave infrared) of 20-meter were used. To cover the reservoir, it was necessary to merge 3 Sentinel-2 images for each analyzed date, totaling 33 dates;

d) Jason-3: RWL data acquired every 10 days from the US Department of Agri-culture, Global Reservoirs and Lakes Monitor website (USDA G-REALM; https://ipad.fas.usda.gov/cropexplorer/global_reservoir) was used for validation, due to its high accuracy and consistency with 3.3 cm in reservoirs with a width greater than 100 m.[29,22,30]

Generation of SWA time series

GEE combines a multi-petabyte catalog of satellite imagery and geospatial datasets with planetary-scale analysis capabilities.[31,32] Scientists, researchers, and developers use Earth Engine to detect changes, map trends, and quantify differences on the Earth's surface. The GEE hosts complete and up-to-date S1, S2, and L8 data files. We produced temporally distributed water masks and calculate the maximum SWA extent included for each date, with selection of suitable thresholds. As mentioned before, water bodies are determined by texture levels in radar images. For S1, we used thresholds between -24 and -18 decibels (dB) in the VH band and between -15 and -5 dB in the VV band.[33] For S2 and L8, the water spectral index method is a commonly used multi-band extraction method, which is combined with other remote sensing indices to select the threshold of significant difference between a water body and a non-water body. We used the spectral index NDWI[18] Eq (1) and MNDWI[19] Eq (2), widely used and robust in water extraction, and applied suitable thresholds for water and non-water pixels 0.0, 0.1, and 0.2.

$$NDWI = (Green-NIR)/(Green+NIR) \quad (1)$$

$$MNDWI = (Green-SWIR)/(Green+SWIR) \quad (2)$$

Where: NDWI is the Normalized Difference Water Index; MNDWI is Modified Nor-malized Difference Water Index; Green is the reflected green visible light; NIR is the reflected near-infrared energy; SWIR is the reflected short-wave infrared energy.

Accuracy assessment

For each image of sensors S1, S2 and L8, the SWA was calculated for the thresholds described in section 2.3. Validation was performed using data from J3 altimetry water levels. J3 data is not as frequent as S1, S2, and L8 imagery, but some dates with occurrence of simultaneously acquisition were used for assessing purposes. In order to evaluate correlation, the coefficient of determination (R^2) and the root mean square error (RMSE) were calculated to verify the imaging sensor with the highest relation-ship with J3 for greater reliability in the SWA calculation.

Results and discussions

SWA and RWL relationship and better thresholds

Based on R^2 and RMSE (Table 1), the linear model that described the best relationship between SWA and RWL was S2 and NDWI and threshold 0, with R reaching 0.94, R^2 = 0.88, and RMSE =11.59 km². In general, multispectral sensors exhibited better results with L8 and NDWI and threshold 0, with R reaching 0.91, R2 = 0.83, and RMSE less than 15 km². S1 was less satisfactory in the HV band (R^2 = 0.45 for thresholds between -23 and -24 dB and the VV band (R^2 equals 0.61 for the -14 dB threshold). Areas near the reservoir edge were sources of S1 error, mislabeling water pixels to exposed soil and wet areas with aquatic vegetation (Figure 3), especially when the water level was lower, causing SWA overestimation.

Table 1 Relationship between SWA and RWL in the reservoir

Satellite	Parameters	Thresholds	R	R^2	RMSE Km²
Sentinel-1	HV	-24	0.67	0.45	
S1		-23	0.67	0.45	13.59
		-22	0.63	0.4	
	VV	-15	0.73	0.53	
		-14	0.78	0.61	14.37
		-13	0.75	0.57	
Landsat 8	MNDWI	0	0.91	0.83	14.46
L8		0.1	0.91	0.82	
		0.2	0.9	0.81	
	NDWI	0	0.9	0.81	
		0.1	0.91	0.82	16.85
		0.2	0.87	0.75	
Sentinel-2	MNDWI	0	0.93	0.87	11.98
S2		0.1	0.93	0.86	
		0.2	0.93	0.86	
	NDWI	0	0.94	0.88	11.59
		0.1	0.93	0.86	
		0.2	0.9	0.81	

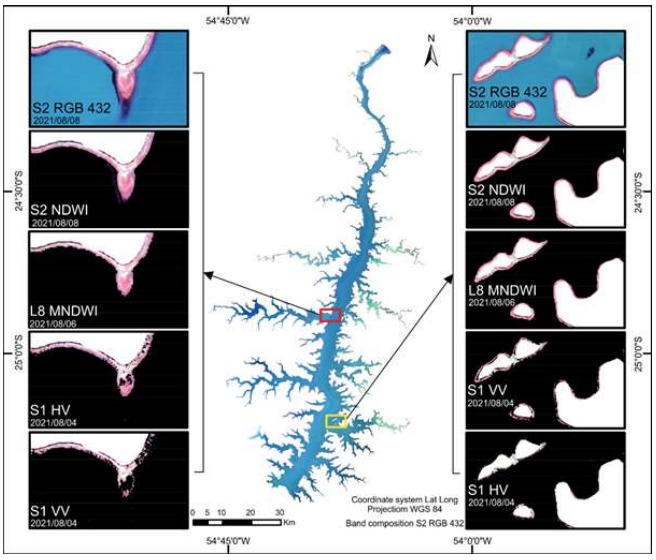

Figure 3 In the center of the Image: Spatial distribution of the water surface of the Itaipu reservoir on the date 08/08/2021 in true RGB432 composition by the S2 sensor SWA and RWL time series. In the column on the left we have a comparison between the sensors with their best parameters for the region the (red rectangle). in the column on the right we have a comparison between the sensors with their best parameters for the region (yellow rectangle).

Water spectral indices for determining SWA are important for establishing the optimal threshold for separating water and non-water pixels.[34] The optimal index depends on the environmental characteristics of the study area, including topography and shadows.[35] The factors that affect the quality of the water mask are different in optical and radar observations. In S1, water detection occurs in low-backscatter areas.[36] When the water body is near wetlands, the SAR response affects low-signal zones on water surfaces.[36] Our results agree with[37] that VV polarization is better for differentiating water and non-water areas compared to VH. Among multispectral sensors, our results agree with,[38,39] which state that S2 is better than L8 considering its spatial and spectral ability to identify water pixels and other coverages. In[40,9] the authors used Landsat 8 water spectral indices to analyze the spatio temporal dynamics of the reservoir.

Both SWA and RWL time series were derived from S2 and J3, which obtained the best discriminating features. Figure 4 contains 33 points, representing the time lapse between 2019 and 2022. The SWA ranged between 1140.2 Km² and 1271.51 km², and the RWL ranged between 215.69 m and 220 m. Figure 4 shows the S2 time series of SWA and RWL, while Figure 5 shows the scatterplot of the S2 and J3 data. The works of[41,42] found that satellite imagery allows the analysis of spatiotemporal variability in res-ervoirs without the requirement of in situ data. A major advance in studying reservoirs with no ground-based observations. J3 data have an error of fewer than 0.30 m and are satisfactory for water height in reservoirs wider than 100 meters.[26,20,28] In this study, the maximum time lag between the orbital image acquisition and the J3 passage was 5 days. Longer delay may lead to an increased SWA detection error. Using J3 for validation was appropriate due to its high accuracy[22,30] while using GEE allowed automating the methodology and process large datasets (Big Earth Data).[43]

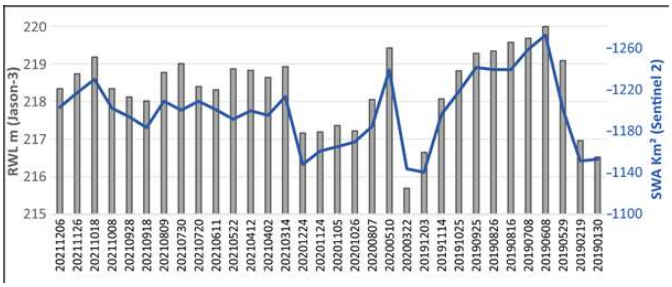

Figure 4 SWA and RWL time series. The gray columns represent the reservoir level in m by the J3 sensor, and the blue line represents the surface area data in Km² by the Sentinel 2.

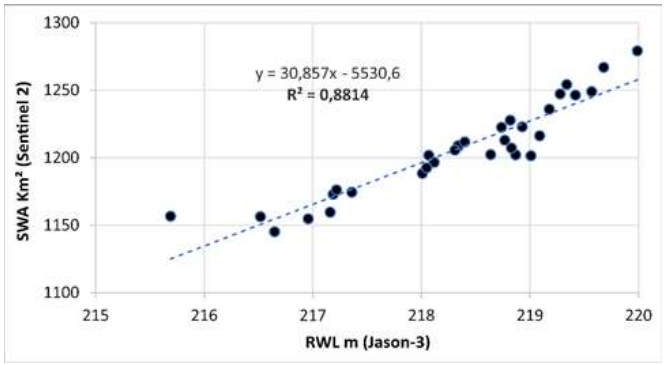

Figure 5 Scatterplot showing the relationship between SWA (Sentinel 2) and RWL (Janson-3) data.

Conclusion

This paper presented an approach to estimating the time series of SWA and RWL variations in reservoirs by combining orbital imagery processed in GEE and J3 altimetry. GEE expedited the mapping of SWA and allowed significantly reduced time and costs in reservoir monitoring. Assessing showed considerable agreement between estimated and observed measures, while SWA and RWL time series from S2 and J3 obtained the best settings. The indirect estimation of important reservoir parameters is able to provide a rapid and reliable water condition. As main limitations, we highlight the cloud cover for the optical images, which can decrease temporal sampling, as well the SAR backscatter response in the presence of bare soil and aquatic vegetation.

Acknowledgments

None.

Conflicts of interest

The author declares there is no confclit of interest.

References

1. Mining 2021. *Water crisis threatens iron transport on key Brazil river*. 2021.
2. Galvão J, Bermann C. Crise hídrica e energia: conflitos no uso múltiplo das águas. *Estudos avançados*. 2015;29:43–68.
3. Mahmoodieh N, Ghomeshi M. Investigation the effect of concentration and radius of bend curvature on turbidity current body thickness in 90 degree bend. *Irrigation Sciences and Engineering*. 2019.
4. Pekel JF, Cottam A, Gorelick N, et al. High-resolution mapping of global surface water and its long-term changes. *Nature*. 2016;540:418–22.
5. Sun S, Wang Y, Liu J, et al. Sustainability assessment of regional water resources under the DPSIR framework. *Journal of Hydrology*. 2016;532:140–148.
6. Liu KT, Tseng KH, Shum CK, et al. Assessment of the impact of reservoirs in the upper Mekong River using satellite radar altimetry and remote sensing imageries. *Remote Sensing* 2016;8:367.
7. Acharya TD, Subedi A, Lee DH. Evaluation of Water Indices for Surface Water Extraction in a Landsat 8 Scene of Nepal. *Sensors*. 2018;18:2580.
8. Beskow S, Timm LC, Tavares VEQ. Potential of the LASH model for water resources management in data-scarce basins: a case study of the Fragata River basin, southern Brazil. *Hydrological Sciences Journal* 2016;61:2567–2578.
9. Facco DS, Guasselli LA, Ruiz LFC, et al. Spectral Reflectance in the Spatial-temporal Dynamic of Turbidity, Itaipu Reservoir, Brazil. *Anuário do Instituto de Geociências* 2021;44.
10. Li J, Wang S. An automatic method for mapping inland surface waterbodies with Radarsat-2 imagery. *International Journal of Remote Sensing* 2015;36:1367–1384.
11. Pipitone C, Maltese A, Dardanelli G, et al. Monitoring Water Surface and Level of a Reservoir Using Different Remote Sensing Approaches and Comparison with Dam Displacements Evaluated *via* GNSS. *Remote Sensing*. 2018;10:71.
12. Yuan C, Gong P, Liu C, et al. Water-volume variations of Lake Hulun estimated from serial Jason altimeters and Landsat TM/ETM+ images from 2002 to 2017. *International Journal of Remote Sensing*. 2018;40:670–692.
13. Cavallo C, Papa MN, Gargiulo M, et al. Continuous Monitoring of the Flooding Dynamics in the Albufera Wetland (Spain) by Landsat-8 and Sentinel-2 Datasets. *Remote Sensing*. 2021;13:3525.
14. Li J, Ma R, Cao Z, et al. Satellite Detection of Surface Water Extent: A Review of Methodology. *Water*. 2022;14:1148.
15. Santoro M, Wegmüller U, Lamarche C, et al. Strengths and weaknesses of multi-year Envisat ASAR backscatter measurements to map permanent open water bodies at global scale. *Remote Sensing of Environment*. 2015;171:185–201.
16. Şerban C, Maftei C, Dobrică G. Surface Water Change Detection via Water Indices and Predictive Modeling Using Remote Sensing Imagery: A Case Study of Nuntasi-Tuzla Lake, Romania. *Water*. 2022;14:556.
17. Yang X, Chu Q, Wang L, et al. Water Body Super-Resolution Mapping Based on Multiple Endmember Spectral Mixture Analysis and Multiscale Spatio-Temporal Dependence. *Remote Sens*. 2022;14:2050.
18. McFeeters SK. The use of the Normalized Difference Water Index (NDWI) in the delineation of open water features. *International journal of remote sensing*. 1996;17(7):1425–1432.

19. Xu H. Modification of normalised difference water index (NDWI) to enhance open water features in remotely sensed imagery. *International journal of remote sensing* 2006;27(14):3025–3033.

20. Zhou S, Kan P, Silbernagel J, Jin J. Application of Image Segmentation in Surface Water Extraction of Freshwater Lakes using Radar Data. *ISPRS International Journal of Geo-Information* 2020;9:424.

21. Bioresita F, Puissant A, Stumpf A, et al. A Method for Automatic and Rapid Mapping of Water Surfaces from Sentinel-1 Imagery. *Remote Sensing*. 2018;10:217.

22. Biancamaria S, Schaedele T, Blumstein D, et al. Validation of Jason-3 tracking modes over French rivers. *Remote Sensing of Environment.* 2018;209:77–89.

23. Neto AR, Behnia S, Tourian MJ, et al. Satellite altimetry over small reservoirs in the Brazilian semiarid region. *Revista Brasileira de Recursos Hídricos* 2021;26.

24. Amani M, Ghorbanian A, Ahmadi SA, et al. Google earth engine cloud computing platform for remote sensing big data applications: A comprehensive review. *IEEE Journal of Selected Topics in Applied Earth Observations and Remote Sensing.* 2020;13:5326–5350.

25. Deng Y, Jiang W, Tang Z, et al. Long-Term Changes of Open-Surface Water Bodies in the Yangtze River Basin Based on the Google Earth Engine Cloud Platform. *Remote Sensing.* 2019;11:2213.

26. Čotar K, Oštir K, Kokalj Ž. Radar Satellite Imagery and Automatic Detection of Water Bodies. *Geode Glass* 2016;50:5–15.

27. Hunt JD, Falchetta G, Zakeri B, et al. Hydropower impact on the river flow of a humid regional climate. *Climatic Change.* 2020;163:379–393.

28. Rocha ASD, Bade MR. *Geografia da bacia hidrográfica do Paraná 3: fragilidades e potencialidades socioambientais,* 3rd edn. Publisher: In House. Jundiaí, São Paulo, Brazil, 2018;314.

29. Le Gac S, Boy F, Blumstein D. *Update and validation of Jason-3 onboard DEM: Enhanced acquisitions over inland water targets, Presentation at OSTST Meeting*. Miami, USA, 2017.

30. Le Gac S, Boy F, Blumstein D, et al. Benefits of the Open-Loop Tracking Command (OLTC): Extending conventional nadir altimetry to inland waters monitoring. *Advances in Space Research.* 2021;68:843–852.

31. Gorelick N, Hancher M, Dixon M, et al. Google Earth Engine: Planetary-scale geospatial analysis for everyone. *Remote sensing of Environment* 2017;202:18–27.

32. Abujayyab SKM, Almotairi KH, Alswaitti M, et al. Effects of Meteorological Parameters on Surface Water Loss in Burdur Lake, Turkey over 34 Years Landsat Google Earth Engine Time-Series. *Land.* 2021;10:1301.

33. Manjusree P, Prasanna Kumar L, Bhatt CM, et al. Optimization of threshold ranges for rapid flood inundation mapping by evaluating backscatter profiles of high incidence angle SAR images. *International Journal of Disaster Risk Science.* 2012;3:113–122.

34. Özelkan E. Water body detection analysis using NDWI indices derived from landsat-8 OLI. *Polish Journal of Environmental Studies.* 2020;29:1759–1769.

35. Zhai K, Wu X, Qin Y, et al. Comparison of surface water extraction performances of different classic water indices using OLI and TM imageries in different situations. *Geo-spatial Information Science.* 2015;18(1):32–42.

36. Peña-Luque S, Ferrant S, Cordeiro MCR, et al. Sentinel-1&2 Multitemporal Water Surface Detection Accuracies, Evaluated at Regional and Reservoirs Level. *Remote Sensing.* 2021;13:3279.

37. Pôssa ÉM, Maillard P, Gomes MF, et al. *On water surface delineation in rivers using Landsat-8, Sentinel-1 and Sentinel-2 data*. In Proceedings of Conference Remote Sensing for Agriculture, Ecosystems, and Hydrology XX, Berlin, Germany, 10 Oct 2018.

38. Marangoz AM, Sekertekin A, Akçin H. *Analysis of land use land cover classification results derived from sentinel-2 image*. In Proceedings of the 17th International Multidisciplinary Scientific GeoConference Surveying Geology and Mining Ecology Management, SGEM 2017, Albena and Varna, Bulgaria, 2017. p. 25–32.

39. Ahady AB, Kaplan G. Classification comparison of Landsat-8 and Sentinel-2 data in Google Earth Engine, study case of the city of Kabul. *International Journal of Engineering and Geosciences.* 2022;7:24–31.

40. Facco DS, Guasselli LA, Ruiz LFC, et al. Comparison of PBIA and GEOBIA classification methods in classifying turbidity in reservoirs. *Geocarto International.* 2021;37(16):1–22.

41. Biancamaria S, Lettenmaier DP, Pavelsky TM. The SWOT mission and its capabilities for land hydrology. *Remote sensing and water resources.* 2016;117–147.

42. Bonnema M, F Hossain. Inferring reservoir operating patterns across the Mekong Basin using only space observations. *Water Resources Research.* 2017;53:3791–3810.

43. Sun Z, Luo J, Yang J, et al. Nation-Scale Mapping of Coastal Aquaculture Ponds with Sentinel-1 SAR Data Using Google Earth Engine. *Remote Sens.* 2020;12:3086.

6 CONSIDERAÇÕES FINAIS

Nossos resultados demonstraram o potencial da utilização de dados exclusivamente de sensoriamento remoto para identificar e analisar padrões de turbidez no reservatório de Itaipu a partir da integração de dados remotos orbitais ativos e passivos e técnicas de processamento digital de imagens.

A escassez de dados de campo motivou a utilização de dados remotos para geração e validação de dados. Ressaltamos a importância de considerar cuidadosamente as vantagens e desvantagens de cada abordagem, e avaliar como os dados remotos se aplicam no contexto da turbidez em reservatórios.

Os dados remotos de média resolução espacial utilizados, ofereceram vantagens, especialmente pela extensão do reservatório de Itaipu, no qual a coleta de dados de campo é difícil, custosa e muitas vezes inviável. Nesse sentido, dados orbitais forneceram informações espaço temporais valiosas além de ter sido econômico e eficiente. Assim, a obtenção de informações espaciais permitiu uma visão abrangente e atualizada da dinâmica da turbidez do ambiente aquático.

Os avanços tecnológicos e o desenvolvimento de novas missões e sensores têm contribuído para a melhoria da qualidade e disponibilidade dos dados de satélite. Mas é importante destacar que os dados remotos têm suas limitações. Dependendo da resolução espacial e espectral, coberturas de nuvens, influências atmosféricas e restrições temporais dos sensores utilizados pode haver lacunas e falhas. A validação com dados terrestres pode ajudar a mitigar essas limitações e fornecer dados mais precisos.

O que pode ser extraído deste estudo é, em primeiro lugar, que a turbidez da água do reservatório de Itaipu é espectralmente ativa e, portanto, pode ser interrogada por sensoriamento remoto. Em segundo lugar, há uma forte conexão entre materiais suspensos, turbidez e precipitação.

A presença de materiais opticamente ativos induz um caráter de alta reflexão espectral na água a partir da dispersão e retroespalhamento da luz. Este fenômeno é muito pronunciado nas regiões do vermelho e do infravermelho médio do espectro eletromagnético no qual o reservatório de Itaipu responde.

Os dados multiespectrais de média resolução utilizados nessa Tese apresentaram resultados positivos. Dados de turbidez utilizados para validação

gerados pela EOMAP possibilitaram averiguar as relações entre a refletância espectral e a precipitação. O que permitiu ilustrar que em sua maioria o material suspenso vem de montante, e que os compartimentos horizontais possuem menor influência nessa dinâmica.

Nossas abordagens para delinear limites espectrais de turbidez consideram estratégias semi-automatizada e multiescala para definir limiares de similaridade e MNP. As classificações GEOBIA foram mais precisas que as classificações PBIA em ambos os algoritmos testados. O classificador RF obteve maiores valores de KA e OA em ambas abordagens de classificação PBIA e GEOBIA.

A estimativa das variações SWA e RWL o GEE agilizou o mapeamento, o que pode permitir uma redução significativa de tempo e custos no monitoramento do reservatório. As séries temporais SWA e RWL de S2 e J3 obtiveram as melhores configurações. Os dados da banda C do Sentinel-1 na polarização VV e VH foram menos capazes de detectar área de superfície da água, havendo confusão entre a detecção das coberturas água solo e vegetação aquática. Da mesma forma destacamos a cobertura de nuvens para as imagens ópticas, que diminuem a amostragem temporal.

Os limites e parâmetros resultantes desta Tese podem servir de orientação para outros trabalhos da mesma temática. Nosso estudo mostra que mesmo sem dados in situ, é possível analisar e quantificar a turbidez do reservatório de Itaipu a partir de sensores acoplados em satélites espaciais. O futuro do sensoriamento remoto para monitoramento de águas interiores é promissor. O uso operacional do sensoriamento remoto para identificação de padrões de águas interiores já é uma realidade, os sensores de satélite continuarão a progredir em suas características espaciais, radiométricas, espectrais e temporais, nos permitindo analises espaciais e multiescalares com mais detalhes e precisão.

REFERÊNCIAS

AGOSTINHO, Angelo Antônio *et al*. **Ecologia e manejo de recursos pesqueiros em reservatórios do Brasil**. Uem, 2007.

AGOSTINHO, Angelo Antonio; JULIO JUNIOR, H. F. Peixes da bacia do alto rio Paraná. 2018.

ALCANTARA, Enner *et al*. A satellite-based investigation into the algae bloom variability in large water supply urban reservoirs during COVID-19 lockdown. **Remote Sensing Applications: Society and Environment**, v. 23, p. 100555, 2021.

ALLAN, Mathew Grant. **Remote sensing, numerical modelling and ground truthing for analysis of lake water quality and temperature**. 2014. Tese de Doutorado. University of Waikato.

ALMEIDA, Viviane LS; MELÃO, Maria da Graça G.; MOURA, Ariadne N. Plankton diversity and limnological characterization in two shallow tropical urban reservoirs of Pernambuco State, Brazil. **Anais da Academia Brasileira de Ciências**, v. 84, p. 537-550, 2012.

ALVADO, Bárbara *et al*. Estimating organic and inorganic part of suspended solids from Sentinel 2 in different inland waters. **Water**, v. 13, n. 18, p. 2453, 2021.

ANDRADE, L. F. *et al*. Fitoplâncton e características físico-químicas do reservatório de Itaipu (BR). **Limnologia e manejo de represas. Série Monografias em Limnologia**, v. 1, p. 205-268, 1988.

ANGELINI, Ronaldo; BINI, Luis Maurício; STARLING, Fernando LRM. Efeitos de diferentes intervenções no processo de eutrofização do lago Paranoá (Brasília-DF). 2008.

ARVOR, Damien *et al*. Monitoring thirty years of small water reservoirs proliferation in the southern Brazilian Amazon with Landsat time series. **ISPRS Journal of Photogrammetry and Remote Sensing**, v. 145, p. 225-237, 2018.

BACALHAU, José Ráurium. **Caracterização volumétrica de reservatórios por meio de sensoriamento remoto**. 2022. Dissertação de Mestrado. Universidade Federal de Pernambuco, Recife, 2022.

BARASA, Bernard; WANYAMA, Joshua. Freshwater lake inundation monitoring using Sentinel-1 SAR imagery in Eastern Uganda. **Annals of GIS**, v. 26, n. 2, p. 191-200, 2020.

BARBAROSSA, Valerio *et al*. Impacts of current and future large dams on the geographic range connectivity of freshwater fish worldwide. **Proceedings of the National Academy of Sciences**, v. 117, n. 7, p. 3648-3655, 2020.

BARBOSA, Claudio Clemente Faria; DE MORAES NOVO, Evlyn Marcia Leão; MARTINS, Vitor Souza (Ed.). **Introdução ao sensoriamento remoto de sistemas aquáticos: princípios e aplicações**. Instituto Nacional de Pesquisas Espaciais, 2019.

BATISTA, Adriana Alves *et al*. Sazonalidade e variação espacial do índice de estado trófico do açude Orós, Ceará, Brasil. **Revista Agro@ mbiente On-line**, v. 8, n. 1, p. 39-48, 2014.

BHATTI, Asif Mumtaz; NASU, Seigo; TAKAGI, M. Assessment of suspended sediment concentration in the surface water using remote sensing. **Global Change Issues in Developing and Emerging Countries: Proceedings of the 2nd Göttingen GIS and Remote Sensing Days 2006, 4th to 6th October, Göttingen, Germany**, v. 4, p. 279, 2007.

BID, Sumanta; SIDDIQUE, Giyasuddin. Identification of seasonal variation of water turbidity using NDTI method in Panchet Hill D

BIERMAN, Paul *et al*. A review of methods for analysing spatial and temporal patterns in coastal water quality. **Ecological Indicators**, v. 11, n. 1, p. 103-114, 2011.

BIORESITA, Filsa *et al*. A method for automatic and rapid mapping of water surfaces from sentinel-1 imagery. **Remote Sensing**, v. 10, n. 2, p. 217, 2018.

BISWAS, Nishan Kumar *et al*. An altimeter height extraction technique for dynamically changing rivers of South and South-East Asia. **Remote Sensing of Environment**, v. 221, p. 24-37, 2019.

BITTENCOURT, CLAUDIA; DE PAULA, MARIA APARECIDA SILVA. **Tratamento de água e efluentes Fundamentos de saneamento ambiental e gestão de recursos hídricos**. Saraiva Educação SA, 2014.

BONANSEA, Matias *et al*. Using new remote sensing satellites for assessing water quality in a reservoir. **Hydrological sciences journal**, v. 64, n. 1, p. 34-44, 2019.

BOWERS, D. G.; BINDING, C. E.; ELLIS, K. M. Satellite remote sensing of the geographical distribution of suspended particle size in an energetic shelf sea. **Estuarine, Coastal and Shelf Science**, v. 73, n. 3-4, p. 457-466, 2007.

BRICAUD, Annick *et al*. Light absorption properties and absorption budget of Southeast Pacific waters. **Journal of Geophysical Research: Oceans**, v. 115, n. C8, 2010.

BRUNKOW, R. F.; ANDRADE, L. F.; XAVIER, C. F. Processo de estratificação térmica e de oxigênio dissolvido no Reservatório de Itaipu, Paraná-BR. **Limnologia e Manejo de Represas. São Carlos: EESC-USP/CRHEA/ACIESP**, 1988.

BUKATA, Robert P. *et al*. **Optical properties and remote sensing of inland and coastal waters**. CRC press, 1995.

BUKATA, Robert P. **Satellite monitoring of inland and coastal water quality: retrospection, introspection, future directions**. CRC Press, 2005.

BUZELLI, Giovanna Moreti; CUNHA-SANTINO, Marcela Bianchessi da. Análise e diagnóstico da qualidade da água e estado trófico do reservatório de Barra Bonita, SP. **Revista Ambiente & Água**, v. 8, p. 186-205, 2013.

CAO, Hongye *et al*. Inversion and distribution of total suspended matter in water based on remote sensing images—A case study on Yuqiao Reservoir, China. **Water Environment Research**, v. 93, n. 4, p. 582-595, 2021.

CARDOSO, Simone J. *et al*. Spatial variation of sediment mineralization supports differential CO2 emissions from a tropical hydroelectric reservoir. **Frontiers in Microbiology**, v. 4, p. 101, 2013.

CARVALHO, Adriana Rosa; SCHLITTLER, Flávio Henrique Mingante; TORNISIELO, Valdemar Luiz. Influence of cattle ranching and agricultural activities on physical chemical parameters of water. **Química Nova**, v. 23, p. 618-622, 2000.

CARVALHO, Gil César Rocha de. Interpretação sísmica e modelagem física do cone do Amazonas, Bacia da Foz do Amazonas, margem equatorial brasileira. 2008.

CHANG, Maoxiang *et al*. Mapping Tidal Flats of the Bohai and Yellow Seas Using Time Series Sentinel-2 Images and Google Earth Engine. **Remote Sensing**, v. 14, n. 8, p. 1789, 2022.

CHEN, Robert F. *et al*. Chromophoric dissolved organic matter (CDOM) source characterization in the Louisiana Bight. **Marine Chemistry**, v. 89, n. 1-4, p. 257-272, 2004.

CHEN, Tan *et al*. Estimating seasonal water budgets in global lakes by using multi-source remote sensing measurements. **Journal of Hydrology**, v. 593, p. 125781, 2021.

CHU, Hone-Jay; KONG, Shish-Jeng; CHANG, Chih-Hua. Spatio-temporal water quality mapping from satellite images using geographically and temporally weighted regression. **International journal of applied earth observation and geoinformation**, v. 65, p. 1-11, 2018.

CILLERO CASTRO, Carmen *et al*. An UAV and satellite multispectral data approach to monitor water quality in small reservoirs. **Remote Sensing**, v. 12, n. 9, p. 1514, 2020.

COLTIN, Brian *et al*. Automatic boosted flood mapping from satellite data. **International Journal of Remote Sensing**, v. 37, n. 5, p. 993-1015, 2016.

COTRIM, John S.; KRAUCH, Hans W.; SARKARIA, Gurmukh S. Itaipu, South America's Grande Dame. **Civil Engineering—ASCE**, v. 54, n. 12, p. 40-43, 1984.

CRÉTAUX, J.-F. *et al*. Lake volume monitoring from space. **Surveys in Geophysics**, v. 37, p. 269-305, 2016.

CUI, Mengying *et al*. Water turbidity retrieval based on uav hyperspectral remote sensing. **Water**, v. 14, n. 1, p. 128, 2022.

CUNHA, Davi Gasparini Fernandes; DO CARMO CALIJURI, Maria; LAMPARELLI, Marta Condé. A trophic state index for tropical/subtropical reservoirs (TSItsr). **Ecological Engineering**, v. 60, p. 126-134, 2013.

DAVRANCHE, Aurélie; LEFEBVRE, Gaëtan; POULIN, Brigitte. Wetland monitoring using classification trees and SPOT-5 seasonal time series. **Remote sensing of environment**, v. 114, n. 3, p. 552-562, 2010.

DE MORAES NOVO, Evlyn ML. **Sensoriamento Remoto: princípios e aplicações**. Editora Blucher, 2010.

DE MORAES RUDORFF, Conrado; DE MORAES NOVO, Evlyn Márcia Leão; GALVÃO, Lênio Soares. Spectral mixture analysis for water quality assessment over the Amazon floodplain using Hyperion/EO-1 images. **Ambiente e Agua-An Interdisciplinary Journal of Applied Science**, v. 1, n. 2, p. 65-79, 2006.

DIAS, Nelson Wellausen *et al*. Caracterização das águas da represa de Paraibuna com o uso de dados hiperespectrais. **Simpósio Brasileiro de Sensoriamento Remoto**, v. 13, p. 3335-3342, 2007.

DÖRNHÖFER, Katja *et al*. Water constituents and water depth retrieval from Sentinel-2A—A first evaluation in an oligotrophic lake. **Remote Sensing**, v. 8, n. 11, p. 941, 2016.

DÖRNHÖFER, Katja; OPPELT, Natascha. Remote sensing for lake research and monitoring–Recent advances. **Ecological Indicators**, v. 64, p. 105-122, 2016.

DU, Zhongxiang; LI, Xuelong; LU, Xiaoqiang. Local structure learning in high resolution remote sensing image retrieval. **Neurocomputing**, v. 207, p. 813-822, 2016.

EDENHOFER, Ottmar *et al*. (Ed.). **Renewable energy sources and climate change mitigation: Special report of the intergovernmental panel on climate change**. Cambridge University Press, 2011.

ELHAG, Mohamed *et al*. Assessment of water quality parameters using temporal remote sensing spectral reflectance in arid environments, Saudi Arabia. **Water**, v. 11, n. 3, p. 556, 2019a.

ELHAG, Mohamed *et al*. Effect of water surface area on the remotely sensed water quality parameters of Baysh Dam Lake, Saudi Arabia. **Hydrology and Earth System Sciences Discussions**, p. 1-20, 2019b.

FERREIRA, Aline Batista; PEREIRA FILHO, Waterloo. Avaliação da reflectância espectral de corpos d'água em Santa Maria-RS por meio de espectrorradiometria de campo. **Geoambiente On-line**, n. 13, p. 01-14 pág., 2009.

FONTANA, Luciane *et al*. Sedimentation rate inferred from 210Pb and 137Cs dating of three sediment cores at Itaipu reservoir (Paraná State, Brazil) the world's second largest hydroelectricity producer. **Journal of Radioanalytical and Nuclear Chemistry**, v. 331, n. 9, p. 3571-3589, 2022.

GARG, Vaibhav; AGGARWAL, Shiv Prasad; CHAUHAN, Prakash. Changes in turbidity along Ganga River using Sentinel-2 satellite data during lockdown associated with COVID-19. **Geomatics, Natural Hazards and Risk**, v. 11, n. 1, p. 1175-1195, 2020.

GHOSAL, S.; ROGERS, M.; WRAY, A. The turbulent life of phytoplankton. In: **Center for Turbulence Research Proceeding of the Summer Program**. 2000. p. 31-45.

GOMINHO, Marize Freitas de Almeida. **Gestão dos recursos hídricos no processo de desenvolvimento sustentável de Cabo Verde: uma proposta**. 2010. Mestrado (Dissertação do programa de pós-graduação em Gestão de Empresas). ISCTE, Business School, Instituto Universitário de Lisboa, Departamento de Gestão. Lisboa, Portugal, 2010.

GORELICK, Noel *et al*. Google Earth Engine: Planetary-scale geospatial analysis for everyone. **Remote sensing of Environment**, v. 202, p. 18-27, 2017.

HAN, Luoheng; RUNDQUIST, Donald C. Comparison of NIR/RED ratio and first derivative of reflectance in estimating algal-chlorophyll concentration: A case study in a turbid reservoir. **Remote sensing of Environment**, v. 62, n. 3, p. 253-261, 1997.

HE, Weiqi *et al*. Water quality monitoring in a slightly-polluted inland water body through remote sensing—Case study of the Guanting Reservoir in Beijing, China. **Frontiers of Environmental Science & Engineering in China**, v. 2, p. 163-171, 2008.

HELLER, Léo; COLOSIMO, Enrico Antonio; ANTUNES, Carlos Mauricio de Figueiredo. Environmental sanitation conditions and health impact: a case-control study. **Revista da Sociedade Brasileira de medicina tropical**, v. 36, p. 41-50, 2003.

INSTITUTO ÁGUA E TERRA (IAT). QUALIDADE DAS ÁGUAS DOS RESERVATÓRIOS DO ESTADO DO PARANÁ. Disponível em: https://www.iat.pr.gov.br/sites/agua-terra/arquivos_restritos/files/documento/2021-03/relatorio_2017.pdf

ITAIPU. Itaipu Binacional, Paraguai, 2023. Disponível em: https://www.itaipu.gov.py. Acesso em: 06 set. 2023.

JAGANNATHAN, S.; KRISHNAVENI, M. Longitudinal sediment profiling and capacity lost in reservoir using multidate Sentinel-2 images. **Journal of the Indian Society of Remote Sensing**, v. 49, p. 317-323, 2021.

JENSEN, John R.; EPIPHANIO, José Carlos Neves. **Sensoriamento remoto do ambiente: uma perspectiva em recursos terrestres**. São José dos Campos: Parêntese Editora, 2009.

JENSEN, John R.; EPIPHANIO, José Carlos Neves. **Sensoriamento remoto do ambiente: uma perspectiva em recursos terrestres**. São José dos Campos: Parêntese Editora, 2009.

JIA, Tianxia; ZHANG, Xueqi; DONG, Rencai. Long-term spatial and temporal monitoring of cyanobacteria blooms using MODIS on google earth engine: A case study in Taihu Lake. **Remote Sensing**, v. 11, n. 19, p. 2269, 2019.

KAVZOGLU, Taskin; GORAL, Merve. Google Earth Engine for Monitoring Marine Mucilage: Izmit Bay in Spring 2021. **Hydrology**, v. 9, n. 8, p. 135, 2022.

KIRK, Kendall R. **Modeling microbial and nutrient dynamics in zero-discharge aquaculture systems**. 2010. Tese de Doutorado. Clemson University.

KOPONEN, Sampsa *et al*. Remote sensing of water quality for Finnish lakes and coastal areas. 2006.

KOPONEN, Sampsa *et al*. Remote sensing of water quality for Finnish lakes and coastal areas. 2006.

KUHN, Catherine *et al*. Performance of Landsat-8 and Sentinel-2 surface reflectance products for river remote sensing retrievals of chlorophyll-a and turbidity. **Remote Sensing of Environment**, v. 224, p. 104-118, 2019.

KULKARNI, Bhargavi N.; KULKARNI, Nagaraj B.; ANANTHARAMA, V. An empirical analysis of surface-level methane emission from anthropogenic sources in India. **Journal of Cleaner Production**, v. 346, p. 131101, 2022.

LACAUX, J. P. *et al*. Classification of ponds from high-spatial resolution remote sensing: Application to Rift Valley Fever epidemics in Senegal. **Remote sensing of environment**, v. 106, n. 1, p. 66-74, 2007.

LAMBROU, Theofanis P.; ANASTASIOU, Christos C.; PANAYIOTOU, Christos G. A nephelometric turbidity system for monitoring residential drinking water quality. In: **Sensor Applications, Experimentation, and Logistics: First International Conference, SENSAPPEAL 2009, Athens, Greece, September 25, 2009, Revised Selected Papers 1**. Springer Berlin Heidelberg, 2010. p. 43-55.

LAMPERT, Winfried *et al*. Phytoplankton control by grazing zooplankton: A study on the spring clear-water phase 1. **Limnology and oceanography**, v. 31, n. 3, p. 478-490, 1986.

LEHNER, Bernhard *et al*. High-resolution mapping of the world's reservoirs and dams for sustainable river-flow management. **Frontiers in Ecology and the Environment**, v. 9, n. 9, p. 494-502, 2011.

LI, Chuan *et al*. Lake Water Quality and Dynamics Assessment during 1990–2020 (A Case Study: Chao Lake, China). **Atmosphere**, v. 14, n. 2, p. 382, 2023.

LI, Xinxin *et al*. Measurement and simulation of topographic effects on passive microwave remote sensing over mountain areas: A case study from the Tibetan Plateau. **IEEE transactions on geoscience and remote sensing**, v. 52, n. 2, p. 1489-1501, 2013.

LIANG, Jiayong; LIU, Desheng. A local thresholding approach to flood water delineation using Sentinel-1 SAR imagery. **ISPRS journal of photogrammetry and remote sensing**, v. 159, p. 53-62, 2020.

LIMA NETO, Iran Eduardo; WIEGAND, Mário Cesar; DE ARAÚJO, José Carlos. Sediment redistribution due to a dense reservoir network in a large semi-arid Brazilian basin. **Hydrological Sciences Journal–Journal des Sciences Hydrologiques**, v. 56, n. 2, p. 319-333, 2011.

LIMBERGER, Salete. **Microalgas perifíticas como bioindicadores ambientais na foz do Rio Ocoy: tributário do lago de Itaipu-PR**. 2011. Trabalho de Conclusão de Curso. Universidade Tecnológica Federal do Paraná.

LING, Feng *et al*. Monitoring surface water area variations of reservoirs using daily MODIS images by exploring sub-pixel information. **ISPRS Journal of Photogrammetry and Remote Sensing**, v. 168, p. 141-152, 2020a.

LING, Zunbin *et al*. Remote sensing estimation of colored dissolved organic matter (CDOM) from GOCI measurements in the Bohai Sea and Yellow Sea. **Environmental Science and Pollution Research**, v. 27, p. 6872-6885, 2020b.

LIU, Xiaohan *et al*. Remote sensing of secchi depth in highly turbid lake waters and its application with MERIS data. **Remote Sensing**, v. 11, n. 19, p. 2226, 2019.

LIU, Yansui; ISLAM, Md Anisul; GAO, Jay. Quantification of shallow water quality parameters by means of remote sensing. **Progress in physical geography**, v. 27, n. 1, p. 24-43, 2003.

LOBO, Felipe L.; COSTA, Maycira PF; NOVO, Evlyn MLM. Time-series analysis of Landsat-MSS/TM/OLI images over Amazonian waters impacted by gold mining activities. **Remote Sensing of Environment**, v. 157, p. 170-184, 2015.

LONDE, L. R. *et al*. Análise quantitativa do comportamento espectral da clorofila-a no reservatório de Salto Grande (SP). **SIMPÓSIO REGIONAL DE GEOPROCESSAMENTO E SENSORIAMENTO REMOTO**, v. 3, 2006.

LOPES, Fernando B. *et al*. Modelagem da qualidade das águas a partir de sensoriamento remoto hiperespectral. **Revista Brasileira de Engenharia Agrícola e Ambiental**, v. 18, p. 13-19, 2014.

LU, Shanlong *et al*. Water body mapping method with HJ-1A/B satellite imagery. **International Journal of Applied Earth Observation and Geoinformation**, v. 13, n. 3, p. 428-434, 2011.

MA, Run *et al*. Estimation of surface shortwave radiation from Himawari-8 satellite data based on a combination of radiative transfer and deep neural network. **IEEE Transactions on Geoscience and Remote Sensing**, v. 58, n. 8, p. 5304-5316, 2020.

MACHADO, Marilia Teresinha de Sousa; BAPTISTA, Gustavo Macedo de Mello. Sensoriamento remoto como ferramenta de monitoramento da qualidade da água do Lago Paranoá (DF). **Engenharia Sanitária e Ambiental**, v. 21, p. 357-365, 2016.

MANSOURMOGHADDAM, Mohammad *et al*. Assessment of Palm Jumeirah Island's construction effects on the surrounding water quality and surface temperatures during 2001–2020. **Water**, v. 14, n. 4, p. 634, 2022.am, India. **Modeling Earth Systems and Environment**, v. 5, p. 1179-1200, 2019.

MANTOVANI, Jose Eduardo; NOVO, E. M. L. M. Comportamento Espectral da Matéria Orgânica Dissolvida. **Simpósio Brasileiro de Sensoriamento Remoto**, p. 7, 1996.

MARKERT, Kel N. *et al*. Comparing sentinel-1 surface water mapping algorithms and radiometric terrain correction processing in southeast asia utilizing google earth engine. **Remote Sensing**, v. 12, n. 15, p. 2469, 2020.

MARKERT, Kel N. *et al*. Historical and operational monitoring of surface sediments in the lower mekong basin using landsat and google earth engine cloud computing. **Remote Sensing**, v. 10, n. 6, p. 909, 2018.

MARTINS, Vitor S. *et al*. Remote sensing of large reservoir in the drought years: Implications on surface water change and turbidity variability of Sobradinho reservoir (Northeast Brazil). **Remote Sensing Applications: Society and Environment**, v. 13, p. 275-288, 2019.

MAYS, Larry W. A very brief history of hydraulic technology during antiquity. **Environmental Fluid Mechanics**, v. 8, p. 471-484, 2008.

MCFEETERS, Stuart K. The use of the Normalized Difference Water Index (NDWI) in the delineation of open water features. **International journal of remote sensing**, v. 17, n. 7, p. 1425-1432, 1996.

MEIBURG, Eckart; KNELLER, Ben. Turbidity currents and their deposits. **Annual Review of Fluid Mechanics**, v. 42, p. 135-156, 2010.

MINELLA, Jean PG *et al*. Estimating suspended sediment concentrations from turbidity measurements and the calibration problem. **Hydrological Processes: An International Journal**, v. 22, n. 12, p. 1819-1830, 2008.

MISHRA, Manoranjan *et al*. Mining impacts on forest cover change in a tropical forest using remote sensing and spatial information from 2001–2019: A case study of Odisha (India). **Journal of Environmental Management**, v. 302, p. 114067, 2022.

MISHRA, Vikalp *et al*. Evaluating the performance of high-resolution satellite imagery in detecting ephemeral water bodies over West Africa. **International Journal of Applied Earth Observation and Geoinformation**, v. 93, p. 102218, 2020.

MOBLEY, Curtis D. The optical properties of water. **Handbook of optics**, v. 1, n. 43, p. 43, 1995.

MOHD HASMADI, I.; NORSALIZA, U. Analysis of SPOT-5 data for mapping turbidity level of river klang, peninsular malaysia. **Appl. Remote Sens. J**, v. 1, p. 14-18, 2010.

NGUYEN, Hong Anh Thi *et al*. Integrating remote sensing and machine learning into environmental monitoring and assessment of land use change. **Sustainable Production and Consumption**, v. 27, p. 1239-1254, 2021.

NOBREGA, I. W. **Análise espectral de sistemas aquáticos da amazônia para a identificação de componentes opticamente ativos. 2002. 87 f**. Tese de Doutorado. Dissertação (Mestrado em Sensoriamento Remoto) Instituto Nacional de Pesquisas Espaciais–INPE, São José dos Campos.

NOGUEIRA, Pollyanna Faria *et al*. Eutrofização no reservatório da UHE foz do Rio Claro (GO). **Revista do Departamento de Geografia**, v. 30, p. 19-33, 2015.

NORTON, L. D. *et al*. Monitoring the sediment loading of Itaipu Lake and modeling of sheet and rill erosion hazards in the watershed of the Parana River: an outline of the Project. 2001.

OEHY, Christoph D.; SCHLEISS, Anton J. Control of turbidity currents in reservoirs by solid and permeable obstacles. **Journal of Hydraulic Engineering**, v. 133, n. 6, p. 637-648, 2007.

OMAR, Ahmad Fairuz Bin; MATJAFRI, Mohd Zubir Bin. Turbidimeter design and analysis: a review on optical fiber sensors for the measurement of water turbidity. **Sensors**, v. 9, n. 10, p. 8311-8335, 2009.

ORGANISATION FOR ECONOMIC CO-OPERATION AND DEVELOPMENT - OECD. The Future of EcoInnovations: the role of business models in green Transformation. Paris: OECD, 2012.

PAGIORO, Thomaz A.; THOMAZ, Sidinei M. Longitudinal patterns of sedimentation in a deep, monomictic subtropical reservoir (Itaipu, Brazil-Paraguay). **Archiv fur Hydrobiologie**, v. 154, n. 3, p. 515-528, 2002.

PAGIORO, THOMAZ AURÉLIO. **Variações espaço-temporais das características físicas e químicas da água, material em sedimentação e produtividade primária fitoplanctônica no reservatório de Itaipu, PR, Brasil**. 1999. Tese de Doutorado. Doctoral Thesis, Universidade Estadual de Maringá, Maringá, Brasil, 59p.

PATRA, Debasmita; BASU, Saikat Kumar. Ecological restoration of earth's ecosystem and the decade of ecosystem restoration. **International Journal on Environmental Sciences**, v. 11, n. 2, p. 117-148, 2021.

PEKEL, Jean-François *et al*. High-resolution mapping of global surface water and its long-term changes. **Nature**, v. 540, n. 7633, p. 418-422, 2016.

PENG, Feng *et al*. Light-scattering features of turbidity-causing particles in interconnected reservoir basins and a connecting stream. **water research**, v. 43, n. 8, p. 2280-2292, 2009.

PHAM-DUC, Binh *et al*. Monitoring Lake Volume Variation from Space Using Satellite Observations—A Case Study in Thac Mo Reservoir (Vietnam). **Remote Sensing**, v. 14, n. 16, p. 4023, 2022.

R CHALOV, Sergey *et al*. Spatio-temporal variation of sediment transport in the Selenga River Basin, Mongolia and Russia. **Environmental Earth Sciences**, v. 73, p. 663-680, 2015.

R CHALOV, Sergey *et al*. Spatio-temporal variation of sediment transport in the Selenga River Basin, Mongolia and Russia. **Environmental Earth Sciences**, v. 73, p. 663-680, 2015.

RAMOLLO, Phetole Peter. **Bioassessing the impact of water quality on the health and parasite composition of Oreochromis Mossambicus at the Phalaborwa Industrial Complex (PIC) and the barrage (Olifants river) in the Limpopo Province, South Africa**. 2008. Tese de Doutorado.

RAMOLLO, Phetole Peter. **Bioassessing the impact of water quality on the health and parasite composition of Oreochromis Mossambicus at the Phalaborwa Industrial Complex (PIC) and the barrage (Olifants river) in the Limpopo Province, South Africa**. 2008. Tese de Doutorado.

REN21 (2021). Renewables 2021 Global Status Report. Technical report, REN21 Secretariat, Paris, France.

RITCHIE, Jerry C.; ZIMBA, Paul V.; EVERITT, James H. Remote sensing techniques to assess water quality. **Photogrammetric engineering & remote sensing**, v. 69, n. 6, p. 695-704, 2003.

ROSA, Roberto. **Introdução ao Sensoriamento Remoto.** Uberlândia: EDUFU, 2009.

RUDKE, Anderson Paulo *et al*. **Dinâmica da cobertura do solo para a bacia hidrográfica do alto rio Paraná**. 2018. Dissertação de Mestrado. Universidade Tecnológica Federal do Paraná.

RUDORFF, Natalia *et al*. Remote sensing monitoring of the impact of a major mining wastewater disaster on the turbidity of the Doce River plume off the eastern Brazilian coast. **ISPRS Journal of Photogrammetry and Remote Sensing**, v. 145, p. 349-361, 2018.

Rycerz, R., BuglerW., Messling, L. and Wade, G. (2020). Itaipú Dam: How natural ecosystems support one of the world's largest hydroelectric dams. Resilience Shift Case Study. https://www.resilienceshift.org/wp-content/uploads/2020/08/Itaipu-Dam-case-studyResilience-Shift.pdf

SANTOS, Ana Paula dos. **Lago de memórias: a submersão das Setes Quedas**. 2006. Mestrado em História. Universidade Estadual de Maringá, Maringá, PR, 2006.

SANTOS, Rafson Varela dos *et al*. Variabilidade espacial e temporal das características limnológicas dos reservatórios Santa Cruz e Umarí, semiárido do Rio Grande do Norte, Brasil. 2014.

SCHLEISS, Anton J. *et al*. Reservoir sedimentation. **Journal of Hydraulic Research**, v. 54, n. 6, p. 595-614, 2016.

SEATON, Dylan; DUBE, Timothy; MAZVIMAVI, Dominic. Use of multi-temporal satellite data for monitoring pool surface areas occurring in non-perennial rivers in semi-arid environments of the Western Cape, South Africa. **ISPRS Journal of Photogrammetry and Remote Sensing**, v. 167, p. 375-384, 2020.

SHAFIQUE, Naseer A. *et al*. Hyperspectral remote sensing of water quality parameters for large rivers in the Ohio River basin. In: **First interagency conference on research in the watershed, Benson, AZ**. Citeseer, 2003. p. 216-221.

SILVA, Diogo Aparecido Lopes *et al*. Life cycle assessment of the sugarcane bagasse electricity generation in Brazil. **Renewable and Sustainable Energy Reviews**, v. 32, p. 532-547, 2014.

SOMVANSHI, S. *et al*. Water turbidity assessment in part of Gomti River using high resolution Google Earth's Quickbird satellite data. In: **Geospatial World Forum**. 2011. p. 18-21.

SONG, Chunqiao *et al*. Remote sensing of alpine lake water environment changes on the Tibetan Plateau and surroundings: A review. **ISPRS Journal of Photogrammetry and Remote Sensing**, v. 92, p. 26-37, 2014.

SOUZA FILHO, EE de; STEVAUX, José Cândido. Geologia e geomorfologia do complexo rio Baía, Curutuba, Ivinheima. **A planície de inundação do alto rio Paraná: aspectos físicos, biológicos e socioeconômicos**, p. 3-46, 1997.

STERNBERG, Rolf. Hydropower's future, the environment, and global electricity systems. **Renewable and Sustainable Energy Reviews**, v. 14, n. 2, p. 713-723, 2010.

STEVAUX, José Candido. **O rio Paraná: geomorfogênese, sedimentação e evolução quaternária do seu curso superior (região de Porto Rico, PR)**. 1993. Tese de Doutorado. Universidade de São Paulo.

SU, Yuan-Fong *et al*. A multivariate model for coastal water quality mapping using satellite remote sensing images. **Sensors**, v. 8, n. 10, p. 6321-6339, 2008.

SURISETTY, Venkata Vijay Arun Kumar *et al*. Improved turbidity estimates in complex inland waters using combined NIR–SWIR atmospheric correction approach for Landsat 8 OLI data. **International Journal of Remote Sensing**, v. 39, n. 21, p. 7463-7482, 2018.

TALLING, Peter J. *et al*. Key Future Directions For Research On Turbidity Currents And Their Depositskey Future Directions For Research On Turbidity Currents And Their Deposits. **Journal of Sedimentary Research**, v. 85, n. 2, p. 153-169, 2015.

TOLENTINO, Franciele Marques. Análise do desempenho de redes neurais artificiais no monitoramento sazonal de macrófitas no reservatório de Salto Grande e nas mudanças no uso e cobertura da terra do entorno. 2019. Mestrado em Ciências Cartográficas - Universidade Estadual Paulista, Presidente Prudente, São Paulo, SP, 2019.

TORTINI, Riccardo *et al*. Satellite-based remote sensing data set of global surface water storage change from 1992 to 2018. **Earth System Science Data**, v. 12, n. 2, p. 1141-1151, 2020.

TRENTIN, Aline Biasoli *et al*. Sensoriamento remoto aplicado ao estudo do comportamento espectral da água no reservatório Passo Real RS. 2009.

TRINH, Nguyen Xuan *et al*. Delimitating inland aqua-ecological zones under different climate conditions in the Mekong Delta region, Vietnam. **Journal of Water and Climate Change**, v. 9, n. 3, p. 463-479, 2018.

TUNDISI, José G. A review of basic ecological processes interacting with production and standing-stock of phytoplankton in lakes and reservoirs in Brazil. **Hydrobiologia**, v. 100, p. 223-243, 1983.

TUNDISI, José Galizia. Recursos hídricos no futuro: problemas e soluções. **Estudos avançados**, v. 22, p. 7-16, 2008.

TURCONI, Roberto; BOLDRIN, Alessio; ASTRUP, Thomas. Life cycle assessment (LCA) of electricity generation technologies: Overview, comparability and limitations. **Renewable and sustainable energy reviews**, v. 28, p. 555-565, 2013.

VON SPERLING, Marcos. **Introdução à qualidade das águas e ao tratamento de esgotos**. Editora UFMG, 1996.

WANG, F. *et al*. Applications of Landsat-5 TM imagery in assessing and mapping water quality in Reelfoot Lake, Tennessee. **International Journal of Remote Sensing**, v. 27, n. 23, p. 5269-5283, 2006.

WANG, Xianwei; XIE, Hongjie. A review on applications of remote sensing and geographic information systems (GIS) in water resources and flood risk management. **Water**, v. 10, n. 5, p. 608, 2018.

WANG, Yi *et al*. Fluid flow mechanisms and heat transfer characteristics of gas recovery from gas-saturated and water-saturated hydrate reservoirs. **International Journal of Heat and Mass Transfer**, v. 118, p. 1115-1127, 2018.

WETZEL, Robert G. **Limnology: lake and river ecosystems**. gulf professional publishing, 2001.

XIA, Haoming *et al*. Changes in water surface area during 1989–2017 in the Huai River Basin using Landsat data and Google earth engine. **Remote Sensing**, v. 11, n. 15, p. 1824, 2019.

XU, Hanqiu. Modification of normalised difference water index (NDWI) to enhance open water features in remotely sensed imagery. **International journal of remote sensing**, v. 27, n. 14, p. 3025-3033, 2006.

YAMAZAKI, Dai; TRIGG, Mark A.; IKESHIMA, Daiki. Development of a global~ 90 m water body map using multi-temporal Landsat images. **Remote Sensing of Environment**, v. 171, p. 337-351, 2015.

YANG, Xiaoying; JIN, Wei. GIS-based spatial regression and prediction of water quality in river networks: A case study in Iowa. **Journal of Environmental Management**, v. 91, n. 10, p. 1943-1951, 2010.

YANG, Yi-Chen E.; CAI, Ximing. Reservoir reoperation for fish ecosystem restoration using daily inflows—Case study of Lake Shelbyville. **Journal of Water Resources Planning and Management**, v. 137, n. 6, p. 470-480, 2011.

YAO, Huang; QIN, Rongjun; CHEN, Xiaoyu. Unmanned aerial vehicle for remote sensing applications—A review. **Remote Sensing**, v. 11, n. 12, p. 1443, 2019.

YUDIANTO, Doddi *et al*. A Framework of Dam-Break Hazard Risk Mapping for a Data-Sparse Region in Indonesia. **ISPRS International Journal of Geo-Information**, v. 10, n. 3, p. 110, 2021.

ZARFL, Christiane *et al*. A global boom in hydropower dam construction. **Aquatic Sciences**, v. 77, p. 161-170, 2015.

ZHANG, Hua *et al*. A remote sensing method for estimating regional reservoir area and evaporative loss. **Journal of Hydrology**, v. 555, p. 213-227, 2017.

ZHU, Lin *et al*. Algal accumulation decreases sediment nitrogen removal by uncoupling nitrification-denitrification in shallow eutrophic lakes. **Environmental science & technology**, v. 54, n. 10, p. 6194-6201, 2020.